



HAL
open science

Study of a new gas-liquid-solid three phase contact mode at millimetric scale: catalytic reactors using “slurry Taylor” flow

Anne-Kathrin Liedtke

► **To cite this version:**

Anne-Kathrin Liedtke. Study of a new gas-liquid-solid three phase contact mode at millimetric scale: catalytic reactors using “slurry Taylor” flow. Chemical and Process Engineering. Université Claude Bernard - Lyon I, 2014. English. NNT : 2014LYO10137 . tel-01140247

HAL Id: tel-01140247

<https://theses.hal.science/tel-01140247>

Submitted on 8 Apr 2015

HAL is a multi-disciplinary open access archive for the deposit and dissemination of scientific research documents, whether they are published or not. The documents may come from teaching and research institutions in France or abroad, or from public or private research centers.

L’archive ouverte pluridisciplinaire **HAL**, est destinée au dépôt et à la diffusion de documents scientifiques de niveau recherche, publiés ou non, émanant des établissements d’enseignement et de recherche français ou étrangers, des laboratoires publics ou privés.

THÈSE

présentée devant

L'UNIVERSITÉ CLAUDE BERNARD - LYON 1

pour l'obtention du

DIPLÔME DE DOCTORAT

(arrêté du 07 août 2006)

École doctorale de Chimie
Spécialité : Génie des Procédés

présentée et soutenue publiquement le 11/07/2014 par

Anne-Kathrin LIEDTKE

Study of a new gas-liquid-solid three phase contact mode at millimetric scale: catalytic reactors using "slurry Taylor" flow.

Laboratoire de Génie des Procédés Catalytiques UMR 5285 CPE Lyon-CNRS

Directeurs de thèse: M. Claude de BELLEFON

<i>Jury:</i> Mme Flavie SARRAZIN	Examineur
M. David W. AGAR	Rapporteur
M. Christophe GOURDON	Rapporteur
M. Hugh STITT	Examineur
M. Pascal FONGARLAND	Président
M. Régis PHILIPPE	Examineur
M. Claude de BELLEFON	Examineur

UNIVERSITE CLAUDE BERNARD - LYON 1

Président de l'Université

M. François-Noël GILLY

Vice-président du Conseil d'Administration

M. le Professeur Hamda BEN HADID

Vice-président du Conseil des Etudes et de la Vie
Universitaire

M. le Professeur Philippe LALLE

Vice-président du Conseil Scientifique

M. le Professeur Germain GILLET

Directeur Général des Services

M. Alain HELLEU

COMPOSANTES SANTE

Faculté de Médecine Lyon Est - Claude Bernard

Directeur : M. le Professeur J. ETIENNE

Faculté de Médecine et de Maïeutique Lyon Sud -
Charles Mérieux

Directeur : Mme la Professeure C.
BURILLON

Faculté d'Odontologie

Directeur : M. le Professeur D.
BOURGEOIS

Institut des Sciences Pharmaceutiques et
Biologiques

Directeur : Mme la Professeure C.
VINCIGUERRA

Institut des Sciences et Techniques de la
Réadaptation

Directeur : M. le Professeur Y.
MATILLON

Département de formation et Centre de Recherche
en Biologie Humaine

Directeur : Mme. la Professeure A-M.
SCHOTT

COMPOSANTES ET DEPARTEMENTS DE SCIENCES ET TECHNOLOGIE

Faculté des Sciences et Technologies

Directeur : M. F. DE MARCHI

Département Biologie

Directeur : M. le Professeur F. FLEURY

Département Chimie Biochimie

Directeur : Mme Caroline FELIX

Département GEP

Directeur : M. Hassan HAMMOURI

Département Informatique

Directeur : M. le Professeur S.
AKKOUCHE

Département Mathématiques

Directeur : M. le Professeur Georges
TOMANOV

Département Mécanique

Directeur : M. le Professeur H. BEN
HADID

Département Physique

Directeur : M. Jean-Claude PLENET

UFR Sciences et Techniques des Activités
Physiques et Sportives

Directeur : M. Y.VANPOULLE

Observatoire des Sciences de l'Univers de Lyon
Polytech Lyon

M. B. GUIDERDONI

Directeur : Directeur : M. P. FOURNIER

Ecole Supérieure de Chimie Physique Electronique

Directeur : M. G. PIGNAULT

Institut Universitaire de Technologie de Lyon 1

Directeur : M. le Professeur C. VITON

Ecole Supérieure du Professorat et de l'Education

Directeur : M. le Professeur A.
MOUGNIOTTE

Institut de Science Financière et d'Assurances

Directeur : M. N. LEBOISNE

For my family.

Curiously enough, the only thing that went through the mind of the bowl of petunias as it fell was *Oh no, not again.*

Many people have speculated that if we knew exactly why the bowl of petunias had thought that we would know a lot more about the nature of the Universe than we do now.

— Douglas Adams

ABSTRACT

Ce travail est consacré à la caractérisation d'un nouveau type de contacteur gaz-liquide-solide. L'approche innovante consiste en l'utilisation d'un écoulement segmenté type "slurry Taylor" pour le transport des particules catalytiques et la conduite des réactions triphasique gaz-liquide-solide dans un tube de section circulaire. Les courants de circulation interne présents dans les segments est utilisé pour maintenir le catalyseur en suspension. Ainsi, le catalyseur sous sa forme pulvérulente conventionnelle peut être facilement changé de manière continue, sans démontage du réacteur.

Dans un premier temps l'étude est focalisée sur la caractérisation de l'hydro dynamique et donc le placement et le comportement des particules solides dans la phase liquide en fonction de différentes conditions opératoire telles que: l'orientation de l'écoulement (horizontal ou vertical descendant), la vitesse totale de l'écoulement (2 cm s^{-1} à 42 cm s^{-1}) et la charge en solide (2.5 g l^{-1} à 50 g l^{-1}). En écoulement horizontal une vitesse totale importante est essentielles pour assurer une mise en suspension homogène sur la hauteur du canal. Pour des vitesses lentes (2.3 cm s^{-1} à 5 cm s^{-1}), les particules se trouvent essentiellement dans la partie basse du segment de liquide et une vitesse minimale critique est nécessaire pour mettre les particules en suspension de façon homogène dans le liquide. Le comportement observé est différent pour l'écoulement vertical descendant: les particules peuplent le segment de liquide de façon homogène dès les très faibles vitesses et même pour des taux de solide important (50 g /L).

Dans un second temps, le transfert de matière liquide-solide (L-S) a été étudié par la réaction de neutralisation d'une solution basique avec une résine échangeuse d'ions acide. L'influence de la vitesse totale de l'écoulement (1 cm s^{-1} à 28 cm s^{-1}), la longueur du segment de liquide (1 mm à 3,5 mm), la nature de la phase liquide (densité et viscosité) et l'orientation de l'écoulement (horizontale et verticale descendant) ont été étudiés. Le coefficient de transfert de matière L-S et donc le nombre de Sherwood sont principalement impactés par la vitesse totale de l'écoulement: en augmentant la vitesse (1 cm s^{-1} à 18 cm s^{-1}) le nombre de Sherwood augmente de 6 à 16. Pour des vitesses plus importantes le nombre de Sherwood reste constant. Une influence de l'orientation de l'écoulement n'a pas été observée. Une première corrélation pour le nombre de Sherwood est proposée et la déviation moyenne de 8 % indique la bonne représentation des résultats.

Cet écoulement qui possède les propriétés de l'écoulement segmenté de Taylor (aire interfaciale élevée, bon transfert G-L, faible dispersion axiale, faible perte de charge), semble donc prometteur pour de nouveaux réacteurs triphasiques avec catalyseur en suspension.

For instance, on the planet Earth, man had always assumed that he was more intelligent than dolphins because he had achieved so much - the wheel, New York, wars and so on whilst all the dolphins had ever done was muck about in the water having a good time. But conversely, the dolphins had always believed that they were far more intelligent than man - for precisely the same reasons.

Douglas Adams, The Hitchhiker's Guide to the Galaxy

ACKNOWLEDGEMENTS

I would like to express my genuine gratitude to Claude de Bellefon and Régis Philippe, my research supervisors, for their guidance, patience and fruitful criticism. I very much appreciate our respectful and enthusiastic discussions: I always found them to be very motivating, encouraging me to look further and reminding me of the bigger picture.

This research work could not have been done without the help of the members of the LGPC.

I would like to express my great appreciation to Frédéric Bornette and Fabrice Campoli for your expertise, input and work concerning the experimental work and set-up. Thank you for your patience and assistance regarding all the small and bigger hiccups we encountered.

I wish to acknowledge the help provided by Stephanie Pallier, Marie-Line Zanota and Valérie Meille. Thank you for various discussions on solid particle matter, suspensions as well as life in general. Thank you Marie-Line for your work on image analysis.

The advice and contribution of Laurent Vanoye and Alain Favre-Réguillon has been a great help. Thank you for your expertise and patience. I really enjoyed working on fluorescent particles with Alain and maybe together with the next PhD student you will make them circulate in Taylor flow.

The work on the L-S mass transfer is the result of a collaboration work with Frederik Scheiff and David Agar. Thank you for this collaboration, your input and our fruitful exchange.

Thank you Leonard Sylla, Radhi Khédhiri and Etienne Croiset, for your work and your contribution to this research study. You spend a few month at this laboratory for your bachelor or master's thesis and I am very thankful for the time we spend together and the lessons you taught me about teaching and supervising.

For everybody who was involved in this journey, I'd like them to know how grateful I am to have met you. I will never forget all the places I got to go with you or because of you, all the people I got to meet, all the experiences I got to explore. These last couple of years have been a joyful and at the same time painful time of personal and professional growing and you had an impact. I am very glad that I had the chance to meet all of you.

CONTENTS

i	INTRODUCTION	1
1	INTRODUCTION	3
1.1	Suspension catalysts and reactors	3
1.2	Gas-liquid-solid “slurry Taylor” flow - an alternative?	4
1.3	Outline of the thesis	9
1.4	Symbols and abbreviations	10
ii	CONCEPT OF “SLURRY TAYLOR” FLOW AND MOTIVATION	11
2	G-L-S “SLURRY TAYLOR ” FLOW: CONCEPT AND MOTIVATION	13
2.1	Introduction	14
2.2	Experimental set-up	15
2.2.1	“Slurry Taylor” flow set-up	15
2.2.2	Stirred tank reactor set-up	16
2.2.3	G-L-S model reaction	16
2.2.4	Validation of the slurry contact mode	17
2.2.5	Hydrogenation in Taylor flow reactor	17
2.2.6	Hydrogenation in stirred tank reactor	17
2.2.7	Gas chromatography analysis	18
2.2.8	Reaction course monitoring by image analysis	18
2.3	Results and discussion	19
2.3.1	Validation of the experimental set-up	19
2.3.2	Hydrogenation in the stirred tank reactor	20
2.3.3	Hydrogenation in the “slurry Taylor” flow reactor	21
2.3.4	Reaction course monitoring by visualization	22
2.3.5	Comparison of the “slurry Taylor” and batch reactors	23
2.4	Conclusion	24
2.5	Symbols and subscripts	25
iii	HYDRODYNAMICS	27
3	HYDRODYNAMIC MAPPING OF GAS-LIQUID “SLURRY TAYLOR” FLOW	29
3.1	Introduction	30
3.2	Experimental set-up	31
3.2.1	Optical device and image analysis	32
3.2.2	Chemicals	33
3.2.3	Experimental procedure for hydrodynamic measurements for horizontal and vertical “slurry Taylor” flow	34
3.3	Results and discussion	35
3.3.1	Stable functioning of suspension supply device	35
3.3.2	Particle placement in liquid slugs	36
3.3.3	Description of particle flow patterns and Matlab™ routine for automatic detection of flow patterns	38
3.3.4	Discussion of relevant mechanisms related to particle entrainment and re-suspension	46
3.3.5	Flow pattern map	60
3.4	Conclusion and perspectives	63

3.5	Symbols	65
iv	LIQUID-SOLID MASS TRANSFER	67
4	CONTINUOUS & DISCONTINUOUS PHASE: IMPACT ON L-S MASS TRANSFER	69
4.1	Introduction	71
4.2	Experimental	73
4.2.1	Principle	73
4.2.2	Set-up	75
4.2.3	Chemicals	76
4.2.4	Intrusive and non-intrusive electrical impedance based measurement devices	77
4.2.5	Mass transfer measurements in "slurry Taylor" flow	79
4.3	Results and discussion	80
4.3.1	Gas-liquid "slurry Taylor" flow	80
4.3.2	Liquid-liquid "slurry Taylor" flow	81
4.3.3	Comparison between G-L and L-L "slurry Taylor" flow	84
4.3.4	Conclusion and perspectives	85
4.4	Symbols	86
5	L-S MASS TRANSFER IN HORIZONTAL AND VERTICAL "SLURRY TAYLOR" FLOW	89
5.1	Introduction	90
5.2	Experimental	91
5.2.1	Principle	91
5.2.2	Set-up	91
5.2.3	Chemicals	92
5.2.4	Mass transfer measurements in "slurry Taylor" flow	92
5.3	Results and discussion	94
5.3.1	Influence of two phase velocity and flow direction on the liquid-solid mass transfer	94
5.3.2	Influence of solid loading and particle diameter	95
5.3.3	Correlation for L-S mass transfer coefficients in horizontal and vertical "slurry Taylor" flow	97
5.3.4	Conclusion and perspectives	98
5.4	Symbols	99
v	CONCLUSION AND PERSPECTIVES	101
6	CONCLUSION AND PERSPECTIVES	103
6.0.1	Conclusion	103
6.0.2	Perspectives	104
	BIBLIOGRAPHY	107

LIST OF FIGURES

Figure 2.1	Experimental set-up used for “slurry Taylor” experiments	15
Figure 2.2	Detailed reactor arrangement in the aluminium plate.	16
Figure 2.3	Reaction scheme for the hydrogenation of 3-methyl-1-pentyn-3-ol.	17
Figure 2.4	Measured catalyst charge for different stirring speeds.	19
Figure 2.5	Typical G/L/S “slurry Taylor” flow obtained for a N ₂ /water system with 6.0 g/L of 100 μm Al ₂ O ₃ particles in suspension	20
Figure 2.6	Substrate conversion in the stirred tank reactor for different operating temperatures	20
Figure 2.7	Evolution of the substrate conversion for different solid catalyst charges in the stirred tank reactor	21
Figure 2.8	Conversion obtained by GC analysis for two reactor lengths in the “slurry Taylor” reactor	21
Figure 2.9	Results obtained for “slurry Taylor” flow	22
Figure 2.10	Comparison between substrate conversion profiles obtained in the stirred tank reactor and in the “slurry Taylor” contactor (by bubble shrinkage visualization and GC).	23
Figure 3.1	Experimental set-up used for hydrodynamic “slurry Taylor” flow visualisation experiments	32
Figure 3.2	Geometry of T-junction used for hydrodynamic visualisation experiments	32
Figure 3.3	Arrangement of injection device for horizontal and vertical “slurry Taylor” flow hydrodynamic visualisation experiments	32
Figure 3.4	Refractive index adaptation device	33
Figure 3.5	SEM photography and particle size distribution of SiO ₂ particles used for hydrodynamic visualisation experiments	35
Figure 3.6	Verification of suspension supply unit	35
Figure 3.7	Examples of particle placement in horizontal flow. Operating parameters are summarized in Table 3.2	36
Figure 3.8	Examples of particle placement in vertical flow. Operating parameters are summarized in Table 3.3	37
Figure 3.9	Exemplary pictures of detected flow regimes in horizontal flow	41
Figure 3.10	Exemplary pictures of detected flow regimes in vertical flow	43
Figure 3.11	Typical image after pretreatment for automatic flow pattern analysis	44
Figure 3.12	Matlab™ routine to automatically detect a flow pattern	45
Figure 3.13	Impact of injection configuration on placement of solid particles in the liquid slug, for a)-d): $Q_L = 3 \text{ ml min}^{-1}$, $Q_L = 2.5 \text{ ml min}^{-1}$, for a)-c) $w_s = 2.5 \text{ g L}^{-1}$, d) $w_s = 5 \text{ g L}^{-1}$, for a), b) and d) same injection method, c) spiral arrangement between T-junction and vertical tubing to better distribute the particles	46
Figure 3.14	Configuration of injection device, possible influence of injection on placement of particles	47
Figure 3.15	Schematic illustration of different sources for lift effect: (A) rotating particle, (B) particle exposed to unsymmetrical flow field due to particle shape, (C-D) asymmetric flow profile	49

Figure 3.16	Horizontal flow: chosen points for simplified force analysis	50
Figure 3.17	Illustration of flow profile for selected points in horizontal flow	51
Figure 3.18	Illustration of influence on gravity on bubble shape and liquid film thickness.	52
Figure 3.19	Distance the solid particle can settle while the gas bubble travels one slug length.	53
Figure 3.20	Influence of channel wall on settling velocity for horizontal and vertical flow	54
Figure 3.21	Relative fluid velocity compared to particle settling velocity	54
Figure 3.22	Vertical flow: selected points for simplified force analysis	55
Figure 3.23	Illustration of flow profile for selected points in vertical flow	55
Figure 3.24	Different mechanisms for particle entrainment	57
Figure 3.25	Different particle positions relative to liquid film thickness	57
Figure 3.26	Effect of two phase velocity on the capability of fluid field to initiate particle movement.	58
Figure 3.27	Effect of two phase velocity on the liquid film thickness for selected experimental points.	58
Figure 3.28	Flow pattern map for horizontal flow based on the dimensionless factor N .	60
Figure 3.29	Flow pattern map for horizontal flow based on the product of Shields parameter and shear Reynolds number.	62
Figure 3.30	Flow pattern map for vertical flow based on the product of Shields parameter and shear Reynolds number.	62
Figure 3.31	Flow pattern map for vertical flow, the solid charge is depicted in function of the two phase velocity.	63
Figure 4.1	Solid handling in micro and millimetric structures.	71
Figure 4.2	Typical flow patterns encountered in liquid slugs in G-L Taylor-flow and in liquid droplets in L-L Taylor-flow	74
Figure 4.3	Illustration of the model used to estimate the external L-S mass transfer	75
Figure 4.4	Experimental set-up used for "slurry Taylor" flow mass transfer experiments	76
Figure 4.5	In-house fabricated 4-port connectors used for mass transfer experiments	77
Figure 4.6	Devices for conductimetric measurements applied in L-S mass transfer experiments	79
Figure 4.7	External L-S mass transfer coefficients estimated for gas-liquid "slurry Taylor" flow	80
Figure 4.8	Influence of slug length on the Sherwood number	81
Figure 4.9	Effect of two phase velocity on external L-S mass transfer coefficient in L-L "slurry Taylor" flow	82
Figure 4.10	Influence of particle size on L-S mass transfer coefficient	83
Figure 4.11	Comparison of Shwerwood numbers obtained for G-L and L-L "slurry Taylor" flow	84
Figure 5.1	Illustration of the model used to estimate the external L-S mass transfer	91
Figure 5.2	Experimental set-up used to determine L-S mass transfer coefficients of "slurry Taylor" flow	92
Figure 5.3	Sherwood numbers for horizontal and vertical gas-liquid "slurry Taylor" flow.	94

- Figure 5.4 Effect of solid charge and particle diameter on L-S mass transfer in “slurry Taylor” flow. 96
- Figure 5.5 Parity diagram illustrating experimental and theoretical L-S mass coefficients. 97

LIST OF TABLES

Table 1.1	Typical properties of g-l-s three-phase suspension reactors.	4
Table 1.2	Literature survey for articles published before 2011 on micro metric particles in millimetric tubes. Flow direction indicates if the study was conducted in a single capillary (s) or in parallel channels (p) and in horizontal (h) or vertical flow (v).	7
Table 1.3	Literature survey for articles published on “slurry Taylor” flow after 2011. Flow direction indicates if the study was conducted in a single capillary (s) or in parallel channels (p) and in horizontal (h) or vertical (v) flow.	8
Table 2.1	Operating conditions in the “slurry Taylor” reactor.	18
Table 2.2	Operating conditions in the stirred tank batch reactor.	18
Table 2.3	Operating conditions for the comparison between the batch and the “slurry Taylor” reactors.	24
Table 3.1	Operating conditions applied for hydrodynamic gas-liquid-solid “slurry Taylor” flow experiments.	34
Table 3.2	Operating conditions for horizontal flow for the exemplary pictures in Figure 3.7. Fluid media 1: pure ethanol, fluid media 2: ethanol-glycerol.	36
Table 3.3	Operating conditions for vertical flow for the exemplary pictures in Figure 3.8. Fluid media 1: pure ethanol, fluid media 2: ethanol/ glycerol.	37
Table 3.4	Importance of centrifugal force compared to submerged weight for vertical flow.	56
Table 3.5	Capability of fluid field to initiate particle movement: effect of lift force, pure ethanol flow	59
Table 3.6	Capability of fluid field to initiate particle movement: effect of lift force, ethanol/ glycerol flow	59
Table 4.1	Operating conditions applied in G-L and L-L “slurry Taylor” flow experiments for L-S mass transfer measurements.	78
Table 4.2	Properties of the liquids and mixtures used for L-S mass transfer measurements in G-L and L-L “slurry Taylor” flow.	78
Table 5.1	Operating conditions applied in G-L “slurry Taylor” flow experiments for L-S mass transfer measurements.	93
Table 5.2	Properties of the liquids used for L-S mass transfer measurements in G-L “slurry Taylor” flow.	93

Part I

INTRODUCTION

INTRODUCTION

1.1 SUSPENSION CATALYSTS AND REACTORS

Three phase gas-liquid-solid (g-l-s) reactions [24, 111, 126] play an important role in the chemical industry. Heterogeneous catalysed hydrogenations, oxidations, hydrodenitrogenations and hydrodesulfurizations for example are fundamental reaction classes commonly used in petrochemistry or for the production of pharmaceuticals and fine chemistry [91]. Not to forget the broad applications in environmental chemistry for cleaning processes of effluents or in biochemistry (fermentation). Three phase reactors [24, 103, 111, 126] are rather complex dynamic systems where chemistry is strongly coupled with many physical phenomena such as gas, liquid and solid phase contacting and mass and heat transfer. For the placement of the solid phase the use of suspension catalysts is often the only option:

- a few catalysts exist only in form of a powder, for example Raney Nickel.
- for economic operation of fast deactivating catalysts, easy and on-line replacement and regeneration and/or continuous introduction of fresh catalysts is required, avoiding thus the shut down of the process unit.
- fine powders provide enhanced internal mass transfer and in contrast to eggshell catalysts the whole particle volume is accessible which enables efficient use of solid volume. Concentration gradients in the particle, promoting potential undesired side products, are avoided.
- suspension catalysts ensure efficient heat removal. The build-up of hot spots in suspension phase reactors is effectively avoided which makes them the ideal choice for highly exothermic reactions.

Three-phase g-l-s contactors with suspension catalysts typically employed in chemical industry are in general:

- **bubble columns:** the gas phase is introduced at the bottom of the vessel and suspends the solid particles, the liquid flow rate is zero or very low and can be in co- or counter-current flow to the gas phase.
- **stirred tank reactors:** particle suspension is assured by means of mechanic agitation. The stirred tank can be operated in batch, semi-batch and also continuous mode.
- **fluidized or ebullated beds:** the liquid phase is injected at the bottom of the column and assures effective suspension of the solid particles. The gas phase is in general operated in co-current flow, but counter-current operation also exists and is a common technique to avoid entrainment of low density particles.

When it comes to choice and design of the reactor technology, typical criteria are for example mass (gas-liquid, liquid-liquid) and heat transfer, degree of mixing and ease of operation and scale-up. Table 1.1 gives an overview of relevant properties for suspension reactors. Bubble columns (BC), fluidized beds (FB) and stirred tanks (STR) appear to have rather similar properties with only slight differences. They all offer:

Table 1.1: Typical properties of g-l-s three-phase suspension reactors.

	bubble column	fluidized bed	stirred tank
\bar{d}_p [mm]	0.01-0.2	0.5-5	0.02-0.2
ϵ_S [$\text{m}_S^2/\text{m}_R^3$]	0.02-0.2	0.2-0.6	0.005-0.1
a_S [$\text{m}_{LS}^2/\text{m}_R^3$]	500-150000	200-7000	100-15000
k_S [m/s]	10^{-5} - $5 \cdot 10^{-4}$	10^{-5} - $5 \cdot 10^{-4}$	10^{-5} - $5 \cdot 10^{-4}$
$k_L a$ [s^{-1}]	0.01-2	0.01-2	0.005-0.8
h_{int} [$\text{kW}/\text{m}^2\text{K}$]	1000-6000	1000-6000	500-5000
Backmixing			
liquid phase	complete	complete	complete
gas phase	plug flow	plug flow	complete
solid phase	complete, axial profile more or less uniform	complete, axial profile more or less uniform	complete
catalyst attrition	+	++	+++

- good mass transfer and heat exchange capacities (STR more advantageous due to mechanical agitation [103]) with simple temperature control
- low power requirements due to overall low pressure drops (higher in STR because of mechanical agitation)
- high flexibility.

Potential problems are linked to the

- risk of catalyst attrition depending on solid properties (more distinct in STR)
- difficult separation of catalytic particles (easier in fluidized beds due to higher particle diameter commonly used)
- difficult scale-up, large variety of correlations available for stirred tanks [98], for bubble columns and fluidized beds correlations often only exist for small column diameters (15cm) and physical phenomena are not well understood.

All suspension reactor technologies in common is the high degree of mixing for the liquid and solid phase (and gas phase for STR). For applications which require the use of suspension catalysts (deactivation, need for high internal mass transfer, ..) and where the reaction kinetics demand plug flow behaviour, up to now no technology is able to answer both demands simultaneously.

1.2 GAS-LIQUID-SOLID "SLURRY TAYLOR" FLOW - AN ALTERNATIVE?

Taylor flow or segmented flow is a popular flow pattern often encountered in micro reaction technology due to its interesting properties [72] namely:

- high surface to volume ratio
- nearly ideal plug flow conditions (Peclet numbers up to 1000)

- circulation pattern in the liquid slug promoting, in combination with the reduced scale, excellent mass and heat transfer in the liquid segments.

Gas-liquid or liquid-liquid slug flows were studied quite extensively [62, 72] and are accepted more and more as useful tools in continuous chemistry.

Joining beneficial properties of slug flow conditions and slurry reactors can be an interesting approach to transport the solid phase and answer the demand for suspension reactors with low backmixing. The internal circulations occurring in the liquid slugs of G/L segmented flow [63, 72] or in the continuous and discontinuous phases of L/L segmented flow [36, 57, 65] can be used to keep catalyst particles in motion and transport them in a stable three-phase flow. In this contact mode, catalysts can be easily removed from the reactor, simple and available commercial catalysts can be employed and good transfer performances can be expected due to the large interfacial areas available for both heat and mass transfer.

The transportation and usage of micrometric particles is a subject which has been addressed in multi-phase micro reaction technology only recently. Due to the fear of clogging or bridging of freely flowing particles [49] the placement of the catalytic solid phase is, when necessary, usually resolved by immobilization either in form of a wall coating film or as a micro packed bed. Coating the catalyst on the reactor wall asks for special procedures, unique for each catalyst type, and renders the reactor system less flexible as the removal due to deactivation or change in active phase is nearly impossible without damaging the reactor wall. Milli or micro fixed beds represent an alternative and hold interesting performances in mass transfer [59, 82, 84] but concerns might be the high linear pressure drop and complex hydrodynamics encountered (wall channelling, local dewetting, wettability problems, etc.) [84].

The approach to immobilize the solid phase is limited to catalytic systems and is not applicable when the product or the reactant itself is a solid. On the other hand the occurrence of solid particles other than catalysts should not be neglected. A study by Roberge et al. [106] identified that out of 86 reactions carried out at Lonza, 31% could benefit from micro reaction technology but involve a solid phase (catalyst, reactant or product) and are thus considered to be difficult to perform in a micro reactor. Nanoparticles are handled quite frequently in micro reaction technology but the application of freely flowing solid particles from 10 μm up to 200 μm has so far only been studied rudimentarily as concerns regarding clogging due to bridging and/ or deposition [49] prevailed.

Table 1.2 gives an overview of published articles before 2011 (the beginning of this study) which focused on the utilization of micrometric particles in millimetric tubes. The concept of segmented flow with slurry contact mode was first mentioned in the literature in 2005/2007 [33–35]. These first studies were oriented mainly to the demonstration of this new contactor's applicability and interesting performance. Diverse catalytic hydrogenation reactions were performed in single and parallel vertical channels and the performance of different catalysts was evaluated. The achieved conversions and selectivities in "slurry Taylor" flow were compared to results in conventional reactors. However the reported hydrodynamic data were scarce and the flow pattern was either not investigated [33, 34] or hydrodynamic evaluations concentrated only on g-l flow [35] ignoring possible effects of solid particles. Also the homogeneity of the L-S suspension was not investigated.

In 2009, the Corning advanced flow reactor was tested in slurry mode and found to perform the multiphase hydrogenation of a pharmaceutical molecule with productivity and selectivity comparable to the classical batch process [13]. In this report, no details were provided con-

cerning hydrodynamics.

Ufer et al. [128] were the first who not only focused on investigating the performance of this new contact mode by studying an exemplary reaction, but focused on more fundamental questions: They examined qualitatively the dependency of solid placement in the liquid slug as a function of materials and solid charges and performed a qualitative mass transfer study by fluorescence showing the importance of recirculation loops. However their research focused on L-L-S flow in a horizontal oriented single capillary.

These first promising results drew the interest of other research groups towards “slurry Taylor” flow. The articles published after 2011 are listed in Table 1.3. A few more investigations were addressed to hydrodynamic studies and gave first quantitative results on the placement of solid particles under varying operating conditions [73, 95, 109]. Also a first study on L-S mass transfer in horizontal L-L-S “slurry Taylor” flow was published by Scheiff et al. [110]. Numerical studies on liquid-liquid and gas-liquid “slurry flow” [17, 29, 58] are also prove for the interest in this new contactor type.

Up to now, most of the studies focus on the transport of a liquid-solid suspension in an inert liquid continuous phase. The main argument for the preference to place the solid particles in the dispersed phase is the hindered danger of clogging as the particles are not in direct contact with the reactor wall [95, 101] due to the discontinuous phase. Nevertheless, for gas-liquid-solid applications the liquid phase is necessarily the continuous one and as established before (see Section 1.1) especially for G-L-S catalytic suspension reactions this new contact mode possibly represents an interesting new feature.

Therefore this study is dedicated to the investigation of gas-liquid-solid “slurry Taylor” flow in horizontal and vertical millimetric pipes with circular cross section. Due to the nature of this contact mode the parameters which can be studied are easily expandable (4 phases involved, parameters linked to geometry and operating conditions). The choice was therefore made to concentrate on two phase velocity, solid loading, fluid media and flow direction. Hydrodynamics, in particular the placement and motion of solid particles in the liquid slugs, were investigated, relevant forces analysed and a flow pattern map established. For potential scale-up it is also necessary to estimate external mass transfer properties more in detail and we concentrate on liquid-solid mass transfer. For high qualitative results several technical challenges had to be overcome first, which are:

- avoiding settling of the particles during flow through the reactor
- designing an adequate and efficient suspension delivery unit
- avoiding pressure fluctuations in the reactor in order to control the flow homogeneity, the behaviour of the gas phase and the global residence time in the reactor.

Ref.	year	d_T [mm]	d_p [μm]	w_S [g L^{-1}]	T [°C]	p [bar]	Exp./ Sim.	Phases	Flow direction	Objective of study
[34]	2005	3.86	18.3	4.05	70	6,12	Exp	G-L-S	s,v \downarrow	hydrogenation of isophorone, demonstration of reactor concept and performance, supposedly no Taylor flow at operating conditions
[33]	2005	3.5- 6.78	45	13.3	50-100	5-17	Exp.	G-L-S	s,v \downarrow	hydrogenation of recorcinol, demonstration of reactor concept and performance, optimisation of operating conditions, no Taylor flow visualisation for operating conditions
[33]	2005						Exp	G-L-S	p,v \downarrow	hydrogenation of 2-butyne-1,4-diol, slurry g-l-s flow in a monolith (62 channels per square inch), no Taylor flow visualisation
[35]	2007	1-2	20-45	3.3-53	100	7-10	Exp	G-L-S	p,v \downarrow	hydrogenation of recorcinol, scale up effect, integrated Chart heat exchange reactor, effect of channel design and slurry G-L-S flow over a monolith (62 channels per square inch), Taylor flow
[13]	2009	-	30	0.4 wt%	30-140	11-17	Exp	G-L-S	p,h	three phase catalytic hydrogenation, performed in slurry mode in Corning Advanced-Flow™ reactor, no Taylor flow
[128]	2011	1.6	20-50	0.5-10	amb., 70	amb	Exp	L-L-S	s,h	Taylor flow conditions, particle placement in cont. and disc. phase, visualisation of L-S mass transfer with fluorescent particles, catalytic transfer hydrogenation of m-nitrotoluene

Table 1.2: Literature survey for articles published before 2011 on micro metric particles in millimetric tubes. Flow direction indicates if the study was conducted in a single capillary (s) or in parallel channels (p) and in horizontal (h) or vertical flow (v).

Ref.	year	d_T [mm]	d_p [μm]	w_s [g L^{-1}]	T [°C]	p [bar]	Exp./ Sim.	Phases	Flow direc- tion	Objective of study
[58]	2012	3.02	20	-	25	1-10	Sim	G-L-L-S	p, v \uparrow	Taylor flow conditions, monolith (50 channels per square inch), demonstration of concept, catalytic CO ₂ hydration with online removal of bicarbonate by suspended ion-exchange beads
[95]	2012	2.2	10	0-5	20-150	amb	Exp	L-L-S	s, h	Taylor flow conditions, particle placement in discontinuous phase, acylation of anisole
[29]	2013	0.1	3	-	20	amb	Sim	L-L-S	s, h	Taylor flow conditions, motion of single particle in disperse phase
[16]	2013	1.038	1-10	1-10	20	amb	Exp	G-L-S	s, h	Taylor flow conditions, influence of fine solid particles on G-L mass transfer
[17]	2013	0.5		-	20	amb	Sim	G-L-S	s, h	Taylor flow conditions, motion of particle in disperse phase
[109]	2014									literature review of "slurry Taylor" flow, analysis of relevant forces, particle handling in millimetric tubes
[110]	2014	1.6	50-200	5-10	amb	amb	Exp	L-L-S	s, h	Taylor flow conditions, L-S mass transfer for particles circulating in discontinuous phase

Table 1.3: Literature survey for articles published on "slurry Taylor" flow after 2011. Flow direction indicates if the study was conducted in a single capillary (s) or in parallel channels (p) and in horizontal (h) or vertical (v) flow.

1.3 OUTLINE OF THE THESIS

Every chapter (with the exception of chapter one and six) of this thesis is written in form of an article. Therefore some repetitions could not be avoided but in this way every chapter can be read independently from one another.

Chapter 1 introduces the concept of “slurry Taylor” flow and details the potential interest of this new contact mode.

The concept of this new contact mode will be described more in detail in **chapter 2**. Stable and repeatable L-S suspension supply is essential for further investigations. Therefore the design of the L-S suspension supplier will be presented in this chapter and validated with non-reactive and reactive experiments with silica and alumina based catalysts. To demonstrate the performance of this new contact mode the catalytic hydrogenation reaction of 3-methyl-1-pentyn-3-ol is used: results in “slurry Taylor” mode will be confronted with the results obtained in a conventional batch reactor and the possibility of on-line non-intrusive reaction monitoring in G-L-S media is evaluated.

In **chapter 3** the hydrodynamics of this innovative contact mode are studied. The focus is on particle dynamics in the liquid slugs and the influence of different parameters for two configurations (horizontal and vertical downflow) is studied.

In **chapter 4** and **chapter 5** the L-S mass transfer properties are investigated. The neutralisation of dilute caustic solution by a strong ion exchanger is used to estimate the L-S mass transfer coefficients. The performance of particles transported in the continuous phase of G-L flow is compared to results obtained for particles transported in the discontinuous phase of L-L flow ¹. In **chapter 5** the influence of gravity on the L-S mass transfer is evaluated. The influence of two phase velocity, solid charge and fluid media is presented for horizontal flow and vertical down flow. The results obtained in this study are used to propound a first correlation for Sherwood numbers in G-L “slurry Taylor” flow.

In **chapter 6** the results obtained in this study are summarized and challenges for future research are briefly depicted.

¹ This chapter is a collaboration work between the technical university Dortmund, Germany and the laboratory for catalytic processes, LGPC-CPE, Lyon, France. The L-L “slurry Taylor” flow experiments were carried out at the Laboratory for Chemical Reaction Engineering and belong to the doctoral research study of Frederik Scheiff. Contact: Prof. David W. Agar ✉ david.agar@bci.tu-dortmund.de.

1.4 SYMBOLS AND ABBREVIATIONS

Symbols

a_s	$\text{m}_{\text{LS}}^2/\text{m}_{\text{R}}^3$	l-s surface area per reactor volume
\bar{d}_p	m	mean particle diameter
d_T	m	tubing diameter
ϵ_s	$\text{m}_{\text{S}}^3/\text{m}_{\text{R}}^3$	solid hold up
h_{int}	$\text{W}/\text{m}^2\text{K}$	heat transfer coefficient
k_{La}	s^{-1}	G/L mass transfer coefficient
T	$^{\circ}\text{C}$	temperature
p	bar	pressure
w_s	g l^{-1}	solid charge

Abbreviations

exp	experiment
sim	simulation
G	gas phase
L	liquid phase
p	parallel channels
P	particle
R	reactor
s	single channel
S	solid phase

Part II

CONCEPT OF "SLURRY TAYLOR" FLOW AND MOTIVATION

GAS-LIQUID-SOLID “SLURRY TAYLOR”: FLOW: EXPERIMENTAL EVALUATION THROUGH THE CATALYTIC HYDROGENATION OF 3-METHYL-1-PENTYN-3-OL

This chapter has been published as A.-K. Liedtke, F. Bornette, R. Philippe, C. de Bellefon, Gas-liquid-solid “slurry Taylor” flow: Experimental evaluation through the catalytic hydrogenation of 3-methyl-1-pentyn-3-ol, Chem. Eng. J. 227 (2013) 174-181.

The aim of this chapter is to present the concept of the gas-liquid-solid “slurry Taylor” reactor and to evaluate its performance performing the fast catalytic hydrogenation of 3-methyl-1-pentyn-3-ol on a palladium catalyst supported on silica. Therefore the results of the “slurry Taylor” flow are compared to a classical lab-scale semi-batch reactor. Also the system to continuously feed the homogeneous liquid-solid suspension without flow fluctuation is described and first results for the validation of a stable and controlled gas-liquid-solid “slurry Taylor” flow delivery are given. Furthermore the suitability of this G-L-S contactor for data acquisition tasks as an attractive and non-intrusive technique to monitor the reaction progress by image analysis is highlighted.

2.1	Introduction	14
2.2	Experimental set-up	15
2.2.1	“Slurry Taylor” flow set-up	15
2.2.2	Stirred tank reactor set-up	16
2.2.3	G-L-S model reaction	16
2.2.4	Validation of the slurry contact mode	17
2.2.5	Hydrogenation in Taylor flow reactor	17
2.2.6	Hydrogenation in stirred tank reactor	17
2.2.7	Gas chromatography analysis	18
2.2.8	Reaction course monitoring by image analysis	18
2.3	Results and discussion	19
2.3.1	Validation of the experimental set-up	19
2.3.2	Hydrogenation in the stirred tank reactor	20
2.3.3	Hydrogenation in the “slurry Taylor” flow reactor	21
2.3.4	Reaction course monitoring by visualization	22
2.3.5	Comparison of the “slurry Taylor” and batch reactors	23
2.4	Conclusion	24
2.5	Symbols and subscripts	25

2.1 INTRODUCTION

In multiphase micro-reaction technology, when an heterogeneous catalyst is needed, the most common way to introduce it in the reactor is by a coating procedure on the reactor walls [66, 87]. This is well suited for fast reactions and for good wall heat transfer but specific coating procedures need to be developed for each catalyst type in order to provide a good adherence whilst maintaining catalyst activity. Moreover, the obtained reactor system is not flexible because the catalyst removal in case of deactivation or change in active phase appears very difficult, even impossible without damage to the reactor walls. An alternative approach being developed is the use of small packed beds. These micro-fixed beds are more flexible concerning the catalyst replacement and present interesting performances in mass transfer [82] but with a high linear pressure drop due to the small particles involved. Another concern is the complex (and still not understood) hydrodynamics in the case of two-phase flow at this scale (wettability problems, wall channelling, local dewetting, etc.) [84]. These constraints seriously reduce the simplicity and the applicability of such contactors.

A new approach consists in joining beneficial properties of micro-or milli-channels under Taylor flow conditions and slurry reactors. The internal circulations occurring in the liquid slugs of a G/L segmented flow [63, 72] can be used to keep catalyst particles in motion and transport them in a stable three-phase flow. In this contact mode, catalysts can be easily removed from the reactor, simple and available commercial catalysts can be employed and good transfer performances can be expected due to the large interfacial areas available for heat and mass transfer. Additionally, the G-L mass transport may be enhanced by the vortices in the slugs [63]. Several G-L-S microreactor concepts different from the wallcoated Taylor flow have been already reported for screening and kinetics investigations [1, 25] but they all involve a coated catalyst. This "new" G-L-S contact mode may be a very promising way to provide a flexible and efficient tool for these purposes by allowing the use of simple and available catalysts. As far as data acquisition is concerned, an additional benefit of this new contacting principle is its usability for non-intrusive online data acquisition by visualization. Indeed, visualising the reaction progress by monitoring the gas bubble shrinkage has been successfully applied for gas-liquid-reactions or mass transfer studies [44, 74, 121] but not yet for gas-liquid-solid reactions.

The concept of a three phase slurry micro-reactor was first mentioned in the literature in 2005 [33, 34]. Sedimentation of the solid and plugging problems were reported thus lowering the robustness of the set-up. Also, no peculiar attention was given to the stability of the flow and to the homogeneity of the L-S suspension which are key to the correct control of the set-up. In 2007, a Chart Heat-Exchange reactor with a single vertical channel was reported for the slurry hydrogenation of resorcinol with a variety of solid catalysts demonstrating increased reaction rates and the applicability of the concept [35]. However, the reported hydrodynamics data were scarce and mainly dealing with gas-liquid MRI visualization. Furthermore, only cocurrent down flow mode was investigated.

In 2009, the Corning advance flow reactor was tested and found to perform the multiphase hydrogenation of a pharmaceutical molecule in slurry mode with an improved productivity and a selectivity comparable to the classical batch process [13]. In this report, no details were provided concerning the hydrodynamics.

Recently, the use of liquid-liquid-solid flow for catalysis was reported [128]. The dependency of solid placement in the liquid slug as a function of materials and solid charges was examined and a mass transfer study by fluorescence was undertaken showing the importance of recirculation loops. These first promising and preliminary works on the subject draw our interest to investigate this new contact mode and to develop it for the G-L-S media. Indeed, this is a widely used media for example in hydrogenations and oxidations but still poorly inves-

tigated and controlled under “slurry Taylor” flow conditions. Furthermore, several technical challenges to be overcome are:

- avoiding settling of the particles during flow through the reactor,
- designing an adequate and efficient suspension delivery unit,
- avoiding pressure fluctuations in the reactor in order to control the flow homogeneity, the behaviour of the gas phase and the global residence time in the reactor.

2.2 EXPERIMENTAL SET-UP

2.2.1 “Slurry Taylor” flow set-up

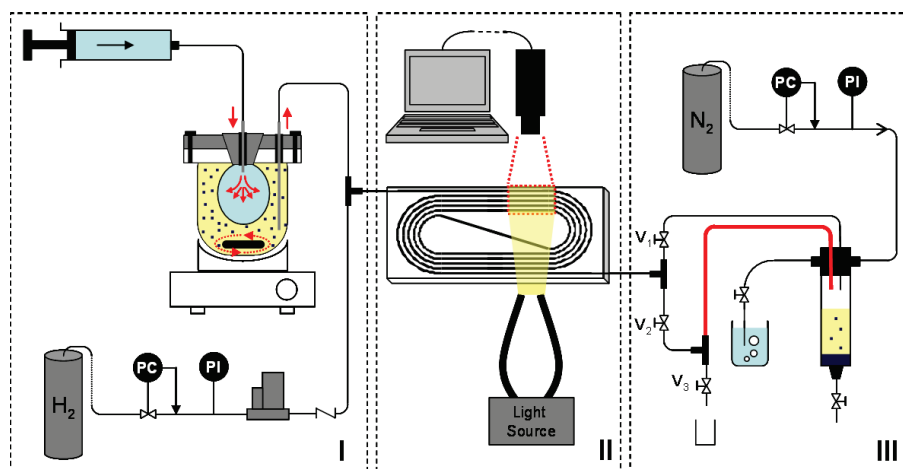


Figure 2.1: Experimental set-up used for “slurry Taylor” experiments: (I) injection zone for gas and liquid-solid suspension; (II) reaction and visualization zone; (III) backpressure regulation and sample collection zone (sample volume appears in red).

Figure 2.1 gives a global view of the experimental set-up employed to perform “slurry Taylor” flow experiments. It can be roughly divided into three main parts: A fluid and suspension supply section (I), a reaction and visualization section (II) and a back-pressure regulation, sampling and waste collection section (III).

The liquid-solid supply unit consists of a glass vessel with a magnetic stirrer covered by a stainless steel plate. The catalyst, the substrate and the solvent are introduced directly into the vessel. The stainless steel cover is fitted with a polypropylene bag of our own construction with a capacity of 200 mL. A syringe pump (Harvard apparatus PHD 4400) injects water into the bag to expand it and push the L-S suspension into the T-junction at the precise flow-rate set at the syringe pump and without any fluctuation. In the T-junction (Upchurch Scientific PEEK tee for a 3.16 mm o.d. tubing), the suspension meets the gas phase fed by a mass-flow controller (Bronkhorst “el flow” able to deliver up to 50 N mL/min of H₂) forming the Taylor flow. With this set-up, typical run durations of more than 1 h can be performed for a water flow rate of 3 mL/min without any problem of fluctuation or clogging. The reactors used in this study consist in a simple PFA capillary tubing (1.65 mm i.d. and 3.16 mm o.d.) with a total length up to 14 m. A special reactor arrangement in a coiled channel has been chosen and designed as a compromise between compactness and high curvature radii for the bends. The coiled shape channel was milled into an aluminium plate (10 mm - 400 mm - 200 mm) allowing the insertion of different tube lengths into the channel (Figure 2.2).

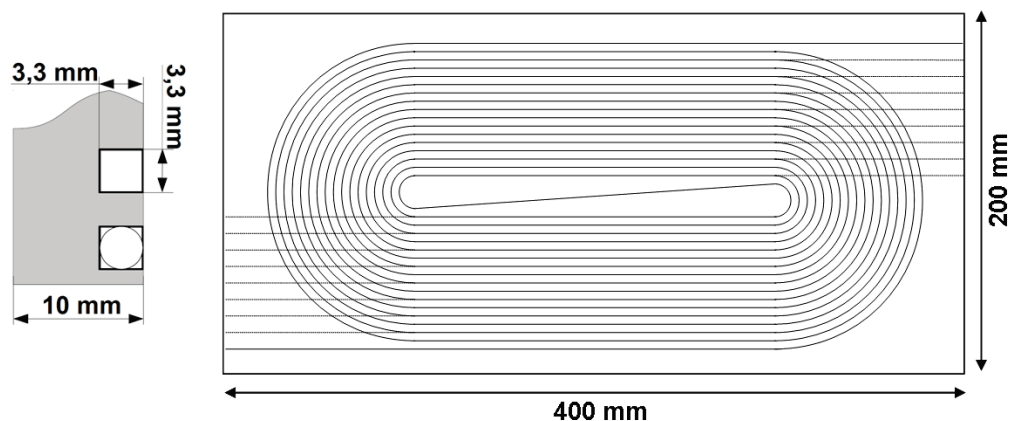


Figure 2.2: Detailed reactor arrangement in the aluminium plate. By choosing specific entries and exits, the total coiled tube length for reaction can be changed.

If necessary, efficient heating via a silicon 270W regulated heating foil (Chromalox CISA 240) attached to the back of the plate is possible. The entire length of the tube is visible and due to the compactness of this design a small area of the plate will give information about the Taylor flow having the lowest, highest and several intermediate residence times. A high speed camera (Optronis CR600x2), a macro-lens (Computar MLH-10X) and a 150W cold illumination system (Dolan Jenner FiberLite PL800) are used to capture the Taylor flow along several channels at the same time. This arrangement has been used for the preliminary hydrodynamic visualizations and to determine the conversion from the bubble shrinkage. In all the experiments described in this article, the plate was arranged vertically as shown in Fig. 2. Downstream of the reaction zone, the G-L-S flow goes into the pressurized waste tank where a classical back-pressure regulator system is used to maintain the pressure in the whole reactor. Sample collection for analysis is ensured by the inversion of the three valves V_1 , V_2 , V_3 allowing the flow to go into the upper tube and to recover the sample volume (in red, Figure 2.1).

2.2.2 Stirred tank reactor set-up

The stirred tank reactor is a 300 mL Parr autoclave equipped with a gas inducing turbine, baffles and operated in a semi batch mode. Hydrogen was constantly fed via a pressure regulator and supplied by a calibrated reserve. The pressure and temperature monitoring in this reserve provides the hydrogen consumption rate and thus the apparent and instantaneous activity of the catalyst.

2.2.3 G-L-S model reaction

The hydrogenation of 3-methyl-1-pentyn-3-ol (reactive scheme shown in Figure 2.3) was chosen as a G-L-S model reaction because of the high reaction rates reported in the literature and the availability of an intrinsic kinetic model [92]. For both stirred tank and "slurry Taylor" experiments the same reagents were used: A 5 wt.% palladium catalyst supported on a silicon oxide powder support with a mean particle diameter of $40 \mu\text{m}$ (Strem Chemicals Inc.) was chosen. Absolute ethanol (Carlo Erba), 3-methylpentyn-3-ol (Merck, >98%) and quinoline (Aldrich, >98%) were used respectively as solvent, substrate and reaction modifier in order to avoid the second hydrogenation leading to the undesired 3-methyl-pentan-3-ol product. For more details see the work of Nijhuis et al. [92].

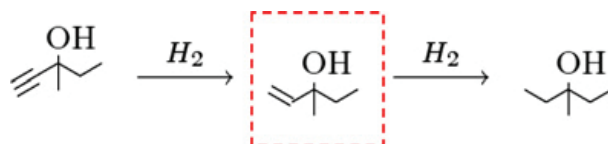


Figure 2.3: Reaction scheme for the hydrogenation of 3-methyl-1-pentyn-3-ol. The desired product is the intermediate 3-methyl-1-penten-3-ol.

2.2.4 Validation of the slurry contact mode

Firstly, qualitative experiments of the set-up were carried out with a non-reactive flow of nitrogen/water/alumina in order to check for issues such as plugging, sedimentation, inhomogeneous suspension supply and unstable Taylor flow. Therefore rather challenging operating conditions in terms of solid charge (6.0 g/L) and particle mean diameter (100 μm) were used. For this suspension, the agitation speed inside the liquid solid supply system was 500 rpm and the syringe pump liquid flow rate was varied from 1.0 to 5.0 mL/min. To check the good homogeneity and the stability of the suspension over time, several quantitative measurements were also made. The following protocol was followed: successive samples were collected at the reactor exit over 20 min, the obtained suspensions were filtered and dried overnight at 120 °C to separate the solid fraction for weighing with a balance (Mettler AE200) in order to determine the effective transported solid fraction. This quantitative study was performed with the Pd/SiO₂ catalyst (Strem chemicals, 5.0 wt.% Pd, mean diameter of 40 μm) at different stirring speeds from 140 rpm to 700 rpm for a solid charge of 5.0 g/L in absolute ethanol and for a constant flow rate of 2.0 mL/min.

2.2.5 Hydrogenation in Taylor flow reactor

In a typical experiment, the desired content of solvent, catalyst, quinoleine, n-pentanol (internal standard) and substrate are placed in the suspension feeding system before sealing and connexion with the reactor. Magnetic stirring is started and a stabilization period of approximately 5 min is allowed. Then the syringe pump is launched to feed the L-S suspension at the desired flow-rate followed by the setting of the gas flow-rate. Finally the back-pressure is set to obtain the desired pressure and residence time in the reactor. During the reaction, video capture of the Taylor flow is recorded and samples are collected by switching the valves V_1 , V_2 , V_3 successively (see Figure 2.1). The reaction is quenched by exposure to air and the liquid is sampled for GC analysis. The operating conditions tested in this reactor are listed in Table 2.1.

2.2.6 Hydrogenation in stirred tank reactor

In a classical experiment, the appropriate charge of solvent, quinoleine, n-pentanol (internal standard) and catalyst are introduced in the reactor before sealing. Then three purges with N_2 are performed at 4 bar followed by three purges with H_2 at the working pressure. After this step, the reactor is connected to the calibrated and regulated H_2 reserve and the stirring is started. After 5 min of stabilization, the substrate is injected quickly through a septum in the reactor by a syringe defining the reference time for the start of the reaction. Throughout the reaction, pressure and temperature in the H_2 reserve are monitored and liquid samples are collected for GC analysis. The operating conditions used for the hydrogenation in the batch reactor are listed in Table 2.2 and include the conditions for the comparison with the “slurry Taylor” reactor. Temperature, substrate concentration and catalyst charge are varied in order

Table 2.1: Operating conditions in the "slurry Taylor" reactor.

L_{tube} (m)	8.8 and 14.4
$d_{tube,int}$ (mm)	1.65
P_{in} (bar)	1.3
T (°C)	20
$C_{substrate}$ (mol/L)	0.11
$C_{quinoline}$ (mol/L)	0.22
Feeding system stirring speed (rpm)	360
Q_L (mL/min)	3
Q_G (N mL/min)	14-30
$u_{tot,0}$ (cm/s)	8.4-17.9
$F_{H_2}/F_{substrate}$ (mol/mol)	1.45-3.71
w_{cat} (g/L)	3.5
Experimental specific pressure drop (kPa/m)	1.1-2.1

Table 2.2: Operating conditions in the stirred tank batch reactor.

V_L (L)	0.18
V_{batch} (L)	0.3
w_{cat} (g/L)	0.76-3.5
Agitation (rpm)	1450
P (bar)	1.2 and 1.5
T (°C)	20-60
$C_{substrate}$ (mol/L)	0.11 and 0.3
$C_{quinoline}$ (mol/L)	0.22

to check the working regime in the batch reactor: reaction or mass transfer limited rate (see results and discussion section for more details).

2.2.7 Gas chromatography analysis

For GC measurements, a Gas Chromatograph (Agilent Technologies 6890N) with an automatic injection system (injector 7683 series) with a HP5 column (15 m × 0.1 mm × 0.1 μm) was used. Mass balances are established with the internal standard method by using the n-pentanol (Aldrich, >99%) as a reference.

2.2.8 Reaction course monitoring by image analysis

A specific Matlab_TM program has been developed to analyze the video captures recorded during the reactive experiments. Each image of the video capture is analyzed (segmentation, thresholding, interface detection) in order to detect the gas bubble edges and to measure their length and distance from each other. Knowing the acquisition rate of the video capture, bubble velocities can be easily estimated by following each bubble and measuring its displacement.

In order to obtain representative lengths and velocities for each position of the reactor plate, a sufficient number of bubbles is necessary. Therefore, the analysis is made line by line of the viewed area for the bubbles flowing through each of them. Mean, upper and lower lengths and velocities can then be associated to the mean abscissa of the corresponding plate line.

2.3 RESULTS AND DISCUSSION

2.3.1 Validation of the experimental set-up

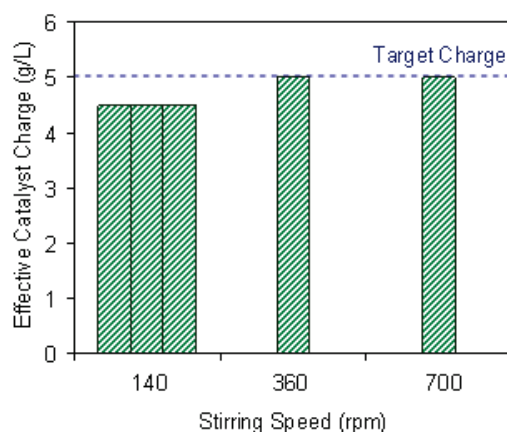


Figure 2.4: Measured catalyst charge for different stirring speeds. Sampling time was 20 min ($w_{cat} = 5.0$ g/L, $Q_L = 2$ mL/min, solvent: ethanol, solid: Pd/SiO₂, $d_{50} = 40$ μ m).

To validate the good delivery of the L-S suspension, the stirring speed in the glass vessel has been changed from 140 to 700 rpm for an ethanol suspension containing 5.0 g/L of 40 μ m Pd/SiO₂ catalyst particles. The solid fraction has been collected and weighed in order to quantify the good delivery of the solid-liquid suspension as explained in the experimental section. The system is able to deliver the target charge of catalyst contained in the stirred tank and to transport it along the reactor for a stirring speed superior to 360 rpm (Figure 2.4). The lower speed tested (140 rpm) shows a repeatable over time and non-negligible difference between the solid charge effectively transported and the target. These results demonstrate the operability and the efficiency of the L-S supply system for the following reactive experiments. Qualitatively, the three-phase Taylor flow is stable, homogeneous and of regular appearance. No plugging of the tube or of any connector was detected. Figure 2.5 shows a typical capture of the “slurry Taylor” flow realized with alumina particles of 100 μ m.

This large particle diameter was used to test a challenging condition and to be able to visualize the suspension with the rather low resolution optical set-up used. For low liquid velocities some solid particles in the suspension feeding tube would sink down back into the supply vessel instead of proceeding to the reacting tube. Therefore a minimal liquid velocity of 1 mL/min was defined. Under this condition stable and uniform Taylor flow was attained over the entire tube length. Visually the solid charge in each liquid slug was homogeneous and mainly circulating in the lower part of the liquid slug. It would sediment for a short period of time until the next gas bubble reaches it pushing the particles back into the vortices that exist in the liquid slug. The placement of the solid in the liquid slug is consistent with previous results which also report partial occupation of the slug height for lower solid charges up to 8 g/L [128]. For more details on hydrodynamics, especially in particular the detection of

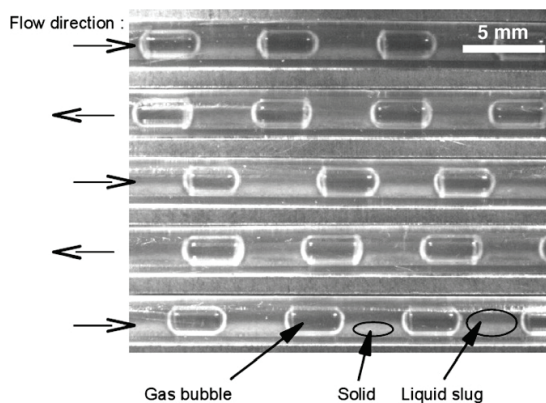


Figure 2.5: Typical G/L/S "slurry Taylor" flow obtained for a N_2 /water system with 6.0 g/L of 100 μm Al_2O_3 particles in suspension (flow velocity of 3.6 cm/s).

different hydrodynamic regimes under broader experimental conditions the reader is referred to chapter 3.

2.3.2 Hydrogenation in the stirred tank reactor

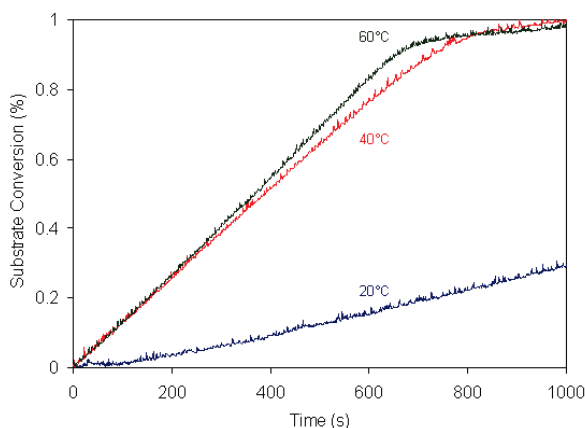


Figure 2.6: Evolution of the substrate conversion in the stirred tank reactor for different operating temperatures (for all three experiments, catalyst charge = 0.75 g/L, stirring speed = 1450 rpm, $P = 1.5$ bar, $C_{substrate} = 0.3$ mol/L and $C_{quinoline} = 0.22$ mol/L).

Figure 2.6 and Figure 2.7 show the results obtained in the stirred tank reactor by varying the temperature and the catalyst charge. The substrate conversions plotted here were calculated according to the temperature and pressure evolution in the gas reserve and to the experimental selectivity towards the desired 3-methyl-1-penten-3-ol. Because of the presence of quinoline, the selectivity is always very close to 1 and the H_2 pressure variation in the reserve can be directly linked to the conversion of 3-methyl-1-pentyn-3-ol with a stoichiometry of 1:1. By varying the temperature (Figure 2.6) an acceleration of the apparent initial reaction rate was observed between 20 °C and 40 °C. No further initial reaction rate acceleration was detected between 40 °C and 60 °C. This probably indicates the appearance of a significant mass transfer limitation for the experiment at 60 °C. Assuming that the experiment carried out at 40 °C is not mass-transfer controlled, an activation energy of 45 kJ/mol is determined. This value is quite close to the 52 kJ/mol reported in the literature for this reaction [92] indicating that the experiments carried out in this work at 20 °C in the stirred tank reactor are not or only slightly mass transfer limited. This conclusion is also supported by the experiments with

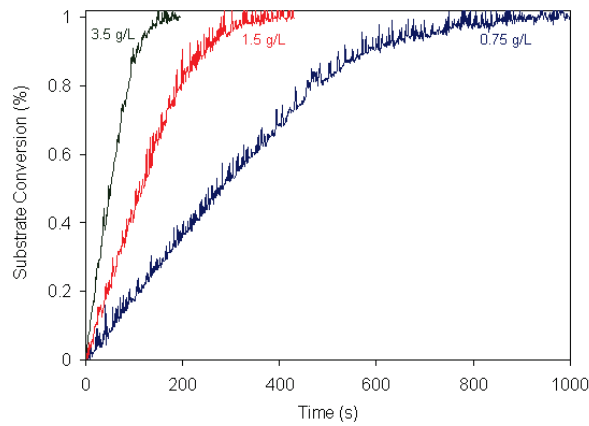


Figure 2.7: Evolution of the substrate conversion for different solid catalyst charges in the stirred tank reactor ($C_{\text{substrate}} = 0.11 \text{ mol/L}$, stirring speed = 1450 rpm, $T = 20^\circ\text{C}$, $P = 1.5 \text{ bar}$ and $C_{\text{quinoleine}} = 0.22 \text{ mol/L}$).

different catalyst charges (Figure 2.7). A constant initial reaction rate of $5 \times 10^{-3} \text{ mol/s/g}_{Pd}$ can be determined for the three catalyst charges tested at a substrate concentration of 0.11 mol/L confirming that a reaction limited regime can be declared in this reactor at 20°C for the range of operating conditions tested.

2.3.3 Hydrogenation in the “slurry Taylor” flow reactor

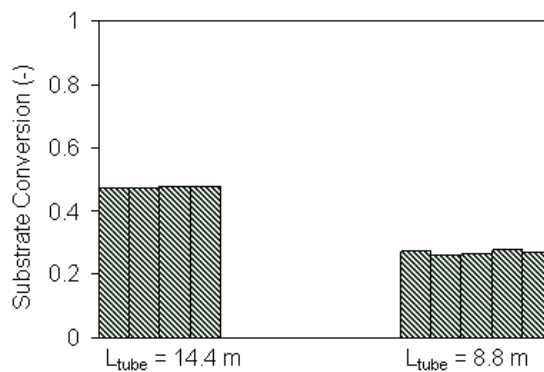
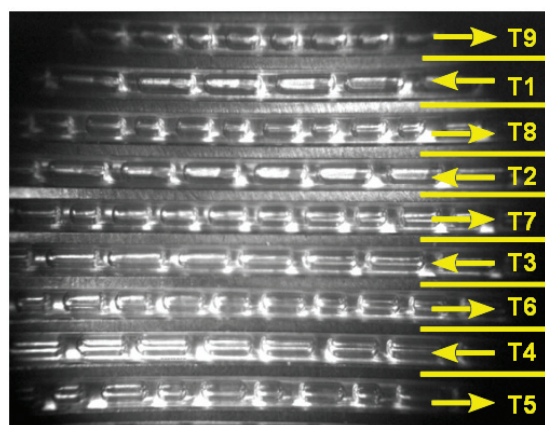


Figure 2.8: Conversion obtained by GC analysis for two reactor lengths in the “slurry Taylor” reactor ($Q_L = 3 \text{ mL/min}$, $Q_{G,0} = 29.4 \text{ Nm L/min}$, $w_{\text{cat}} = 1.5 \text{ g/L}$, $d_{\text{int,tube}} = 1.65 \text{ mm}$, $T = 20^\circ\text{C}$, $P_{\text{in}} = 1.3 \text{ bar}$).

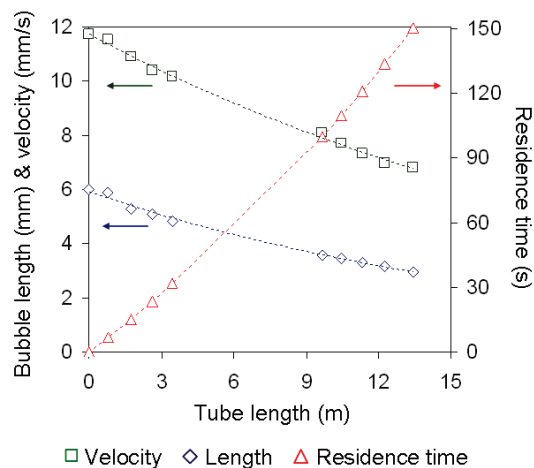
To validate the experimental set-up under reactive conditions, the test reaction was performed under two different operating conditions by varying the tube length (8.8 m and 14.4 m). The final conversion was determined via GC analysis taking several samples over time at the exit of the reactor (Figure 2.8). As for the cold experiments, good repeatability is also found in the case of experiments with reaction. In fact, under the different reaction conditions tested, a standard deviation around 1.4% is obtained. This repeatability indicates that the target catalyst charge in the liquid slugs and the residence time in the reactor remain unchanged over time leading to a good control of the set-up under steady state. It is important to notice that the conditions tested here were always performed with an excess of hydrogen in order to keep a sufficient gas hold up and to maintain a Taylor flow. Some preliminary experiments

with a stoichiometric or a default flow of hydrogen (not shown here) lead to a substantial decrease in repeatability. This is due to the large bubble shrinkage that occurs, leading to coalescence of non-Taylor gas bubbles travelling at different velocities and in the worst case to total consumption of them and thus to solid particle deposition at the bottom of the tube wall. Under these conditions, even if a homogeneous suspension supply and a stable Taylor flow formation are ensured at the inlet, the residence time and the solid hold-up along the reactor become unsteady with time and uncontrolled. This is a limit of operability of this system.

2.3.4 Reaction course monitoring by visualization



(a) Photograph of the "slurry Taylor" flow profile obtained under reactive conditions (see Table 3)



(b) corresponding experimental profiles of bubble lengths, velocities and residence times

Figure 2.9: Results obtained for "slurry Taylor" flow

The reaction progress can be easily monitored over time by simple recording of images of the gas bubbles in several regions of the reaction tube with a high speed camera. Bubble lengths and velocities can be measured simultaneously at different locations due to the specific reactor arrangement. A typical example is given in Figure 2.9. The gas bubble length decreases steadily from line T1 to line T9 (Figure 2.9a) and this evolution is directly linked to the amount of hydrogen consumed over the reactor length. To calculate precisely and easily the substrate conversion through the H_2 consumption by using the local bubble length several reasonable assumptions are made:

- The gas phase obeys the ideal gas law.
- The bubble shrinkage does not alter the bubble shape which is modelled as a cylindrical body with two hemispherical caps having a diameter nearly equal to the tube diameter.
- The pressure drop profile is assumed to be linear along the reactor.
- The ethanol vapour pressure and the inlet hydrogen concentration are negligible for the specific conditions tested here.

In order to precisely attribute a residence time to a location in the tube, the experimental velocity profile needs to be integrated along the channel length. To determine an accurate conversion level, the pressure drop, leading to a small expansion of the gas bubbles, has to be taken into account along the whole reactor length. Based on the measured pressure drop over

the total reactor length, a theoretical and reference bubble length profile without conversion is determined. The difference between their actual length under reaction and their expected length without reaction yields the consumption of hydrogen and, consequently, the hydrogen conversion which enables the calculation of the substrate conversion. Bubble lengths, bubble velocities and corresponding residence times determined by this method are plotted in Figure 2.9b as an example. The first exploitable gas bubbles from the line T1 correspond to a short residence time (here 6 s). It implies that the initial bubble length and velocity are extrapolated according to the encountered profiles and the initial theoretical gas velocity. Figure 2.10 presents a validation of the visual reaction progress monitoring as the conversions obtained by this method are close to the final GC analysis. Nonetheless, it is important to notice that this method is only efficient in quite a restrained range of operating conditions. For example, an excess of hydrogen is needed but a too large excess of hydrogen leads to indistinguishable differences even for a large degree of substrate conversion.

2.3.5 Comparison of the “slurry Taylor” and batch reactors

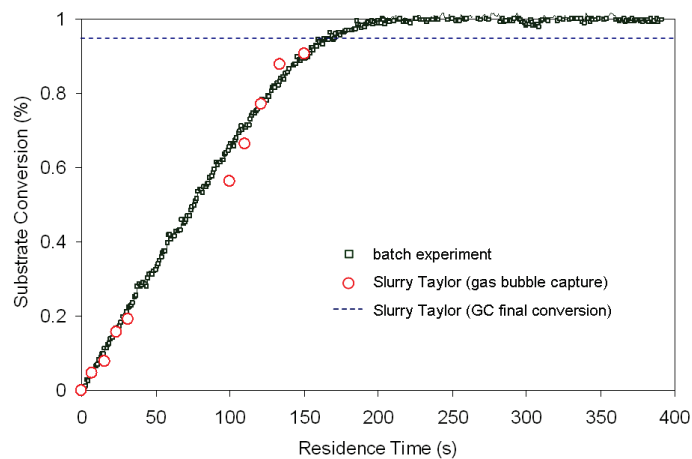


Figure 2.10: Comparison between substrate conversion profiles obtained in the stirred tank reactor and in the “slurry Taylor” contactor (by bubble shrinkage visualization and GC).

To compare the “slurry Taylor” reactor to the batch reactor, a similar experiment was performed in these two different reactors. The experimental conditions tested can be found in Table 3. This comparison is reliable because of the analogy between the residence time in an ideal plug flow reactor and the reaction time in a well-stirred batch reactor. Figure 2.10 shows the superposed experimental conversion profiles obtained in the batch reactor (consumption of the H_2 reserve) and in the “slurry Taylor” reactor (movie analysis and final GC measurement). It can be seen that good agreement is obtained in these two different reactors. The preliminary experiments done in the batch reactor had a mass transport coefficient, $k_L a$, in the range $1 - 2s^{-1}$ [88] and this allows us to say that this Taylor flow experiment is occurring under a reaction limited regime and that a good overall mass transfer is reached in our slurry set-up for this quite fast reaction. For more insights into liquid-solid mass transfer performances of this contactor the reader is referred to chapter 4 where first results for the l-s mass transfer constant are presented.

Table 2.3: Operating conditions for the comparison between the batch and the "slurry Taylor" reactors.

Batch reactor		"Taylor reactor"	
V_R (L)	0.30	V_R (L)	0.031
V_L (L)	0.18	Q_L (mL/min)	3
		$Q_{G,0}$ (N mL/min)	13.9
Reactor agitation speed (rpm)	1450	L-S suspension supplier agitation speed (rpm)	360
P (bar)	1.2	P (bar)	1.2
T °C	20	T °C	20
w_{cat} (g/L)	3.5	w_{cat} (g/L)	3.5
$C_{substrate}$ (mol/L)	0.11	$C_{substrate}$ (mol/L)	0.11
$C_{quinoleine}$ (mol/L)	0.22	$C_{quinoleine}$ (mol/L)	0.22
$F_{H_2}/F_{substrate}$ (-)	Not applicable	$F_{H_2}/F_{substrate}$ (-)	1.72
Reaction duration (s)	400	Residence time (s)	150

2.4 CONCLUSION

The G-L-S "slurry Taylor" contact mode was investigated in a simple capillary reactor. A L-S suspension supplier has been designed and was successfully validated with "cold" and reactive experiments with silica and alumina based catalysts in water or ethanol. Mean diameters up to 100 μm and solid loadings up to 6 g/L have been used successfully. A stable G-L-S slurry Taylor flow was generated with an homogeneous and targeted content of particles fluidized in the lower recirculation streamlines existing in the liquid slugs. This contacting mode was used under a pressurized flow of H_2 for the catalytic hydrogenation reaction of 3-methyl-1-pentyn-3-ol. Results were in agreement and as good as those obtained in a conventional batch reactor confirming the good mass transfer performances attainable in this contact mode. Conversion levels for each experiment carried out in excess of hydrogen did not vary for a duration of several hours indicating the efficiency and the regularity of the flow and particularly the stability of the L-S suspension feed throughout time. A method of monitoring reaction progress via bubble shrinkage was also exemplified and validated for the first time in a G-L-S media.

These first promising results encourage further studies considering the influence of particle, wall and liquid properties on hydrodynamics. Also the range of operability and mass transfer performances need to be investigated. Therefore the subsequent work is concentrated on two parts:

- by varying solid charge, flow direction and gas and liquid velocities the occurrence of different hydrodynamic regimes is investigated and the involved forces are characterized
- the solid-liquid mass transfer performance is evaluated by using ion exchange particles.

2.5 SYMBOLS AND SUBSCRIPTS

Symbols		
C	mol/L	molar concentration
d	m	diameter
F	mol/min	molar flow rate
L	m	length
P	bar	pressure
Q	ml/min or Nml/min	volumetric flow rate
rpm	-	rotations per minute
T	°C	temperature
u	cm/s	velocity
w	g/L	mass concentration

Subscripts	
o	initial or inlet conditions
batch	batch reactor
cat	catalyst
G	gas phase
in	inlet
int	internal
L	liquid phase
out	outlet
R	reactor
tot	total
tube	tube reactor

Part III
HYDRODYNAMICS

HYDRODYNAMIC MAPPING OF HORIZONTAL AND VERTICAL GAS-LIQUID-SOLID “SLURRY TAYLOR” FLOW

The objective of this chapter is to evaluate the hydrodynamics of G-L-S “slurry Taylor” flow. The study focuses mainly on the placement and behaviour of solid particles in the liquid slugs. The influence of two phase velocity, solid charge and fluid media is investigated for two configurations: horizontal and vertical flow. A simplified force analysis serves to explain the observed phenomena and to establish a flow pattern map.

A publication based on this work will be submitted.

3.1	Introduction	30
3.2	Experimental set-up	31
3.2.1	Optical device and image analysis	32
3.2.2	Chemicals	33
3.2.3	Experimental procedure for hydrodynamic measurements for horizontal and vertical “slurry Taylor” flow	34
3.3	Results and discussion	35
3.3.1	Stable functioning of suspension supply device	35
3.3.2	Particle placement in liquid slugs	36
3.3.3	Description of particle flow patterns and Matlab™ routine for automatic detection of flow patterns	38
3.3.4	Discussion of relevant mechanisms related to particle entrainment and re-suspension	46
3.3.5	Flow pattern map	60
3.4	Conclusion and perspectives	63
3.5	Symbols	65

3.1 INTRODUCTION

The transportation and usage of freely moving micro-metric particles ($10\ \mu\text{m} < \bar{d}_p < 300\ \mu\text{m}$) in milli-metric tubes ($0.25\ \text{mm} < d_T < 3\ \text{mm}$) has been until recently a rather rare application in multi-phase micro reaction technology [130]. The fear of clogging or bridging [50] and difficult solid handling [49] prevailed and led often to approaches where the immobilization of the solid phase is favoured [30, 55, 62, 66, 69, 82, 84] by using monolith reactors or micro packed beds for example. Nonetheless the utilization of nanoparticles ($d_p < 10\ \mu\text{m}$) in micro reaction technology or millimetric particles in macroscopic applications ($d_T > 3\ \text{cm}$) is manifold.

Laminar, liquid-solid phase flow in small channels is used for biochemical or analytical applications (analysis of cells, blood, DNA, proteins). Here microfluidics offer continuous operation in contrast to conventional solutions (centrifugation, filtration, chromatography) and are advantageous concerning speed and resolution [97]. Microfluidic technologies are used for example for particle concentration or focusing [6, 19, 61, 131, 135], ordering [19], separation [97] and subsequent analysis (i.e.g. counting). For particle focusing for example the particle motion in the channel was studied and lift and drag forces were identified and characterized as crucial for particle placement [18, 19, 89]. Therefore the geometry is often characterized by high aspect ratios and the operating conditions are such that particle Reynolds numbers are close to 1. Another large application is the synthesis of nanoparticles in Taylor flow contact mode. The typical properties of Taylor flow (no axial dispersion) are advantageous for the production of particles with controlled morphology and narrow size distribution. Though in general the synthesis is performed in the liquid droplets of L-L Taylor flow [101, 113, 117, 132] to avoid particle adhesion at the wall, a few examples for the synthesis in the liquid slugs of G-L Taylor flow [104] exist. For the synthesis of nano particles the flow is often oriented horizontally and hydrodynamic studies are conducted to estimate the effect of operating parameters on particle size and distribution [104]. Visualisation of particle motion for example or quantification of involved forces is rare.

In macroscopic flow freely moving solid particles can be found for horizontal [118] or vertical [38] oriented pipes in liquid-solid, gas-solid [102] and gas-liquid-solid [96] flow. Applications are for example the economic transport of slurries. Here relevant phenomena for entrainment of particles are often studied [100] with the focus on estimating the critical velocity for particle entrainment, homogeneous suspension and establishing flow pattern maps [3, 26, 27, 32]. In this context the entrainment of sediment (rivers, dunes) in geology [54] should also be mentioned. Relevant physical phenomena in this macroscopic applications were identified as lift forces and shear stress. Particle diameters range from a few micro meters up to a few milli meters and turbulent flow is usually dominant.

Enache et al. [33, 34] and Buisson et al. [13] were the first to employ micrometric particles in millimetric tubes for gas-liquid-solid catalysed reactions. First studies on segmented flow with slurry contact mode were oriented mainly to the demonstration of this new contactor's applicability and interesting performance (tube oriented horizontally [13, 80, 128] or vertically [35]). Only few investigations were addressed to hydrodynamic studies and gave first qualitative results on the placement of solid particles under varying operating conditions [73, 95] or estimated relevant forces for particle motion [109]. Numerical studies on liquid-liquid and gas-liquid "slurry Taylor" flow [17, 29, 58] are also prove for the interest in this new contactor type. So far more studies focus on the transport of a liquid-solid suspension in an inert liquid continuous phase to avoid potential clogging. Nevertheless, for the performance of

gas-liquid-solid reactions the liquid phase is necessarily the continuous one and studies on particle hydrodynamics for G-L-S “slurry Taylor” flow important to estimate good operating parameters for a certain application.

The aim of this chapter is therefore to study particle motion and flow patterns of G-L-S “slurry Taylor” flow for horizontal and vertical oriented channels. Special attention is paid to evaluate reproducibility and clogging behaviour for high solid loadings (up to 50 g L^{-1}). In consideration of the broad range of possible parameters (4 phases involved: gas, liquid, solid particles, tubing material) the study was limited to one particle type and one channel geometry and material. The influence of solid loading, two phase velocity, fluid media and liquid slug length was investigated.

3.2 EXPERIMENTAL SET-UP

The main focus is to gain quantitative and qualitative insights on the behaviour of micro-metric particles in millimetric sized tubes. Therefore we considered image quality and robust operating conditions crucial and identified the following criteria as essential for our experimental set-up:

- precise image quality, maximum zoom and high frame rate, both constant for all operating conditions, identical lightning, so that the background grey-scale is as constant as possible for all experimental runs
- exact adjusted horizontal and vertical tubing
- easily recognizable particles, as spheric and mono-disperse as possible
- automatic analysis of slug and bubble length, two phase velocity, objective assignment of identified flow regimes to the corresponding operating conditions to avoid subjective judgement.

Figure 3.1 gives a global view of the experimental set-up used for the visualisation experiments. It can roughly be divided in three main parts: A fluid and suspension supply system (I), the observation zone (II) and a section (III) for sampling and waste collection. The fluid and suspension supply section is similar to the one described in an earlier work [80]. An in-house built T connector (PMMA, inner diameter 1.6 mm) is used to generate the slug flow. An additional inlet is used to purge the contactor in between different operating points with the working solvent to increase repeatability. The contactor used in this study consists in a simple $1/8$ " PFA capillary tubing with an internal diameter of 1.65 mm. The tubing was arranged and straightened either horizontally or vertically and the observation of the particle pattern was made 1 m downstream from the Taylor flow generation.

The liquids were supplied with syringe pumps (Harvard apparatus PHD 4400, equipped with a 100 mL stainless steel syringe) and the gas phase was fed by mass flow controllers (Brooks instruments 58505 for flow rates higher 10 N mL min^{-1} and Bronkhorst “el flow” for flow rates lower 12 N mL min^{-1} for nitrogen). The different operating conditions can be found in Table 3.1. The geometry of the T-junction is detailed in Figure 3.2. The suspension phase is introduced perpendicularly to the flow direction. The same T-junction was used for horizontal and vertical flow. That’s why for vertical flow, the flow was horizontal for the first 10 cm and was then conducted vertically (Figure 3.3).

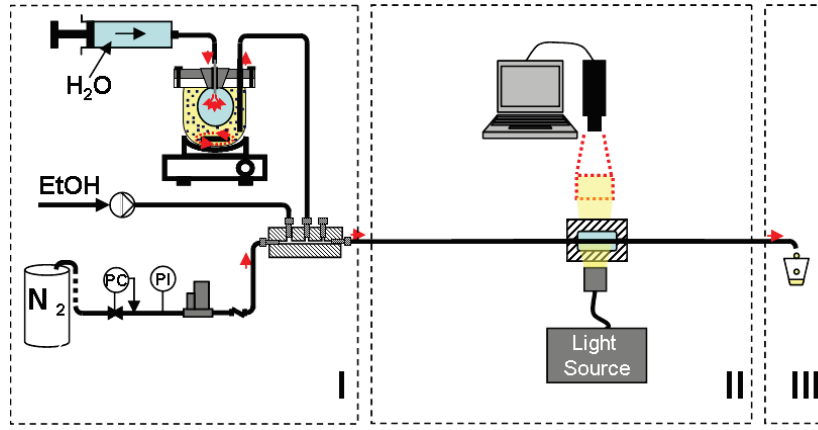


Figure 3.1: Experimental set-up used for G-L "slurry Taylor" flow visualisation experiments: (I) injection zone for gas and liquid-solid suspension; (II) reaction and visualization zone; (III) sample collection zone.

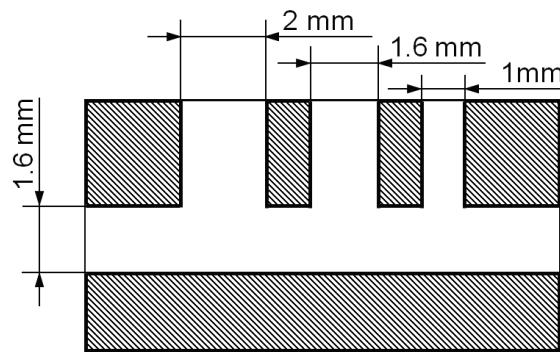


Figure 3.2: Geometry of T-junction used for hydrodynamic visualisation experiments.

3.2.1 Optical device and image analysis

For visualisation of the solid behaviour in the liquid slugs a high speed camera (Optronis CR600x2), a microscopic zoom (Solini 7:1 modular zoom, 0.9x-6.34x) and an illumination system consisting of a mercury lamp (Olympus ILP-2), a fibre optic cable and a focuser (Olympus) are used to capture the particle motion. The light source is placed in the same axis as the camera lens allowing to work with transmitted light. (see Fig. 3.4) A viewing cell, based on the work of [124], was used to eliminate refraction on the tubing and to obtain clear images of the particle flow. The viewing cell was fabricated in-house (acrylic glass) and has the form of a frame with a center cut-out. The connections to the tubing are realized with two Swagelok fittings, it is therefore possible to vary the outer tubing diameter from 1/16 to 1/4 inch. A

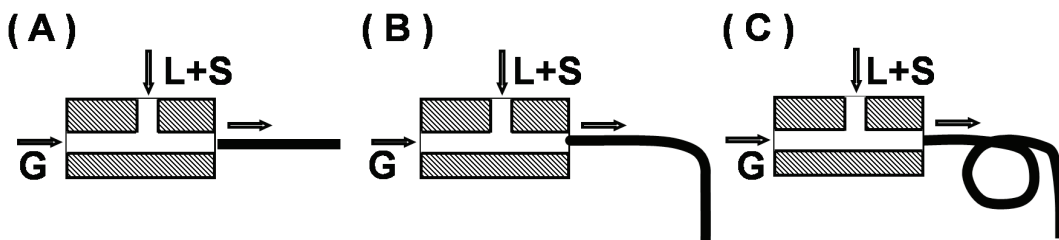


Figure 3.3: Arrangement of injection device for (A) horizontal and (B) vertical visualisation experiments. The suspension phase is injected from above, perpendicular to the gas phase. A few experiments in vertical flow were conducted with the arrangement depicted in (C).

pyrex glass plate is glued on each side of the frame (Plastiform D.A.V.) which allows to easily remove the plate in case the tubing has to be replaced. The viewing cell is filled with distilled water to match the refractive index of the PFA tube. In order to ensure that all air bubbles will leave the cell while filling it with distilled water, first ethanol is used to clean and provide better wettability. After this cleaning process, distilled water is cautiously and slowly inserted in the cell with a plastic syringe to allow bubbles to raise and leave the cell over the Swagelok fitting. To better diffuse the light, tracing paper was fixed at the back of the cell.

A specific Matlab™ program has been developed to analyse the images captured during hydrodynamic experiments. The aim was to extract information on slug and bubble length, bubble velocity and particle flow behaviour. The automatic analysis was necessary due to manifold reasons:

- large amount of data (over 400 films) to exploit
- objective recognition and determination of particle flow pattern
- estimate the deviation of overall flow pattern for succeeding slugs during the same run as well as reproducibility for the same operating conditions
- generate significant and representative visualisation images for particle flow patterns.

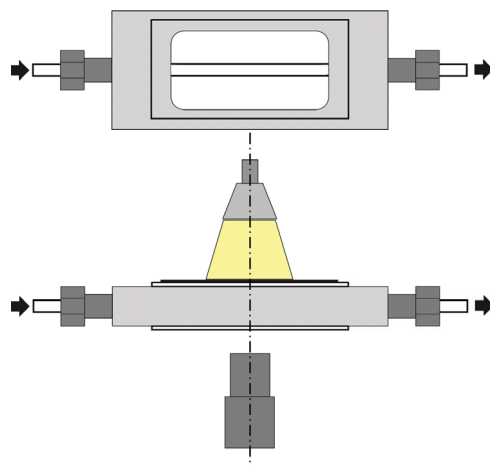


Figure 3.4: Sketch of the in-house built viewing cell (acrylic glass) to adapt the refractive index. The tubing can be fixed via Swagelok connectors and two PYREX glass plates are glued on each side of the frame, covering the cut-out. The device is filled with a liquid matching the refractive index of the tubing material and tracing paper was fixed on one side to ensure better light distribution.

3.2.2 Chemicals

Ethanol (technical grade, 96vol.%, VWR), glycerol (Laurylab) and nitrogen were used as received. We chose to work with silica as a typical catalytic support. Silica particles (dichrom SiliCycle® SiliaSphere™ PC, 40-75 μm 70 \AA spherical Silica Gel) were commercially available in spherical form and a narrow size distribution (Figure 3.5). As the visualisation and easy detection of these particles is crucial to identify and analyse solid flow patterns, the silica particles were treated with nickel nitrate (nickel nitrate (II) hexahydrate, 99%, acros) according to [114]. The nickel oxide gives them a dark, greyish tint which enhances their visibility on the films and results in better image quality.

Table 3.1: Operating conditions applied for hydrodynamic gas-liquid-solid "slurry Taylor" flow experiments.

Liquid phase	EtOH	EtOH/glycerol
Q_L [mL min ⁻¹]	1.5-8	1.5-8
$w_{glycerol}$ [wt.%]	0	34
ρ_L [g/cm ³]	0.791 [41]	0.946[5]
μ_L [Pa s]	0.001153 [41]	0.009096 [5]
σ [N m ⁻¹]	0.02225 [41]	0.0235 [5]
Gas phase	N₂	N₂
Q_G [mL min ⁻¹]	1.5-40	1-40
Solid phase	SiO₂	SiO₂
w_s [g L ⁻¹]	2.5-50	5
\bar{d}_P [μ m]	56.5	56.5
ρ_P [g/cm ³] ¹	1.6	1.6
Tubing material	PFA	PFA
$d_{T,int}$ [mm]	1.65	1.65
Operating conditions		
T [°C]	ambient	ambient
p [bar]	ambient	ambient

3.2.3 Experimental procedure for hydrodynamic measurements for horizontal and vertical "slurry Taylor" flow

For horizontal and vertical flow the experimental procedure was the same. In order to be able to evaluate potential settling and accumulation of solid particles in the liquid film and to analyse solid flow patterns consistently, particular measures for invariant operation conditions were kept: a) before each experiment the tube was thoroughly cleaned for 30 minutes by passing ethanol and b) in between each parameter change, ethanol flow was used to remove potential settled particles. Attention was also paid to the constant and even illumination of the flow. Therefore all videos were recorded under the same recording parameters (frame rate 4000 frames/s, exposure time 1/10000s, 512x256 pixel) which allows the use of the same illumination intensity for all tested parameters. For all experiments the focuser and with it the lamp, was placed at the same distance to the viewing cell. ImageJ was used to verify that the lighting is constant from one day to another and uniform vertically and horizontally on one image. The L-S supply unit was filled with the solvent and the desired amount of silica particles, sealed and connected with the T-junction. The respective flow rates were adjusted and a stabilisation time of 10 minutes was permitted before the first video was taken. In order to evaluate visually potential accumulation of solid particles in the liquid film, a second video was taken after another 10 to 15 min. Videos were taken only from the side, no view from above was realized. At the exit of the contactor two samples for each operating parameter were taken to determine the actual solid charge delivered by the suspension supply unit under flow conditions. Therefore the sample time was recorded and the sample was weighed after being dried in a cabinet drier at 60 °C for at least 24 h.

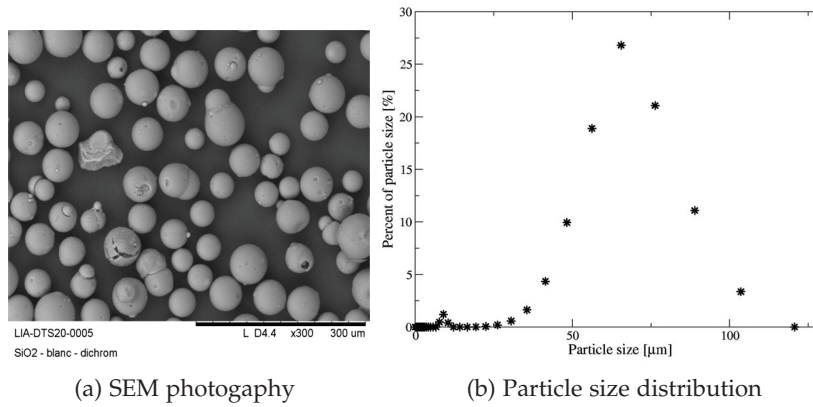


Figure 3.5: SEM photography and particle size distribution of SiO_2 particles used for hydrodynamic visualisation experiments

3.3 RESULTS AND DISCUSSION

3.3.1 Stable functioning of suspension supply device

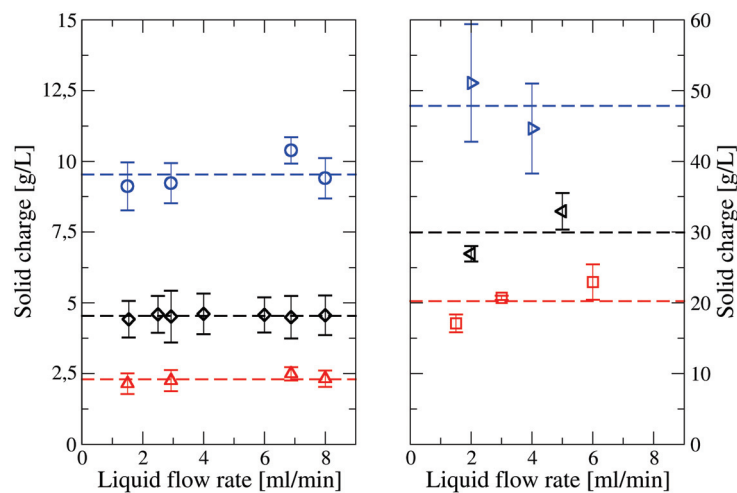


Figure 3.6: Verification of steady functioning of suspension supply unit: the mean solid charge is indicated by the dashed line and was obtained from all experiments for one target charge without consideration of total flow rate or flow direction, the symbols indicate the solid charge per liquid flow rate for both flow directions and without considering the gas flow rate. The left figure indicates solid charge up to 10 g L^{-1} and the figure on the right solid charge between 20 g L^{-1} to 50 g L^{-1} .

In order to analyse the particle behaviour and detect and assign potential flow patterns it is necessary that the suspension supply unit delivers a constant and reliable solid charge throughout the experiment and from one operating day to another. Also the solid charge has to be independent from flow conditions (liquid and gas flow rates). For each operating parameter at least two samples were taken, and the mean solid charge was determined for over 526 samples. Figure 3.6 shows the good agreement between target and measured solid

charge. For higher solid loadings ($w_s > 10 \text{ g L}^{-1}$) the mean deviation is increased (12.7%) compared to lower loadings (4.7%).

3.3.2 Particle placement in liquid slugs

The influence of solid loading, two phase velocity and viscosity of the fluid media for horizontal and vertical flow is illustrated in Figure 3.7 and Figure 3.8. The corresponding operating conditions are detailed in Table 3.2 and Table 3.3. In the following the influence of the selected parameters is briefly described before the identified flow regimes are summarized.

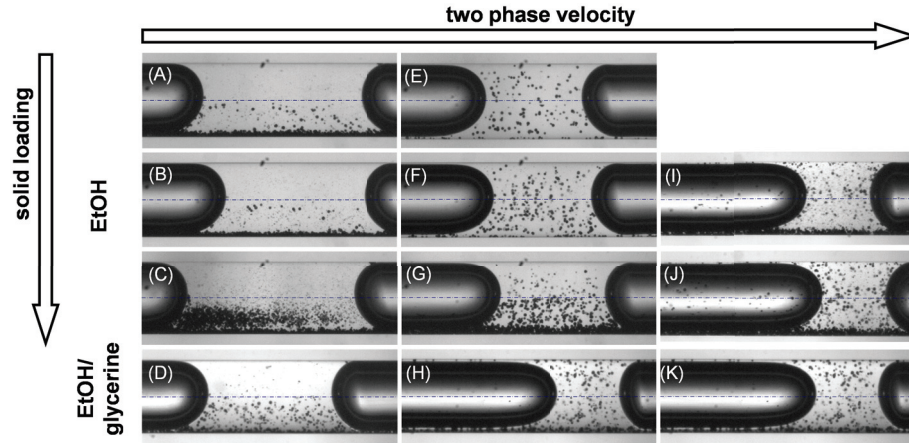


Figure 3.7: Examples of particle placement in horizontal flow. Operating parameters are summarized in Table 3.2

Table 3.2: Operating conditions for horizontal flow for the exemplary pictures in Figure 3.7. Fluid media 1: pure ethanol, fluid media 2: ethanol-glycerol.

#	Fluid	w_s [g L^{-1}]	Q_L [mL min^{-1}]	Q_G [mL min^{-1}]	u_{TP} [cm s^{-1}]	L_{slug} [mm]	Re_T [-]	Ca [-]
A	1	2.5	1.5	1	2.3	3.14	26.1	0.0012
B	1	5	1.5	1	2.3	3.14	26.1	0.0012
C	1	10	1.5	1	2.3	3.14	26.1	0.0012
D	2	5	2	2	3.4	2.8	5.8	0.0132
E	1	2.5	8	10	15	2.2	169.9	0.0077
F	1	5	6.88	10	14.9	2.1	198.8	0.0076
G	1	10	8	10	15	2.2	169.9	0.0077
H	2	5	4	8	12	1.8	20.6	0.0464
I	1	5	3	20	22.9	1.4	259.4	0.0117
J	1	10	3	20	23.3	1.3	264	0.0119
K	2	5	4	16	21.3	1.3	36.6	0.0824

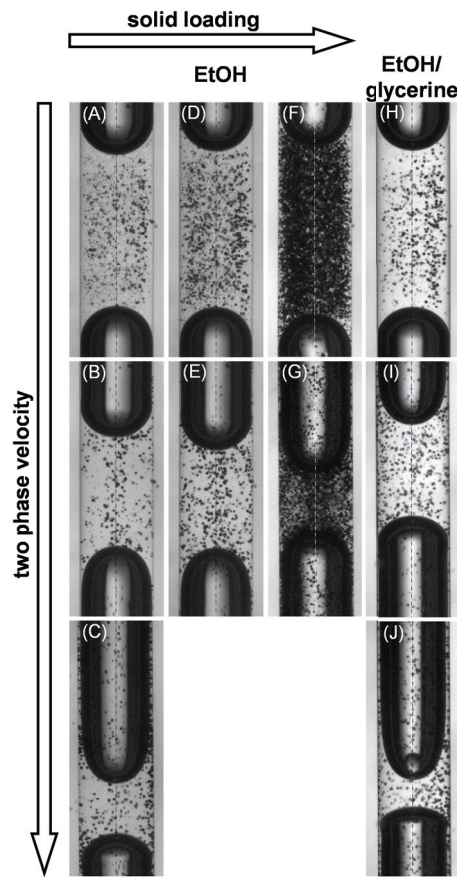


Figure 3.8: Examples of particle placement in vertical flow. Operating parameters are summarized in Table 3.3

Table 3.3: Operating conditions for vertical flow for the exemplary pictures in Figure 3.8. Fluid media 1: pure ethanol, fluid media 2: ethanol/ glycerol.

#	Fluid	w_s [g L ⁻¹]	Q_L [mL min ⁻¹]	Q_G [mL min ⁻¹]	u_{TP} [cm s ⁻¹]	L_{slug} [mm]	Re_T [-]	Ca[-]
A	1	5	1.5	1	2.3	3.7	26.1	0.0012
B	1	5	8	10	15.7	2.4	177.9	0.008
C	1	5	3	30	31.4	1	355.8	0.0161
D	1	10	1.5	1	2.3	3.7	26.1	0.0012
E	1	10	8	10	15.7	2.4	177.9	0.008
F	1	50	2	2	3.1	3.4	35.1	0.0016
G	1	50	3	30	14	1.5	158.6	0.0072
H	2	50	1.5	1	1.9	3.4	3.3	0.0074
I	2	5	6	30	17.9	1.9	30.7	0.0693
J	2	5	8	10	40.3	0.8	69.2	0.156

3.3.2.1 Influence of two phase velocity

Horizontal flow: for low two phase velocities ($u_{TP} \approx 2 \text{ cm s}^{-1}$), the particles are mainly situated in the lower part of the liquid slug, a non negligible amount is settled and forms a stationary bed on the liquid tubing. Increasing the two phase velocity suspends the particles more homogeneously over the entire slug height and less particles are settled. For very high

two phase velocities ($u_{TP} > 20 \text{ cm s}^{-1}$), particles can be observed over the entire slug height, but not uniformly distributed. Particles are placed close to the upper channel tubing but seem to be trapped not only in the lower liquid film but also, to a minor degree in the upper liquid film (particles placed between gas bubble and channel wall).

Vertical flow: for low two phase velocities ($u_{TP} \approx 2 \text{ cm s}^{-1}$), particles are homogeneously distributed over the entire slug volume, almost no particles are placed in the liquid film. Increasing the velocity ($u_{TP} > 8 \text{ cm s}^{-1}$) leads to a less homogeneous distribution where the majority of the solid particles is placed in the tubing center leaving the inner vortex depopulated. More particles are visible in the liquid film. For very high two phase velocities the amount of particles in the liquid film is even more increased.

3.3.2.2 *Influence of solid loading*

Horizontal flow: it seems that higher solid loadings ($w_s > 10 \text{ g L}^{-1}$) need higher two phase velocities to be homogeneously suspended. For the same velocity ($u_{TP} = 15 \text{ cm s}^{-1}$) particles populate the entire slug for the lower solid loading ($w_s < 5 \text{ g L}^{-1}$) whereas if the solid charge is increased the particles are mostly situated in the lower part and a high amount seemed to be settled.

Vertical flow: for higher solid charges (50 g L^{-1}), more particles seem to be trapped in the liquid film between gas bubble and channel wall.

3.3.2.3 *Influence of viscosity of the fluid media*

Horizontal flow: an influence of viscosity on particle placement can be observed for the lower and upper region close to the channel tubing. It is difficult to evaluate the amount of particles settled in the stationary bed layer but it appears that for low two phase velocities ($u_{TP} \approx 2 \text{ cm s}^{-1}$) less particles are settled in the higher viscous media than in pure ethanol flow. Regardless the two phase velocity, for ethanol/ glycerol a non negligible amount of particles is always observed in the liquid film in contrast to ethanol flow, where for high two phase velocities ($u_{TP} > 8 \text{ cm s}^{-1}$) only a few isolated particles can be observed. The stationary particle bed in glycerol/ ethanol flow seems less dense than the one in ethanol flow. For ethanol flow, for moderate velocities ($u_{TP} = 15 \text{ cm s}^{-1}$) particles are situated over the entire height but the region close to the upper channel tubing is rather empty. In ethanol/ glycerol flow, ($u_{TP} = 12 \text{ cm s}^{-1}$) more particles are visible in this area.

Vertical flow: it appears that no influence of liquid viscosity on particle placement in a vertical oriented tube can be detected. One reason might be that it is rather difficult to distinguish between particles placed in the liquid film and particles circulating in the vortex of the liquid slug.

3.3.3 *Description of particle flow patterns and Matlab™ routine for automatic detection of flow patterns*

3.3.3.1 *Horizontal flow*

In horizontal flow, particle motion was in general introduced by the passage of the gas bubble. Mainly the approaching bubble nose conducted to particle entrainment but also the rear end of the bubble led to a minor degree to particle movement and loosening of the deposited particle bed. Five different flow regimes could be detected and will be described in detail in the

following. Except otherwise mentioned the operating parameters given in the descriptions are those for pure ethanol, the lower viscous media used for visualisation experiments.

Regime H-I: For very low two phase velocities ($u_{TP} = 2 \text{ cm s}^{-1}$ to 4 cm s^{-1}), a large amount of particles rests on the bottom of the tube and a bed is formed consisting of more than two layers of particles (Figure 3.9 A1). The gas bubble slides over the rough particle bed and the passage of the bubble nose entrains some particles. The path of particle movement is slightly inclined, an observation for which two possible explanations can be given: a sign for particle sedimentation or just a reflection of the streamline pattern of the liquid phase [55, 78]. In spite of this downward movement, particles reach the other end of the slug before colliding with the tubing bottom and descend with upwards directed streamlines. Despite the low velocity, once the particles are in movement they do not deposit although they circumference settled particles when they follow the outer streamlines close to the settled particles.

For these low velocities, irregularities in the solid loading between successive liquid slugs are visible (Figure 3.9 A2). An accumulation of particles close to the bubble nose and a higher particle loading than in the average slug could be detected approximately every 6 slugs. This phenomena occurs only at low two phase velocities and is attributed to the creation of Taylor flow and not part of the flow pattern. It seems that at these low two phase velocities the suspension supply is not constant and the liquid slugs are not fed uniformly with the same solid amount. The same liquid flow rates at higher two phase velocities do not have the same effect (no irregularities were observed), this behaviour must also be linked to the low gas flow rate and thus to the initial Taylor flow formation. The effect of Taylor flow formation is discussed more in detail further on (see 3.3.4).

Regime H-II. Increasing the two phase velocity ($u_{TP} = 5 \text{ cm s}^{-1}$ to 8 cm s^{-1}) leads to a homogeneous particle distribution in the lower recirculation (Figure 3.9 B1 and B2). Two different patterns are visible: particles can follow mainly the velocity streamline with the highest velocity and the inner part of the vortice, where the local streamline velocity is lower, seems mostly empty (Figure 3.9 B1). In Figure 3.9 B2 the particles are distributed over the entire lower part of the liquid slug and a depopulation of the inner lower vortex is not visible. Even for these higher velocities, a non negligible amount of particles is still deposited in the liquid film. As the observation is made only from the side and a top view is missing, it is difficult to differentiate the source of the different patterns. It is possible that the observed effect is mainly due to the low solid charge ($w_s = 2.5 \text{ g L}^{-1}$ to 5 g L^{-1}). We therefore consider both observations as one flow regime.

Regime H-III: If the two phase velocity is increased further on ($u_{TP} > 9 \text{ cm s}^{-1}$), the particles are distributed over the entire slug height (Figure 3.9 C). The particle concentration is higher in the lower recirculation loop but a non negligible amount circulates also in the upper part of the slugs. Only a few isolated particles are settled in the liquid film but keep continuously moving due to the high frequency of bubble passage.

Regime H-IV: By further increasing the two phase velocity ($u_{TP} > 12 \text{ cm s}^{-1}$, ethanol/ glycerol flow) particles are homogeneously distributed over the entire slug height (Figure 3.9 D).

The decision if particles are homogeneously distributed over the entire slug height (regime H-IV) and the differentiation towards the transitional regime (regime H-III) is probably the most difficult and questionable due to two reasons: the formulated threshold is possibly too strict. Also the analysis is based only on one picture per slug and thus a stationary represen-

tation of flow conditions neglecting the continuous aspect of particle motion. According to the results of our Matlab analysis, we did not reach this regime for the operating conditions studied. But, by further increasing the two phase velocity it should be possible to suspend more particles in the upper recirculation loop.

Regime H-V: By further increasing the two phase velocity ($u_{TP} > 20 \text{ cm s}^{-1}$), particles are still located over the entire slug height but a non negligible amount of particles is deposited at the bottom of the tubing channel and a few are even trapped in the liquid film between the gas bubble and the upper part of the channel tubing (Figure 3.9 E).

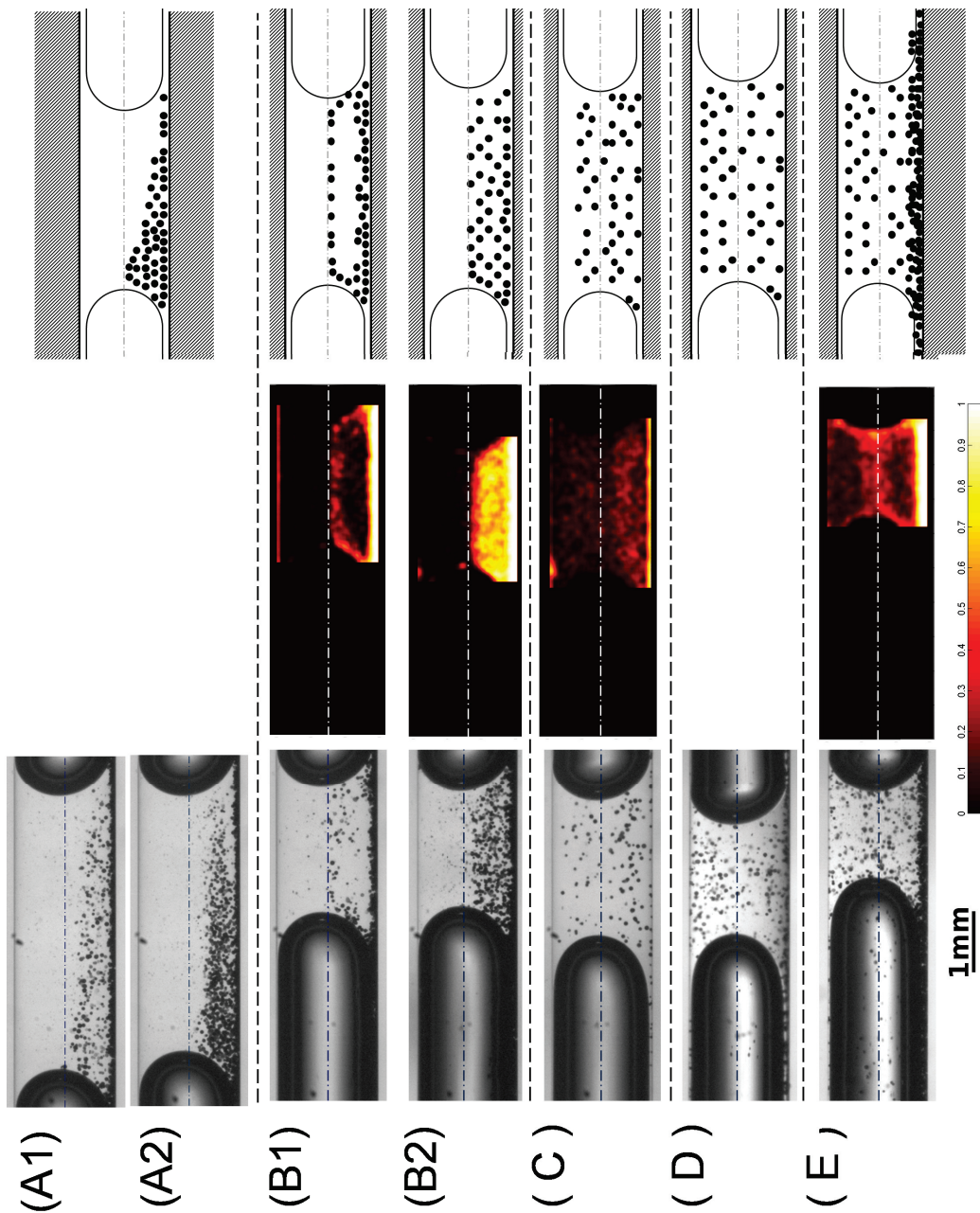


Figure 3.9: (The picture was flipped by 90° .) For each flow pattern, a photograph, the representative image indicating the probability of particle presence as a result of the Matlab program and the symbol used in the following discussion for the flow pattern are given. For the particle probability images, 0 signifies absence of solid particles and 1 means a probability of 100% that solid particles are present. The fluid media is pure ethanol (A, B, C, E) and ethanol/glycerol (D). **(A1)**: Regime H-I, $w_S = 5 \text{ g L}^{-1}$, $u_{TP} = 3.1 \text{ cm s}^{-1}$, **(A2)**: regime H-I, illustrates the observed irregularities every 6 slugs, **(B1)**: regime H-IIa, $w_S = 5 \text{ g L}^{-1}$, $u_{TP} = 6.4 \text{ cm s}^{-1}$, **(B2)**: regime H-IIb, $w_S = 10 \text{ g L}^{-1}$, $u_{TP} = 4.7 \text{ cm s}^{-1}$, **(C)** regime H-III, $w_S = 2.5 \text{ g L}^{-1}$, $u_{TP} = 14.9 \text{ cm s}^{-1}$, **(D)** regime H-IV, $w_S = 5 \text{ g L}^{-1}$, $u_{TP} = 12 \text{ cm s}^{-1}$, **(E)** regime H-V, $w_S = 5 \text{ g L}^{-1}$, $u_{TP} = 23.2 \text{ cm s}^{-1}$

3.3.3.2 *Vertical flow*

For vertical flow three different regimes were identified.

Regime V-I: At low two phase velocities ($u_{TP} < 8 \text{ cm s}^{-1}$) the solid particles are homogeneously suspended over the entire slug height (Figure 3.10 A). No accumulation neither in the film nor on the preceding bubble rear end can be detected. It seems that the particles do not populate the film region. Nevertheless as the camera focuses on the center of the tube this might be misleading and only due to visual effects.

Regime V-II: If the two phase velocity is increased ($u_{TP} > 8 \text{ cm s}^{-1}$), the solid particles are pushed towards the outer recirculation loop where the fluid velocity is high. Solid particles are observed mainly at the centre of the tube and along the wall region, both inner vortex centres appear depopulated (Figure 3.10 B). Also more particles are situated in the liquid film zone.

Regime V-III: For very high two phase velocities ($u_{TP} > 18 \text{ cm s}^{-1}$), more particles are pushed towards the outer recirculation loop and accumulate in the film region (Figure 3.10 C). The particles trapped in the liquid film are observed to move slowly downwards.

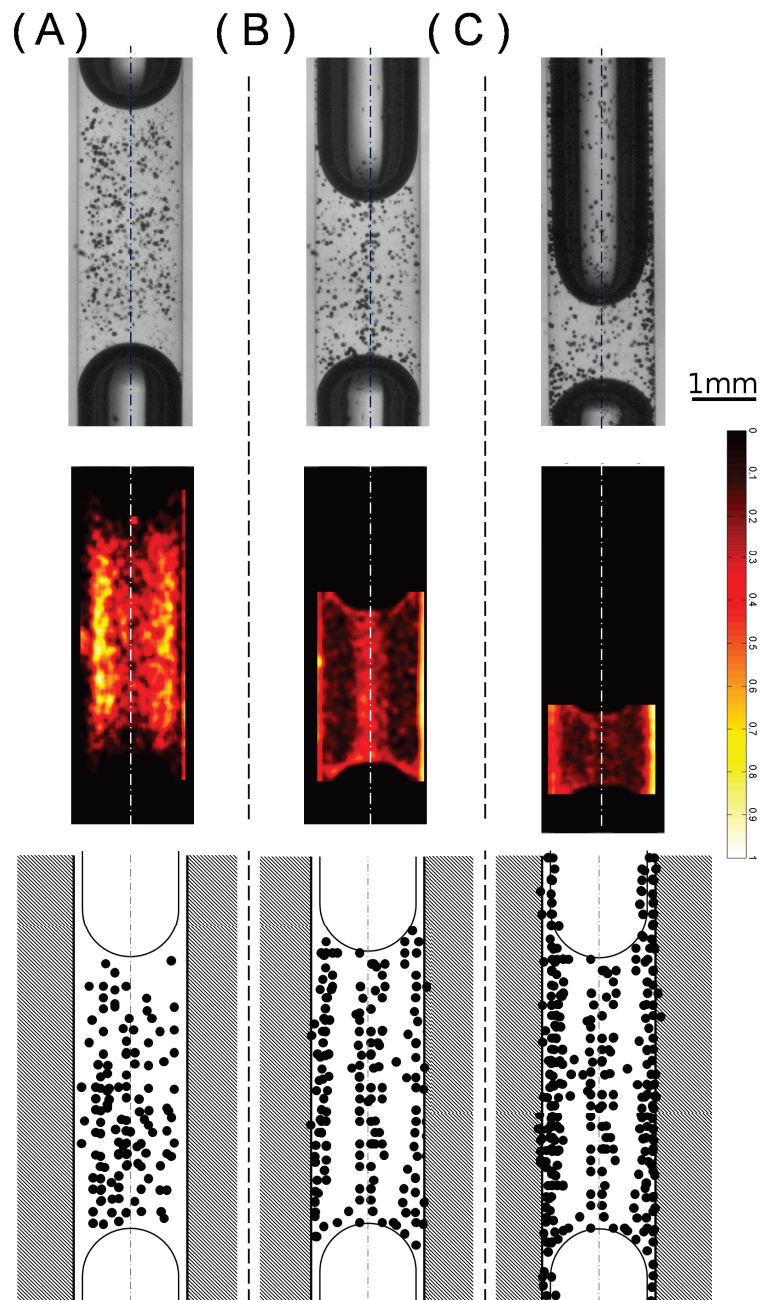


Figure 3.10: For each flow pattern, a photograph, the representative image indicating the probability of particle presence as a result of the Matlab program and the symbol used in the following discussion for the flow pattern are given. For the particle probability images, 0 signifies absence of solid particles and 1 means a probability of 100% that solid particles are present. The fluid media is pure ethanol, $w_S = 5 \text{ g L}^{-1}$ (A): Regime V-I, $u_{TP} = 4.6 \text{ cm s}^{-1}$, (B): regime V-II, $u_{TP} = 10.7 \text{ cm s}^{-1}$, (C): regime V-III, $u_{TP} = 31.4 \text{ cm s}^{-1}$

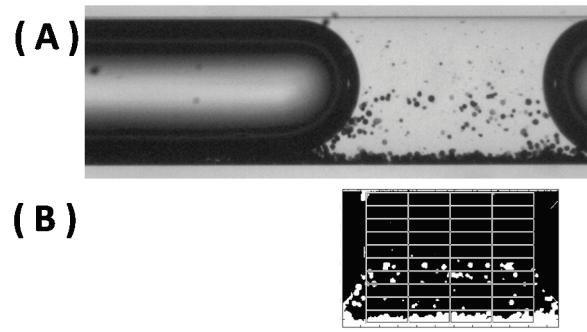
3.3.3.3 *Matlab routine for automatic detection of flow patterns*

Figure 3.11: Typical image for automatic flow pattern analysis after increasing the contrast, binarization and reversing black and white

For each video one image per slug is extracted (thresholding, binarization) and analysed with a Matlab™ routine. The algorithm was constructed according to the identified flow patterns and characteristic observations served to establish threshold conditions for each pattern. Each slug was divided into 4×10 zones. The height of the observation area is slightly smaller than the tubing diameter: even though reflections due to the curved tubing could be avoided, a marginal shadow can be observed at the upper and lower channel wall. This shadow does not deteriorate the image quality but could alter the results for the automatic flow pattern assignment.

After increasing the contrast to account also for less visible particles (gray scale image, pixel values $p_{i,j}$ between 0 and 255), binarization (particles are black: $p_{i,j} = 0$, bubble and channel wall white: $p_{i,j} = 1$), and reversing black and white "colors" (particles are white: $p_{i,j} = 1$, bubble and channel wall black $p_{i,j} = 0$) a characteristic image looks like the one depicted in Figure 3.11.

The algorithm is based on the decision if a zone or a certain region (group of zones) is more or less populated than another one. Therefore in a first step, it was determined if a zone is populated with particles or not. For each zone the particle concentration c_p was determined as the ratio of white pixels to the total amount of pixels in one zone.

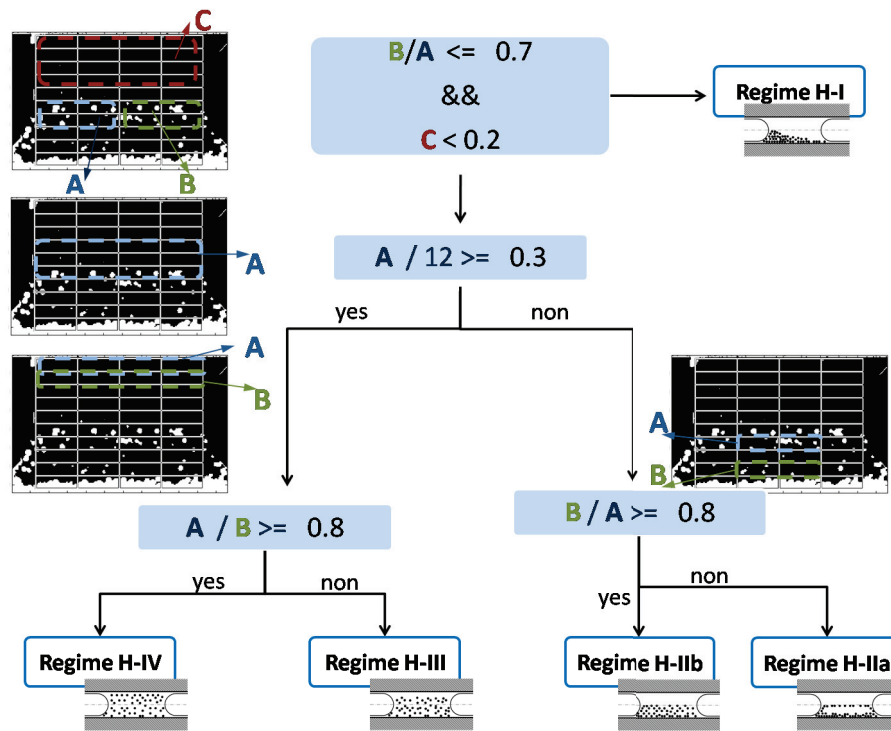
$$c_p = \frac{\sum_{i,j} p(i,j)}{i \cdot j} \quad (3.1)$$

Then, the mean particle concentration \bar{c}_p was calculated and a zone was considered to be populated by solid particles if the particle concentration in this respective zone is superior to a certain percentage of the mean concentration:

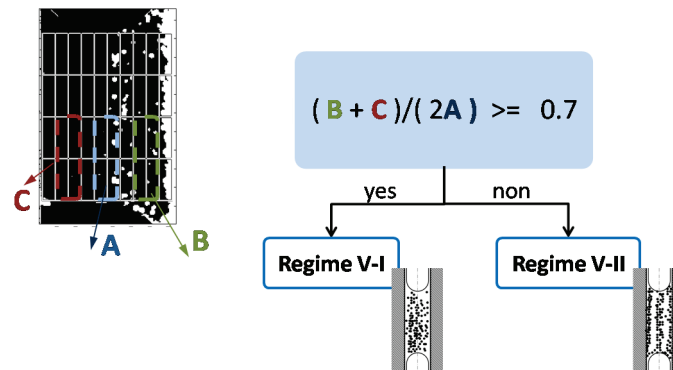
$$c_p \geq 0.65 \cdot \bar{c}_p \quad (3.2)$$

Now that every zone is either "populated" or "not populated" by particles, different groups of zones are compared according to the algorithm depicted in Figure 3.12. For each group (A, B or C) the ratio of populated to total number of zones is calculated and compared to a defined threshold (as indicated in Figure 3.12).

One flow pattern is thus attributed to each slug present in the recorded video. The maximum count of one regime for all slugs of one video will determine the flow pattern for the specific experiment.



(a) Detection for horizontal flow pattern



(b) Detection for vertical flow pattern

Figure 3.12: Matlab™ routine to automatically detect a flow pattern

Unfortunately for the ethanol/ glycerol experiments it was not possible to use this procedure as the background was not uniform enough and the lighting led to shadowy regions. Also high solid loadings ($w_s > 20\text{g/L}$) led to quite uniform appearance of slug and bubble regions which made it not possible to use the Matlab program for operating conditions with high solid loadings. For these video films a flow pattern was assigned manually, adding a possible source of uncertainty and subjectivity. The Matlab program analyses one picture for each slug passing in front of the camera. This adds another uncertainty as only the instantaneous placement of particles is taken into consideration. To get high quality pictures and a good representation of the circulating particles, the zoom was chosen in such a way that the inner tubing diameter fills almost the entire height of the picture. By doing so it is not possible to follow one slug over a longer period of time. Therefore the assignment of a certain flow pattern to one operating condition has to be handled with caution.

3.3.4 Discussion of relevant mechanisms related to particle entrainment and re-suspension

The placement of particles in the liquid slug and the particle movement is influenced by three main mechanisms:

- the initial formation of the Taylor flow
- the availability of flow conditions to keep particles in motion
- the capability of flow profile to entrain settled particles by bubble passage

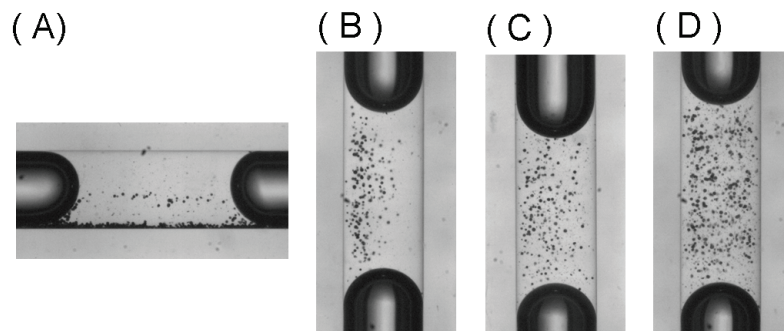


Figure 3.13: Impact of injection configuration on placement of solid particles in the liquid slug, for a)-d): $Q_L = 3 \text{ ml min}^{-1}$, $Q_L = 2.5 \text{ ml min}^{-1}$, for a-c) $w_s = 2.5 \text{ g L}^{-1}$, d) $w_s = 5 \text{ g L}^{-1}$, for a), b) and d) same injection method, c) spiral arrangement between T-junction and vertical tubing to better distribute the particles

For both configurations the suspension phase is introduced perpendicular to the gas phase and is directed downwards to the tubing bottom (Figure 3.3, see Section 3.2). One example for the influence of injection method on particle placement is illustrated in Figure 3.13 where (A) and (B) illustrate particle behaviour for identical operating parameters in horizontal (A) and vertical (B) flow. Particles initially located in the lower recirculation loop of horizontal flow do not populate the entire slug height/ width by simply passing in vertical flow mode but keep circulating preferentially on the left side which coincides with the former lower part of the liquid slug. By adding a coil formed passage (Figure 3.3 C) it seems possible to better distribute the particles (Figure 3.13 C). For higher concentrated suspensions ($w_s = 5 \text{ g L}^{-1}$ in comparison to $w_s = 2.5 \text{ g L}^{-1}$) the modification of the injection procedure is not necessary and particles redistribute homogeneously over the entire liquid volume without the additional coil (Figure 3.13 D).

Apart from the solid loading, one might assume that the frequency of gas bubble passage is a crucial parameters and determines if the particles have the time to sediment to the bottom of the tube or are entrained with the upper recirculation loop (Figure 3.14).

For horizontal flow, the injection and formation process of "slurry Taylor" flow is important insofar as it seems rather impossible that a particle passes from the lower to the upper recirculation loop: in the centre region the streamlines are facing towards each other so that even for high upwards directed velocities close to the lower front side of the bubble, the same high velocity will be directed towards the bottom in the upper region. Therefore the only possibility for particles to be able to populate the upper part of the liquid slug is during the formation of the Taylor flow (Figure 3.14 C). We assume that whereas there can be an exchange of particles from the upper to the lower part of the slug due to sedimentation, there is no movement directed from the lower to the upper part. The influence and effect of the initial

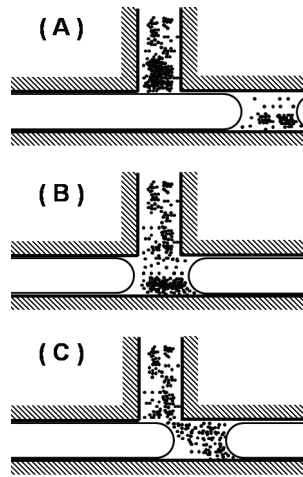


Figure 3.14: Possible influence of injection method on placement of particles. While the gas bubble passes the liquid feed, the particles are trapped above the gas bubble (A). If the gas flow rate is small, the particles are entrained with the liquid flow which is directed downward to the tubing bottom and can thus settle (B). If the gas flow rate and with it the frequency of gas bubbles passing in front of the liquid phase inlet is high, the particles are entrained together with the liquid phase horizontally and do not settle on the tubing bottom. Particles can thus populate the upper part of the liquid slug (C).

formation of “slurry Taylor” flow was however not further investigated nor quantified. We focused on the two other criteria for good particle distribution: does the flow profile allow that solid particles are kept in motion? If particles sediment to the bottom, can they be entrained by the passing gas bubble and the deformed flow profile? Relevant parameters are therefore liquid and particle properties and the velocity profile.

In the following a short overview of the forces relevant to the motion of particles in fluids is given and subsequently we will estimate the effect of these forces on maintaining particle transport and the possibility of particle entrainment.

3.3.4.1 Forces on particles

The motion of particles is in general described by the so called Basset-Boussinesq-Oseen-equation [68, 116, 120]. Relevant forces are the drag force \vec{F}_D , inertia due to fluid acceleration and the local pressure gradient \vec{F}_P , the added mass force \vec{F}_{AddM} , the history force \vec{F}_H , the buoyancy \vec{F}_B and the gravitational force \vec{F}_G . Additionally the lift force \vec{F}_L and the centrifugal force \vec{F}_Z as a special form of inertia might be relevant in our case.

The **gravitational force** and the **buoyancy force** are both body forces and depend only on fluid and solid properties and the gravitational or centrifugal field the particle is exposed to.

$$\vec{F}_G = m_P \vec{g} = \rho_P \frac{\pi}{6} d_P^3 \vec{g} \quad (3.3)$$

$$\vec{F}_B = m_F \vec{g} = \rho_F \frac{\pi}{6} d_P^3 \vec{g} \quad (3.4)$$

The **drag force** acts in the direction of the relative velocity between particle and surrounding fluid.

$$\vec{F}_D = 0.5 C_D \rho_F (\vec{u}_F - \vec{u}_P)^2 A_P \quad (3.5)$$

The drag force depends on the projected area of the particle towards the flow A_P , fluid density ρ_F and a drag coefficient C_D . The coefficient is a lumped parameter which accounts

for the various sources for drag like friction and correlations are usually given as a function of particle Reynolds number Re_P (Equation 3.6).

$$Re_P = \frac{\rho_F d_P (\vec{u}_F - \vec{u}_P)}{\mu_F} \quad (3.6)$$

The drag coefficient is influenced by the flow conditions of the surrounding fluid, the surface roughness and shape of the particle [116]. Also the proximity of a wall and the particle concentration can effect the magnitude of the drag coefficient.

In the Stokes regime, meaning for small particle Reynolds numbers ($Re_P \rightarrow 0$) an analytical solution for the drag coefficient for spherical particles is possible (Equation 3.7).

$$C_{D,Stokes} = \frac{24}{Re_P} \quad (3.7)$$

Particle motion in proximity of a rigid wall increases the drag coefficient [133] and for particles (radius r_P) in normal (Equation 3.8, [12, 23]) or parallel (Equation 3.9, [40]) movement towards a wall, the drag coefficient is increased and depends on the distance a between particle and wall.

$$\frac{C_D}{C_{D,Stokes}} = 1 + \frac{9}{8} \frac{r_P}{a} + \left(\frac{9}{8} \frac{r_P}{a} \right)^2 \quad (3.8)$$

$$\frac{C_D}{C_{D,Stokes}} = \left[1 - \frac{9}{16} \frac{r_P}{a} + \frac{1}{8} \left(\frac{r_P}{a} \right)^3 - \frac{45}{256} \left(\frac{r_P}{a} \right)^4 - \frac{1}{16} \left(\frac{r_P}{a} \right)^5 \right]^{-1} \quad (3.9)$$

The **pressure force** represents the fluid acceleration in absence of the particle and results from the local pressure gradient. It describes the inertia of the liquid phase (Equation 3.10).

$$\vec{F}_P = m_P \frac{\rho_F}{\rho_P} \frac{d\vec{u}_F}{dt} \quad (3.10)$$

The acceleration of a certain fraction of the fluid surrounding the particle is accounted for by the **added mass force** (Equation 3.11). The **Basset** or **history force** (Equation 3.12) describes the delayed response of the boundary layer surrounding the particle to a change in relative velocity. For both forces an analytical solution is only possible for low particle Reynolds numbers.

$$\vec{F}_{AddM} = 0.5 C_{AddM} \rho_F \frac{m_P}{\rho_P} \frac{d}{dt} (\vec{u}_F - \vec{u}_P) \quad (3.11)$$

$$\vec{F}_H = 9 \sqrt{\frac{\rho_F \mu_F}{\pi}} \frac{m_P}{\rho_P d_P} C_H \left[\int_0^t \frac{d}{dt} (\vec{u}_F - \vec{u}_P) \frac{d\tau}{(t-\tau)^{0.5}} + \frac{(\vec{u}_F - \vec{u}_P)_0}{\sqrt{t}} \right] \quad (3.12)$$

The parameters C_{AddM} and C_H are a function of slip velocity.

When particles are exposed to unsymmetrical flow profiles and thus a non symmetric pressure gradient surrounding it, they are exerted to a **lift force**. This lift force is directed perpendicular to the flow direction. A general expression of this lift force is defined analogous to the drag force in function of particle cross section, relative velocity and a lift coefficient C_L (Equation 3.13)

$$\vec{F}_L = 0.5 C_L A_P \rho_F (\vec{u}_F - \vec{u}_P)^2 \quad (3.13)$$

The source of this unsymmetrical flow profile can have several reasons (Figure 3.15). Unsymmetrical particle shapes, rotating particles after particle-wall collisions or unsymmetric

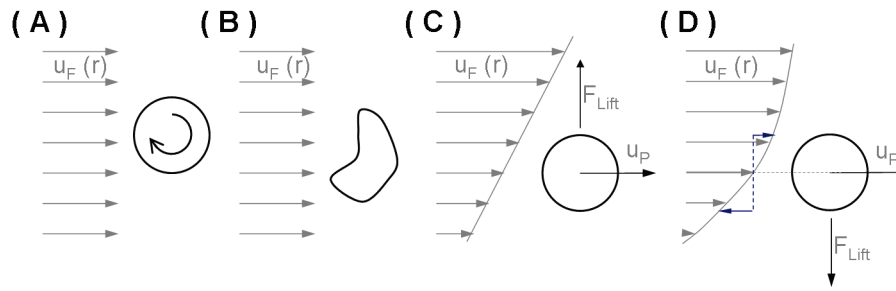


Figure 3.15: Schematic illustration of different sources for lift effect: (A) rotating particle, (B) particle exposed to unsymmetrical flow field due to particle shape, (C-D) asymmetric flow profile, illustrations based on [15, 26, 85, 133].

flow profiles in vicinity to the reactor wall are a few examples. Due to the laminar flow profile in slug flow, especially the latter reason seems relevant for the description of particle movement in “slurry Taylor” flow and its relevance was already discussed for L-L “slurry Taylor” flow [109]. A popular expression for lift resulting from two dimensional shear flow and nonuniform relative velocity profile was described by Saffman [107] and is valid for low Reynolds numbers.

The shear rate $\dot{\gamma}$ is defined as

$$\dot{\gamma} = \frac{du_F}{dy} \quad (3.14)$$

The **Saffman lift force** characterizes the lift experienced by a particle in two-dimensional shear flow :

$$F_{L,saff} = 1.615\rho_F (u_F - u_P) d_P^2 \sqrt{\frac{\mu}{\rho_F} \cdot \dot{\gamma} \text{sgn}(\dot{\gamma})} \quad (3.15)$$

A special expression for the Saffman lift force was developed for a particle touching a solid plane ([77], Equation 3.16). In this case the force points always away from the wall.

$$F_{L,resting} = 0.576\rho_L d_P^4 \dot{\gamma}^2 \quad (3.16)$$

Particles in a centrifugal field experience a special form of inertia. The **centrifugal force** \vec{F}_C is effective on objects moving along a circular path and acts perpendicular to the angular velocity ω away from the rotation center [120].

$$\vec{F}_c = m_P \vec{r} \omega^2 \quad (3.17)$$

After this summary of all the main forces that can act on a particle in motion, we will analyse more in detail how they influence the particle transport in “slurry Taylor” flow.

3.3.4.2 Maintaining particle transport

To estimate if the flow conditions meet the requirements to maintain the transport of suspended settling-particles a few assumptions were made:

- The analysis is limited to drag, gravity, buoyancy and lift forces only. For vertical flow centrifugal forces are additionally considered. Forces depending on the change of fluid velocity or relative velocity ($\vec{u}_F - \vec{u}_P$) with respect to time are neglected in this simple approach. This simplification is necessary as otherwise knowledge of the fluid profile is needed which can only be provided by proper numerical fluid modelling and evaluation if the particles present in the flow alter the typical velocity profile of Taylor flow.

- The analysis is made for an isolated particle and possible effects of solid concentration are not accounted for. Single settling particles entrain a certain fluid volume. For continuity reasons this has to result in an upward fluid flow. In concentrated suspensions this upward movement is important enough to hinder the sedimentation and the settling velocity of concentrated suspensions $u_{T,S}$ is thus decreased compared to single particles [105, 120]. The effect of volume concentration V_S on the settling velocity is generally described by the Richardson and Zaki equation (Equation 3.18) where the exponent α is a function of particle Reynolds number $\alpha = f\{\text{Re}_{P,0}(u_t)\}$. In the Stokes regime α equals 4.65. For a volume concentration of 5%, corresponding to the highest solid charge applied in this study, the settling velocity is decreased by 22% compared to a single particle. However, the concentration is not uniform over the entire slug height and actual concentrations may lead to even lower settling velocities. Nevertheless the study concentrated only on a single particle, accounting for the maximum settling velocity in order to over-predict conditions necessary to keep particles in motion rather than underestimate sedimentation.

$$\frac{u_{T,S}}{u_T} = (1 - V_S)^\alpha \quad (3.18)$$

In liquid-solid fluidisation, particles are kept in motion when the upward flow of liquid equals the settling velocity [105] in a stationary fluid. This context is used in hydraulic classification [120] or for fluidized beds [111, 126] to define equilibrium conditions. The settling velocity u_T in a stationary fluid can be obtained by considering the force balance of drag, gravity and buoyancy forces (Equation 3.19, 3.20 and 3.21, [120]).

$$\vec{F}_G - \vec{F}_B = \vec{F}_D \quad (3.19)$$

$$\rho_P \frac{\Pi}{6} d_P^3 g - \rho_F \frac{\Pi}{6} d_P^3 g = \frac{\rho_F \Pi}{2} \frac{d_P^2}{4} u_T^2 C_D(\text{Re}_{P,t}) \quad (3.20)$$

In the Stokes regime ($\text{Re}_{P,t} < 0.25$) an analytical solution for the drag coefficient can be given and in order to be able to judge the influence of the wall on the settling velocity we set $a = \frac{C_D}{C_{D, \text{stokes}}}$ (see Equation 3.8 and 3.8). The settling velocity can be estimated as:

$$u_T = \frac{1}{a} \frac{(\rho_P - \rho_F) d_P^2 g}{18\mu} \quad (3.21)$$

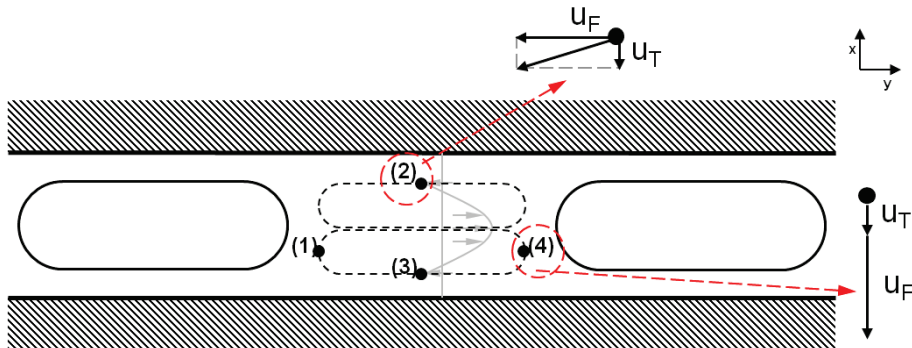


Figure 3.16: Horizontal flow: chosen points for simplified force analysis

First, the experiments for **horizontal flow** are commented. To estimate the influence of the particular forces or mechanisms four exemplary operating conditions are chosen to illustrate

the different regimes. Four characteristic positions in the recirculating pattern were identified (Figure 3.16). As a simplification two assumptions are made:

- At positions 2 and 3 the influence of the approaching gas bubble is negligible, Poiseuille flow is predominant (Figure 3.17 B) and therefore there is only a horizontal component for the fluid velocity \vec{u}_F .

$$\vec{u}_F = \begin{pmatrix} 0 \\ u_{F,lam}(r) \end{pmatrix} \quad (3.22)$$

where $u_{F,lam}(r)$ is defined as

$$u_{F,lam}(r) = 2 \cdot u_{TP} \left[1 - \left(\frac{r}{R} \right) \right] \quad (3.23)$$

- At points 1 and 4, the influence of the gas bubble on the flow profile is dominant, the fluid velocity has only a vertical component (see Equation 3.24).

$$\vec{u}_F = \begin{pmatrix} u_{F,rel}(r) \\ 0 \end{pmatrix} \quad (3.24)$$

To simplify the analysis the absolute value of the fluid velocity is assumed to be constant along the same circulation loop as illustrated in Figure 3.17 (A). The relative velocity $u_{F,rel}(r)$ is therefore defined as indicated in Equation 3.25.

$$u_{F,rel}(r) = 2 \cdot u_{TP} \left[1 - \left(\frac{r}{R} \right) \right] - u_B \quad (3.25)$$

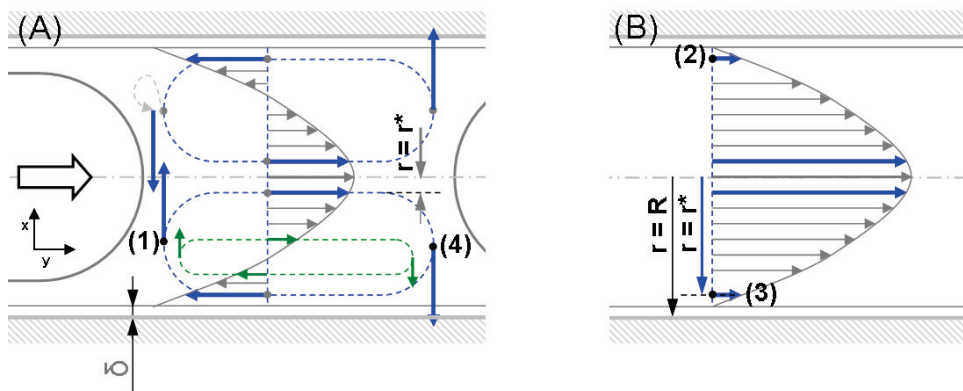


Figure 3.17: Illustration of simplified flow profile for selected points in horizontal flow. (A) indicates conditions where the gas bubble influences the flow profile, (B) influence of the gas bubble was neglected.

Particles are considered to follow the streamlines of the liquid flow in horizontal direction (denoted y on Figure 3.16, [120]), therefore $u_p(y) = u_F(y)$. For the vertical direction (denoted x) the particle settling velocity has to be accounted for.

For horizontal flow the velocity in the liquid film is assumed to be zero [70]. Therefore the possibility of particles trapped in the liquid film is evaluated using the correlation of Aussilous and Qu ere [11] to estimate the film thickness (Equation 3.26). The correlation actually describes the film thickness between the gas bubble and the channel wall. For Capillary numbers smaller than 0.05 the film thickness between the circulating liquid in the liquid slug and the channel wall is comparable in size. Exceeds the Capillary number 0.05 the liquid film in the slug is increased compared to the one between gas bubble and channel wall, limiting thus

the recirculation zone in the slug [70]. In this study the Capillary number exceeds only this threshold for high velocities in ethanol/glycerol flow ($Ca=0.07$) and operating conditions are always far away from complete bypass flow for $Ca>0.5$ [122].

$$\frac{\delta_{film}}{d_T} = \frac{0.67Ca^{2/3}}{1 + 3.35Ca^{2/3}} \quad (3.26)$$

Due to the rather large inner channel diameter (1.65 mm) compared to tubing generally employed when dealing with horizontal segmented flow experiments, an impact of gravity on the flow profile is easily detectable: the liquid film (see Figure 3.18) is enlarged under the gas bubble. The bubble itself is also slightly deformed. A typical bullet type profile can be observed for vertical and horizontal flow and the front is not symmetrical for horizontal flow.

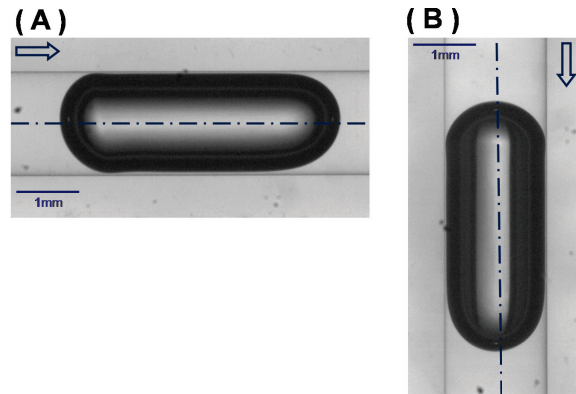


Figure 3.18: Illustration of influence on gravity on bubble shape and liquid film thickness: exemplary image for (A) horizontal flow and (B) vertical flow.

The influence of gravity on the liquid film thickness for millimetric sized channels has been studied [45, 78] and indeed an enlarged film thickness and thus an effect of gravity on the liquid film was reported. Unfortunately there exists no correlation yet to estimate the actual value in conditions where gravity is not negligible. Therefore the film thickness is calculated according to Equation 3.26 and the fact that its actual size is larger is kept in mind.

The approaching gas bubble induces the particular flow pattern which is characteristic for Taylor flow and is responsible for the recirculating movement. Therefore particle motion is maintained if two requirements are fulfilled:

- during the time the gas bubble travels the distance of one slug length $t_{B \rightarrow L_s}$, the particle does not settle (valid for position 2 and 3 on Figure 3.17).
- the vertical fluid component at position 1 (Figure 3.17) is larger than the settling velocity of the solid particle.

The discussion is based on representative operating conditions and ethanol-nitrogen flow is mainly taken into consideration as the settling velocity in higher viscous media is lower: if a relevant distinction can be made for pure ethanol flow, it is interesting to consider a higher viscous flow. If this is not the case, the effect will be even less remarkable for ethanol/glycerol flow. Unless otherwise indicated, all values given for this analysis were obtained for ethanol-nitrogen "slurry Taylor" flow.

For positions 2 and 3 (Figure 3.17), we compare the distance a particle can settle while the gas bubble travels one slug length $u_T \cdot t_{B \rightarrow L_s}$ with the distance between the particle and the

tubing bottom ($R - r^*$ for particles located in the lower part of the slug, Figure 3.17). The threshold for maintaining particles in suspension is therefore:

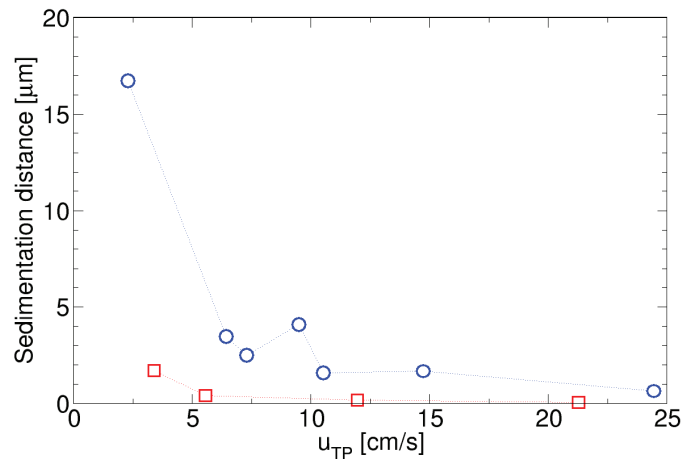


Figure 3.19: Effect of two phase velocity on the distance the solid particle can settle while the gas bubble travels one slug length. Results are given for ethanol (\circ) and ethanol/ glycerol (\square) flow. Pictures in Table 3.5 and 3.6 indicate the flow pattern for selected operating parameters.

$$u_T \cdot t_{B \rightarrow L_s} < R - r^* \quad (3.27)$$

for particles in the lower part and

$$u_T \cdot t_{B \rightarrow L_s} < R + r^* \quad (3.28)$$

in the upper part of the recirculation loop for a particle located at $r = r^*$. In the operating range studied, for the lowest two phase velocity employed, the gas bubble needs 0.14 s to travel one slug length. The settling velocity in ethanol yielded $u_T = 0.12 \text{ cm s}^{-1}$ and in ethanol/glycerol $u_T = 0.013 \text{ cm s}^{-1}$. The particle is thus able to settle $16.7 \mu\text{m}$ in ethanol and $1.04 \mu\text{m}$ in the higher viscous media for the lowest two phase velocity (see Figure 3.19). Compared to the channel diameter ($d_T = 1.65 \text{ mm}$) the settling of particles would effect only particles located close to the tubing bottom. However, when the particle approaches the channel wall, the drag coefficient increases according to Equation 3.8 and 3.8, meaning that the settling is slowed down and the settled distance even smaller. This influence is illustrated in Figure 3.20.

Indeed, visually even for very low two phase velocities it was never observed, that a particle would settle on the bottom of the channel, even particles in motion very close to the channel bottom do not deposit but appear to be circumventing settled particles in the liquid film.

For position 1 (Figure 3.17) the fluid velocity component in vertical direction has to be higher than the settling velocity of the particle in order to prevent sedimentation and to entrain the particle. The typical flow profile for Taylor flow is considered (see Equation 3.25) and the absolute velocity along one recirculation loop is assumed to be constant. The threshold for maintaining particles in suspension is accordingly (Equation 3.29):

$$\frac{u_{F,rel}(r^*)}{u_T} > 1 \quad (3.29)$$

In Figure 3.21 this ratio is plotted against a non-dimensionless tube radius. It can be seen, that over a large range the ratio is superior to 1, for the lowest two phase velocity only for

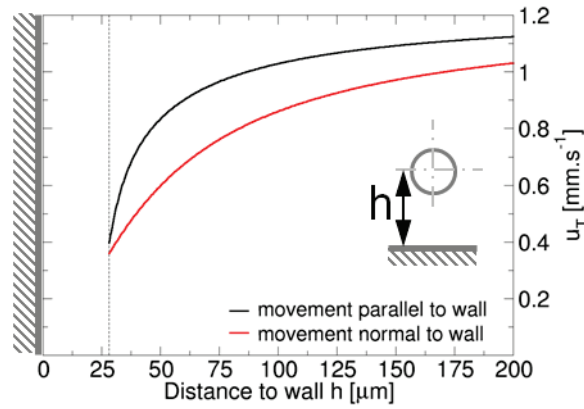


Figure 3.20: Influence of channel wall on settling velocity for horizontal and vertical flow, dashed vertical line indicates center of particle touching the channel wall

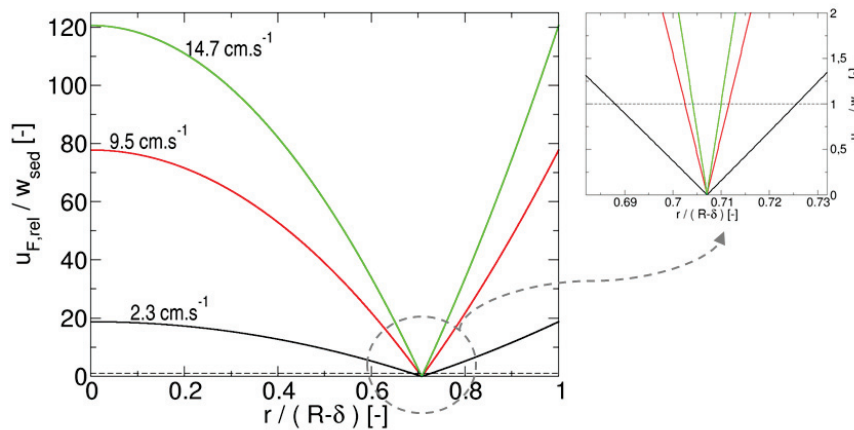


Figure 3.21: Relative fluid velocity compared to particle settling velocity for different two phase velocities. The ratio was plotted against a non-dimensional tube radius $\frac{r}{R-\delta}$ to account for the different liquid film sizes. The dashed line indicates the threshold $\frac{U_{F,rel}(r^*)}{u_T} > 1$

5% of the area the velocity ratio falls below the defined threshold meaning that the fluid velocity is lower than the settling velocity. It seems that even though for a small area the fluid velocity is indeed not sufficient enough to lift the solid particles, the majority of the fluid field exceeds the settling velocity. Also, visually, particles were never observed to not be able to follow the streamlines at position 1. This criteria cannot be the reason for the large amount of particles settled on the tubing bottom for certain experiments. In general, even for low two phase velocities it was not observed that circulating particles would settle at any point. Point 4 can be decisive imagining that the particle is accelerated towards the wall and due to its high inertia is not capable to follow the streamlines towards point 3 but settles. To judge this scenario, more details on the flow profile are necessary. However, as mentioned before, settling was generally not observed.

For **vertical flow** the procedure is similar. Representative operating points for the detected flow patterns were chosen. The selected positions for the detailed analysis are illustrated in Figure 3.22. As the settling velocity was found to be negligible compared to the overall fluid velocity, only the "turning points" 1 and 2 are interesting. The focus is especially to investigate the difference between homogeneously suspended particles and conditions where the particles populate mainly the center of the slug. Therefore the centrifugal force as a special form of

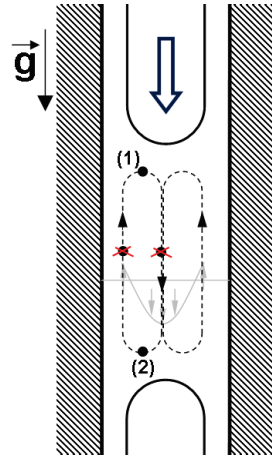


Figure 3.22: Chosen characteristic points for simplified force analysis for “slurry Taylor” flow in vertical oriented tubing.

inertial force is taken into consideration here.

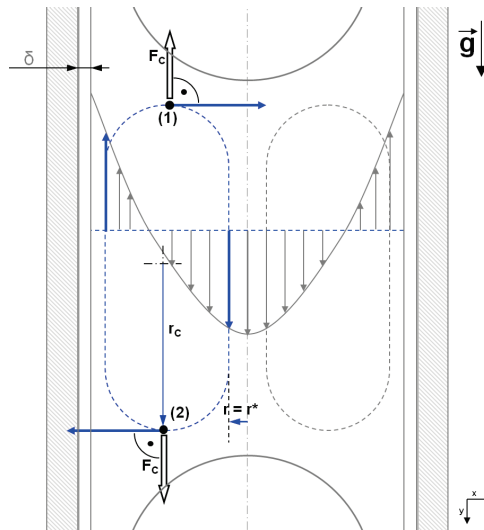
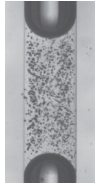
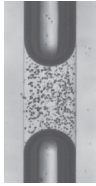
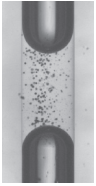
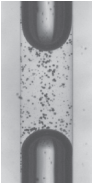



Figure 3.23: Illustration of simplified flow profile for selected positions in vertical flow.

The centrifugal force is effective on objects moving along a circular path and acts perpendicular to the angular velocity away from the rotation center (Figure 3.23, [120]). Following the same approach as for horizontal flow, the absolute velocity is assumed to be constant along one recirculation loop. The centrifugal force being proportional to the distance between the object and the rotation center, the maximum impact of the centrifugal force would be close to the tubing wall, for solid particles following the outer streamline. The distance between the center of the loop and this outer streamline is approximated by half of the channel radius. The centrifugal force is compared to the submerged weight ($\vec{F}_G - \vec{F}_B$) of the particle. The assumption is, that if the centrifugal force is more important than the submerged weight, particles are pushed towards the channel wall, leaving thus the center depopulated. The threshold is hence

$$\frac{\vec{F}_G - \vec{F}_B}{\vec{F}_C} < 1 \quad (3.30)$$

Table 3.4: Effect of two phase velocity on the capability of fluid field to keep particle in motion. Importance of centrifugal force compared to submerged weight $(F_G - F_B)/F_C$ for selected operating points. Pure ethanol flow, $w_S = 5 \text{ g L}^{-1}$.

					
L_{slug} [mm]	3.7	1.9	2.3	2.3	1
u_{TP} [cm s^{-1}]	2.33	5.24	7.4	15.64	31.4
$(F_G - F_B)/F_C$ [-]	3.78	0.74	0.37	0.08	0.02

The results are illustrated in Table 3.4. While for the lowest two phase velocities employed (2.3 cm s^{-1}) the ratio is in fact higher than 1 ($\frac{F_G - F_B}{F_C} = 3.8$) it shifts to values lower than 1 for higher velocities (for 15.6 cm s^{-1} $\frac{F_G - F_B}{F_C} = 0.08$). Nevertheless even for operating conditions which yield a particle placement detected as homogeneously suspended, the ratio is already below the threshold (for 5.2 cm s^{-1} $\frac{F_G - F_B}{F_C} = 0.74$). A possible explanation can lie in the simplifications and assumptions taken for the calculation of the centrifugal force.

3.3.4.3 Initiation of particle entrainment from the tubing bottom

While a possible interpretation for the occurrence of the detected flow regimes could be given for vertical flow, the simplified analysis of relevant forces could not explain the observed flow patterns in horizontal flow as the settling velocity compared to the mean fluid velocity seems generally negligible. Therefore it is necessary to investigate in a subsequent step if the velocity profile is eligible to initiate the entrainment of particles. The prevailing questions are consequently:

- Can the fluid flow entrain particles settled on the bottom of the tubing? By which mechanism?
- Can the amount of particles trapped in the liquid film in ethanol and ethanol/ glycerol flow be directly explained by the increase of liquid film thickness due to increasing two phase velocity?

The initiation of particle transport plays an important role in several different fields such as sedimentation technology (rivers, propagation of sand dunes), cleaning of heat exchangers, pneumatic and hydraulic conveying [118]. Different mechanisms are defined for the initiation of movement as illustrated in Figure 3.24.

- horizontal movement
 - sliding of particles, reported especially for non-spherical particles [115]
 - rolling of particles, reported for spherical particles [15, 115]
- vertical movement:
 - hydraulic lift [51, 115]
 - lift as a result of a torque balance around a pivot point [4, 56, 115]

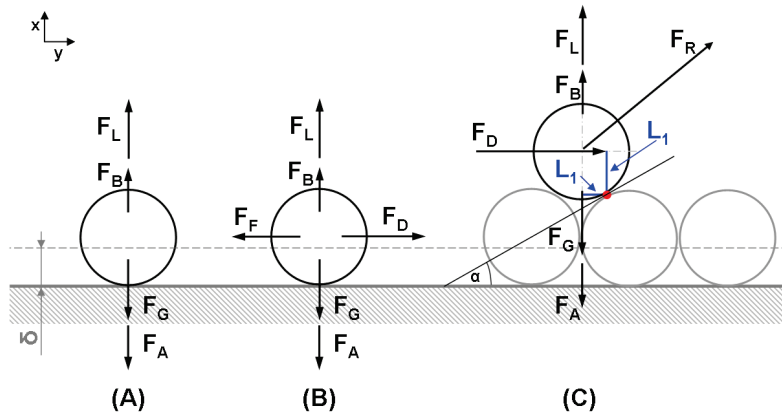


Figure 3.24: Different mechanisms for particle entrainment and the corresponding relevant forces: (A) lift, (B) sliding, (C) rolling and lift, illustrations based on [4, 26, 90, 115, 119].

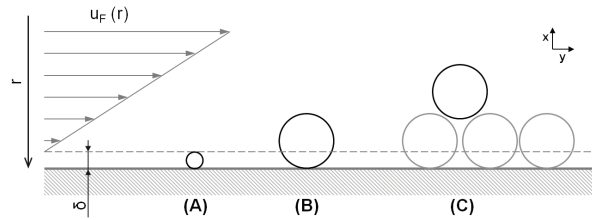


Figure 3.25: The solid particle can be completely settled in the liquid film (A), partially (B) or freely exposed to the liquid flow (C).

Particles are reported to start first rolling or sliding [15, 115] before vertical movement begins. In the literature empirical or mechanistic models [115], usually for turbulent flow, are used to derive a correlation for the critical fluid velocity relative to the initiation of particle motion. According to the particular point of interest, a particle can be defined to be in motion if it starts moving horizontally or vertically.

Also the placement of the particle relative to the liquid film can play a crucial role, as the velocity in the film is considered to be zero. As illustrated in Figure 3.25 the particle can be situated completely in the liquid film, partially or not at all. First we consider that the particle is fully exposed to the flow, secondly the film thickness is estimated for different two phase velocities and compared to the mean particle size.

To estimate the effect of flow conditions on initiation of particle motion, vertical motion is considered to be crucial. The same flow conditions as previously (see 3.3.4.2) are chosen as an example and the analysis focuses on the lift force. The adhesive force is considered to be negligible. Saffman lift force and lift for a particle resting on a plane surface (Equation 3.16 and 3.15) are used to estimate, if the flow conditions allow the initiation of particle motion. The threshold condition is :

$$\frac{\vec{F}_G - \vec{F}_B}{\vec{F}_L} < 1 \quad (3.31)$$

As gravity, buoyancy and lift have all only a component in the vertical direction (Figure 3.24), in the following the notation of the forces is simplified to F . The lift force is proportional to the shear rate $\dot{\gamma} \sim \frac{\Delta u_F}{\Delta x}$ (Figure 3.25). For the lowest two phase velocity ($u_{TP} = 2.3 \text{ cm s}^{-1}$) the ratio $\frac{F_G - F_B}{F_{L,Saff}}$ and $\frac{F_G - F_B}{F_{L,resting}}$ is higher than 1 (see Table 3.5 and 3.5), indicating that particle entrainment due to lift is not possible. For higher velocities, the ratio quickly decreases ($u_{TP} = 14.7 \text{ cm s}^{-1}$: $\frac{F_G - F_B}{F_{L,Saff}} = 0.74$ and $\frac{F_G - F_B}{F_{L,resting}} = 1.27$). For these high velocities the

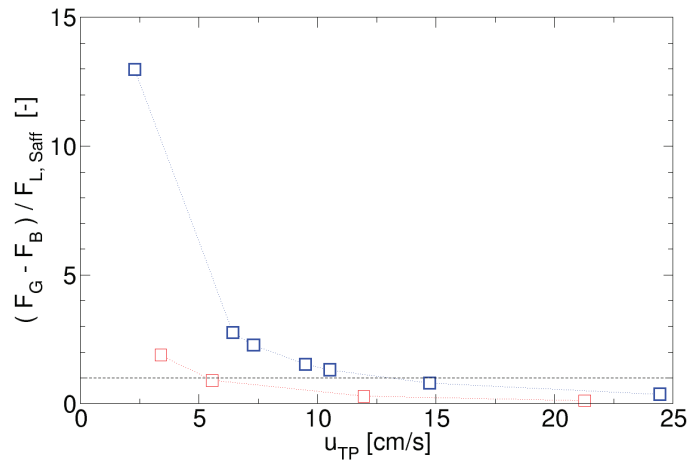


Figure 3.26: Effect of two phase velocity on the capability of fluid field to initiate particle movement. Importance of lift force compared to submerged weight. Results are given for ethanol (\circ) and ethanol/ glycerol (\square) flow. Pictures in Table 3.5 and 3.6 indicate the flow pattern for selected operating parameters.

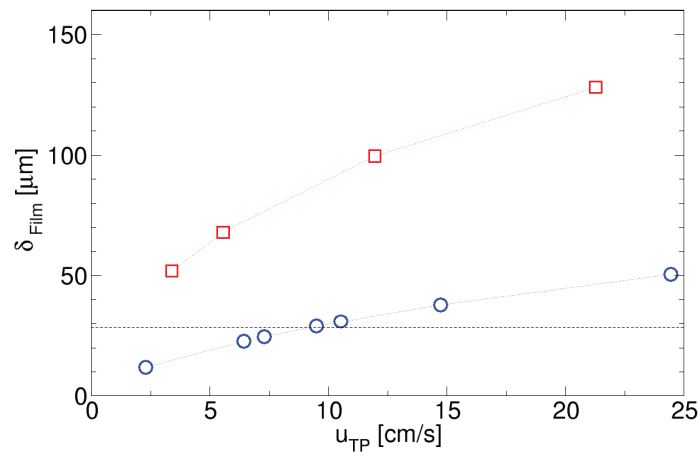


Figure 3.27: Effect of two phase velocity on the liquid film thickness for selected experimental points for ethanol and ethanol/ glycerol flow. Results are given for ethanol (\circ) and ethanol/ glycerol (\square) flow. Pictures in Table 3.5 and 3.6 indicate typical flow patterns for the selected parameters.

lift force is comparable to the submerged weight of the particle ($F_G - F_B$) (see Figure 3.26).

Lastly the influence of the film thickness is evaluated (see Figure 3.27) and its size compared to the mean particle diameter. For low two phase velocities and ethanol flow, the film thickness is rather low ($12 \mu\text{m}$ for $u_{TP} = 2.3 \text{ cm s}^{-1}$) that even an increase of 100% to account for the influence of gravity, particles are not entirely trapped in the liquid film. For increasing two phase velocities, the film thickness augments, and reaches for very high velocities the size of the particle diameter ($50 \mu\text{m}$ for $u_{TP} = 24.4 \text{ cm s}^{-1}$). This could explain the increased amount of particles settled on the bottom of the tubing for high velocities. For glycerol, the film thickness is already for low velocities comparable to the particle diameter, so that particles can possibly get trapped in it. This higher liquid film thickness for ethanol/glycerol compared to pure ethanol flow can be the reason for the non negligible amount of particles settled on the channel tubing for all operating conditions for glycerol flow.

Table 3.5: Effect of two phase velocity on the capability of fluid field to initiate particle movement. Importance of lift force compared to submerged weight $\frac{F_G - F_B}{F_L}$ and liquid film size for selected operating points. Pure ethanol flow, $w_S = 5 \text{ g L}^{-1}$.

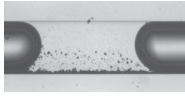
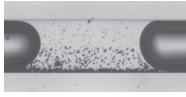
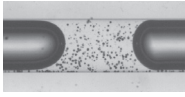
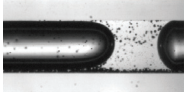
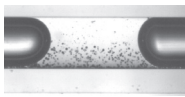
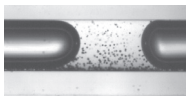
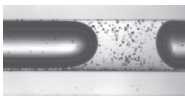
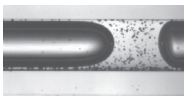
				
L_{slug} [mm]	3.1	3.2	2.0	1.3
u_{TP} [cm s^{-1}]	2.29	9.5	14.73	24.4
$\frac{F_G - F_B}{F_{L,Saff}}$ [-]	12.99	1.54	0.80	0.37
$\frac{F_G - F_B}{F_{L,resting}}$ [-]	52.11	3.04	1.27	0.46
δ_{film} [μm]	12	29	38	50

Table 3.6: Effect of two phase velocity on the capability of fluid field to initiate particle movement. Importance of lift force compared to submerged weight $\frac{F_G - F_B}{F_L}$ and liquid film size for selected operating points. Ethanol/ glycerol flow, $w_S = 5 \text{ g L}^{-1}$.

				
L_{slug} [mm]	2.82	1.9	1.81	1.26
u_{TP} [cm s^{-1}]	3.4	5.56	11.96	21.27
$\frac{F_G - F_B}{F_{L,Saff}}$ [-]	1.89	0.91	0.29	0.12
$\frac{F_G - F_B}{F_{L,resting}}$ [-]	16	6	1.3	0.4
δ_{film} [μm]	51.9	67.2	99.5	128

To sum up the analysis of relevant mechanisms, it seems that maintaining particles in motion does not represent an obstacle as liquid flow velocity in general is always larger than the settling velocity. In spite of this simplified analysis, it appears reasonable to say, that particles once suspended do not settle which can be confirmed by visual observations. The difficulty seems to lie in the initiation of motion. For low velocities, the submerged weight outweighs the induced vertical motion by the fluid. By increasing the two phase velocity, the shear rate increases and thus the lift force. It is difficult to define an exact threshold as a) the lift force is difficult to measure therefore a lot of different expressions exist and have been employed for the same purpose and b) the entrainment is a combination of lift due to shear stress and vertical fluid motion due to the approaching bubble. Nevertheless the analysis shows that wall shear rate may weigh more than settling of particles, at least for the particle and fluid properties considered in this study.

3.3.5 Flow pattern map

After analysing the relevant mechanisms effecting the placement of particles in the liquid slug, the results are used to establish a flow pattern map for horizontal and vertical flow.

3.3.5.1 Flow pattern map for horizontal flow

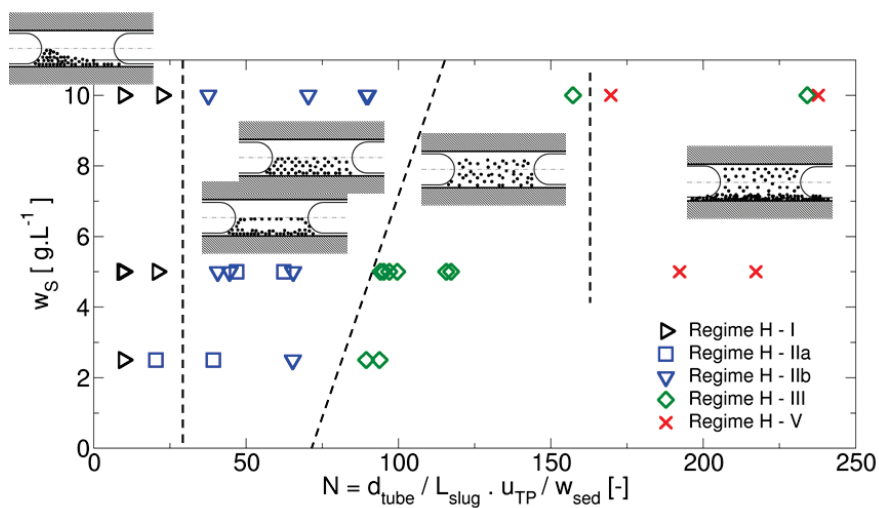


Figure 3.28: Flow pattern map for horizontal flow based on the work of Olivon and Sarrazin [95]. The dimensionless factor N (Equation 3.32) is used to discriminate between the different flow patterns.

In the literature two flow pattern maps for horizontal L-L "slurry Taylor" flow with particles transported in the discontinuous phase exist. Olivon et al. [95] used a dimensionless factor N which compares the time a solid particle needs to sediment over the entire slug height t_S with the time needed by the liquid droplet to travel one droplet length t_F .

$$N = \frac{t_S}{t_F} = \frac{d_T}{L_{slug}} \frac{u_{TP}}{u_S} \quad (3.32)$$

The flow pattern map obtained using this approach is illustrated in Figure 3.28. Olivon et al. [95] operate at very low two phase velocities (up to 1.46 cm s^{-1}) and expected a threshold of 1 for the transition between a regime where sedimentation and segregation prevails and a homogeneous pattern. Instead they found values higher than 1 ($N=5-100$) for the operating conditions studied, even though particles were reported to rest only close to the rear end of

the droplet. They explain the deviation with a recirculation efficiency affecting the time a particle needs to follow one total loop in the droplet. In agreement with them we found values for N higher than 1 and detect only a minor influence of the the solid concentration on the transition between the different regimes. For the transition between particles circulating in the lower part of the liquid slug and over the entire slug height, we found values around 80 for G-L flow compared to 32 for L-L flow reported by Olivon et al. [95]. The same analysis for the higher viscous experiments with the ethanol/ glycerol mixture led to very high values for N (150-2000) and the transition between semi-homogeneous and a homogeneous distribution was found at around 300.

However, comparing the settling velocity with the two phase velocity, or the corresponding characteristic times does not seem adequate if we consider that settling is negligible (see Section 3.3.4.2) and seems not to be the reason for the occurrence of the different observed regimes.

Another approach is the one from Kurup and Basu [73] who chose to work with the Shields parameter Θ which is often used in sedimentation technology to estimate the entrainment of sediment in fluid flow and the necessary critical velocity [26, 27, 56, 86, 115]. The Shields parameter (Equation 3.33) compares destabilizing forces (shear stress τ) with stabilizing forces (gravity and buoyancy) [81]:

$$\Theta = \frac{\tau}{gd_P(\rho_P - \rho_F)} \quad (3.33)$$

Shields presented his results not in form of a correlation but traced the dimensionless Shields parameter Θ as a function of boundary Reynolds number (Equation 3.34, [27, 115]) which takes the shear velocity u^* into consideration.

$$Re^* = \frac{u^* d_P \rho_F}{\mu_F} \quad (3.34)$$

$$u^* = \sqrt{\frac{\tau_0}{\rho_F}} \quad (3.35)$$

The shear stress τ is directly proportional to the velocity gradient of the fluid:

$$\tau = \mu_F \frac{\partial u}{\partial r} \quad (3.36)$$

For laminar flow (see Equation 3.23) the shear stress at the pipe wall is thus $\tau_0 = 8\mu_F u_{TP} / (d_T)$ which defines the Shields parameter as:

$$\Theta = \mu_F \frac{8u_{TP}}{d_T} \frac{1}{gd_P(\rho_P - \rho_F)} \quad (3.37)$$

To be able to represent the results for ethanol and ethanol/glycerol in one graph the product of Shields parameter and boundary Reynolds number $\Theta \cdot Re^*$ is used. As can be seen from Figure 3.29, the different regimes are well distinguished and the operating points for ethanol and ethanol/glycerol are situated in the same area. The fact that certain regimes overlap, may be caused by the difficult assignment to a certain regime as described earlier and the very progressive transitions. If only the Shields parameter is chosen, the same difficulty is detected as with the dimensionless number N : for two different fluids, the regimes are well represented but the values of the Shields parameter differ so much between low and higher viscous media that it is not possible to present both experimental sets on one graph nor to establish threshold conditions valuable for both media. Thorpe et al. [123] pointed out, that the critical velocity to suspend particles in stirred tanks as well as pipelines, is not a function

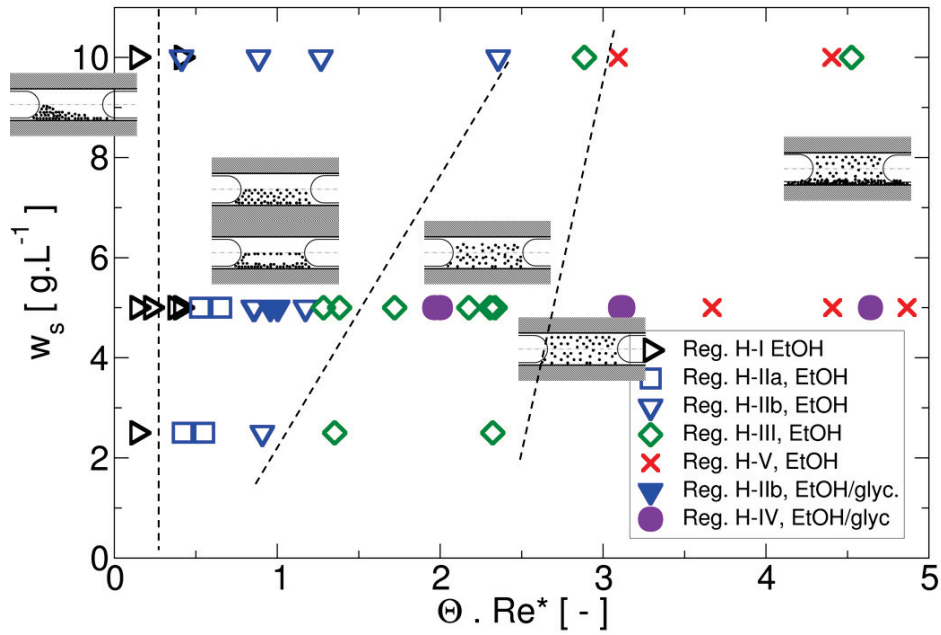


Figure 3.29: Flow pattern map for horizontal flow, the product of Shields parameter and shear Reynolds number is used to differentiate between the different detected flow patterns.

of viscosity. This might be the reason, why the attempt to represent the flow map using only N or Θ for both fluid media failed as both parameters are directly proportional to the liquid viscosity ($N \propto \mu_F$ as well as $\Theta \propto \mu_F$).

3.3.5.2 Flow pattern map for vertical flow

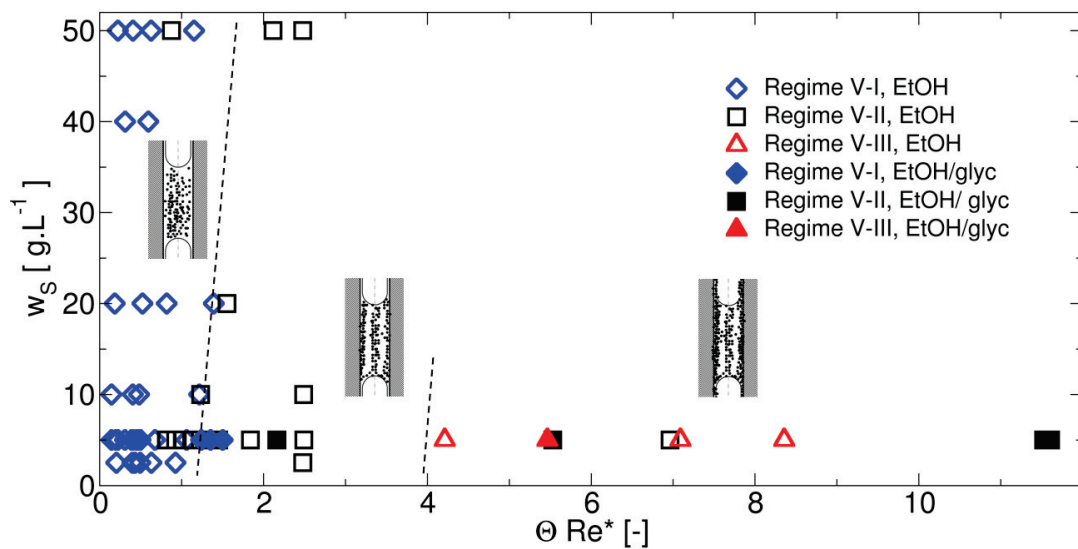


Figure 3.30: Flow pattern map for vertical flow, $\Theta \cdot Re^*$ is used to differentiate between the different flow patterns.

The flow map obtained in vertical flow using $\Theta \cdot Re^*$ is illustrated in Figure 3.30. The representation is not as good as for horizontal flow, but as mentioned earlier, the manual

detection of the flow regimes may have led to erroneous assignments especially for the higher viscous flow. As the initiation of motion was not an issue in vertical flow, and sedimentation is in the same axis as the flow direction, the different flow regimes are represented using the two phase velocity only. From Figure 3.31 it can be seen, that for the operating conditions tested here, the two phase velocity is sufficient to discriminate the different identified flow regimes.

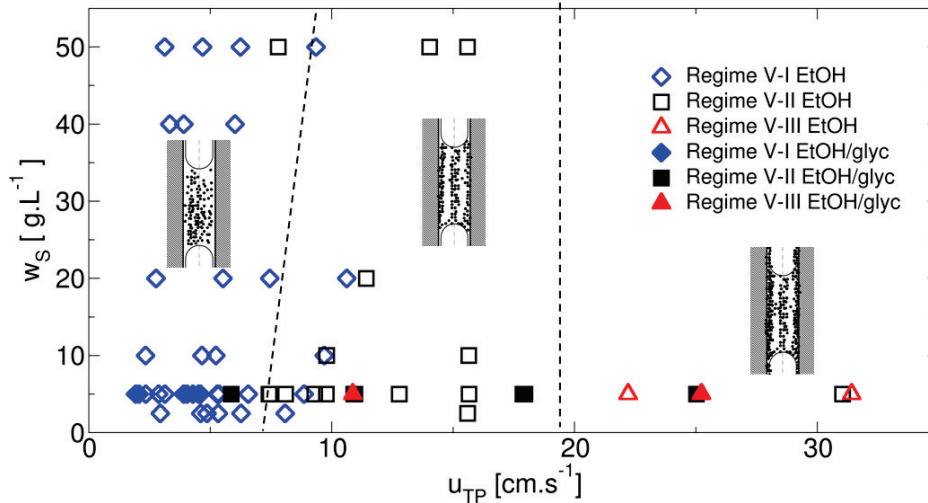


Figure 3.31: Flow pattern map for vertical flow, the solid charge is depicted in function of the two phase velocity.

3.4 CONCLUSION AND PERSPECTIVES

The hydrodynamics of G-L-S “slurry Taylor” flow were investigated for two distinct fluid couples: ethanol-nitrogen and ethanol/glycerol-nitrogen flow and the influence of solid charge and two phase velocity on particle placement was investigated for a horizontal and vertical oriented capillary. It was shown that even for high solid loadings up to 50 g L^{-1} a stable and repeatable solid supply is possible. For the operating conditions examined in this study, clogging of the contactor or the tubing fittings did not occur. For horizontal flow five different flow patterns were observed: for low two phase velocities particles circulate in the lower part of the liquid slug, a non negligible amount is settled on the channel bottom in a stationary bed. By increasing the velocity, particles start to populate also the upper part of the liquid slug, less particles are settled on the bottom and particle dispersion becomes more homogeneous. In vertical flow, even for very low velocities ($u_{TP} = 2 \text{ cm s}^{-1}$) particles were observed to be homogeneously distributed over the entire slug volume. For the operating conditions studied, no accumulation on the rear end of the gas bubble, nor sticking to the subsequent bubble nose was observed at any point, even for high solid loadings. Increasing the two phase velocity pushes the particles in the outer recirculation loop, depopulating the inner center of the vortex. For horizontal as well as vertical flow, at very high velocities ($u_{TP} > 15 \text{ cm s}^{-1}$) the amount of particles trapped in the stationary liquid film increases again. This indicates that there exists an upper border concerning two phase velocity for good operation conditions. A simplified analysis of the relevant mechanisms affecting particle placement showed that for the operating conditions studied, sedimentation appears to be only secondary. The injection of suspension phase as well as entrainment of settled particles is more influential. It was shown that a good representation of the detected regimes is possible by using a coefficient of Shields parameter and boundary Reynolds number $\Theta \cdot \text{Re}^*$ for horizontal flow. For vertical

flow, the two phase velocity seems to impact mostly the placement of particles. In agreement with the literature only a marginal influence of viscosity and solid charge was found.

In order to confirm the findings it is essential to broaden the study by investigating the influence of other operating parameters:

- Tubing diameter: To investigate the influence of shear rate and the impact of scale-up the diameter of the tube is an essential parameter. If initiation of particle motion and with it lift force really is discriminating for efficient particle suspension, by decreasing the channel diameter, shear rate increases and particles should be homogeneously suspended at lower two phase velocities. This is especially crucial for horizontal flow as bigger channel diameters might require higher two phase velocities for a homogeneous particle distribution.
- Slug length: The injector used for this study did not allow to create different slug length for the same velocity. By changing the ratio of gas and liquid flow rate, for low velocities only rather long slug length could be obtained (for $u_{TP} = 4.4 \text{ cm s}^{-1}$ slug length were between 3 and 6 mm) and for higher velocities only rather short slugs were observed (for $u_{TP} = 7.6 \text{ cm s}^{-1}$ slug length were between 1.6 and 2.3 mm). This is not sufficient to detect any influence of slug length on the behaviour of solid particles in the liquid slug. It might be interesting to observe particle motion in short slugs for low velocities and in long slugs for higher velocities.
- Material properties: Studying the influence of material properties on the placement of particles and the required conditions to achieve homogeneous suspension is necessary to predict if a certain reaction can be easily carried out in this new contact mode. Particles having a higher or lower density as the fluid media, hydrophilic particles in hydrophobic fluid media and the influence of gas phase (CO_2 vs. N_2) are parameters worth investigating.

3.5 SYMBOLS

Roman Symbols

a	m	distance between particle and wall
a	-	ratio of drag coefficient for particle settling close to a wall and drag coefficient for an freely settling particle in Stokes regime
A_P	m ²	particle cross section
c_P	-	“particle concentration”: ratio of white pixels to the total amount of pixels in one zone
\bar{c}_P	-	mean “particle concentration”
C_{AddM}	-	added mass coefficient
C_D	-	drag coefficient
$C_{D,Stokes}$	-	drag coefficient in Stokes regime
Ca	-	capillary number
\bar{d}_P	m	mean particle diameter
d_T	m	internal tubing diameter
F_{AddM}	N	added mass force
F_B	N	buoyancy
F_C	N	centrifugal force
F_D	N	drag force
F_G	N	gravity
F_H	N	history force
F_L	N	lift force
$F_{L,resting}$	N	lift force for particles resting on a plane
$F_{L,Saff}$	N	Saffman lift force
F_P	N	pressure force
g	m/s ²	gravitational constant, $g = 9.81\text{m/s}^2$
h	m	distance between wall and particle center
L_{slug}	m	slug length
m_P	kg	particle mass
N	-	dimensionless number, compares convection time with sedimentation time
p	bar	pressure
$p_{i,j}$	-	value of pixel at position i,j
Q_G	ml/min	gas flow rate
Q_L	ml/min	liquid flow rate
r	m	distance between particle position and centre-line of channel
r_P	m	particle radius
R	m	tubing radius
Re^*	-	boundary Reynolds number

Re_p	-	particle Reynolds number
$Re_{p,0}$	-	particle Reynolds number for settling velocity
t	s	time
$t_{B \rightarrow L_s}$	s	time a bubble needs to travel one slug length
T	°C	temperature
u^*	m s^{-1}	shear velocity
u_B	m s^{-1}	bubble velocity
u_F	m s^{-1}	fluid velocity
$u_{F,lam}$	m s^{-1}	fluid velocity (laminar flow)
$u_{F,rel}$	m s^{-1}	relative velocity between fluid and gas bubble
u_p	m s^{-1}	particle velocity
u_t	m s^{-1}	settling velocity
$u_{t,S}$	m s^{-1}	settling velocity for particles in high concentrated suspensions
u_{TP}	m/s	two phase velocity (sum of discontinuous and continuous superficial velocity)
V_S	$\text{m}_S^3 / \text{m}_L^3$	solid volume concentration
w_S	g/L	solid loading
$w_{glycerol}$	-	mass fraction of glycerol
y	m	distance, perpendicular to flow direction

Greek symbols

α	-	exponent in Richardson-Zaki equation for swarm settling velocity, in Stokes regime $\alpha = 4.65$
$\dot{\gamma}$	1/s	shear rate
δ	m	liquid film thickness
μ_L	Pa.s	dynamic viscosity of liquid phase
ρ_L	kg/m^3	liquid phase density
ρ_P	kg/m^3	particle density
σ	Nm	superficial tension
τ	s	time
τ	Pa	shear stress
Θ	-	Shields parameter

Abbreviations

G	gas phase
L	liquid phase
P	particle
R	reactor
S	solid phase

Part IV

LIQUID-SOLID MASS TRANSFER

PARTICLES TRANSPORTED IN CONTINUOUS AND DISCONTINUOUS PHASE OF “SLURRY TAYLOR” FLOW: IMPACT ON LIQUID-SOLID MASS TRANSFER

This chapter has been submitted for publication as A.-K. Liedtke, F. Scheiff, F. Bornette, R. Philippe, D. Agar and C. de Bellefon, Liquid-solid mass transfer for microchannel suspension catalysis in gas-liquid and liquid-liquid segmented flow. submitted to Industrial & Engineering Chemistry Research.

In the previous chapter different flow patterns for horizontal and vertical downward flow were presented and it was established that the distribution of solid particles is fundamentally different according to the flow direction: whereas for horizontal flow a minimum velocity is necessary to achieve a homogeneous distribution over the entire slug volume, for vertical flow this is not the case and particles are always equally distributed in the liquid slug. In a subsequent step the influence of particle placement and flow direction on mass transfer properties will be examined. Here we concentrate on the external liquid-solid mass transfer. The recirculation pattern in the continuous and the discontinuous phase of Taylor flow is essentially different and the localisation of particles (in the cont. or disc. phase) is thus an interesting parameter for L-S mass transfer studies. As for G-L Taylor flow the liquid phase is necessarily the continuous phase, the localisation of particles in the discontinuous phase can only be studied using L-L-S Taylor flow. For this reason we focus on liquid-solid mass transfer in gas-liquid and liquid-liquid “slurry Taylor” flow and propose to confront the mass transfer properties of solid particles circulating either in the dispersed phase in liquid-liquid or in the continuous phase of gas-liquid Taylor flow. In this chapter the influence of particle placement, recirculation pattern, two phase velocity and particle size on the liquid-solid mass transfer coefficient will be described for horizontal “slurry Taylor” flow. The L-L “slurry Taylor” flow experiments were carried out at the technical university Dortmund and belong to the doctoral research study of Frederik Scheiff ¹. If the flow direction and with it gravity (horizontal vs. vertical downflow) has an impact on the L-S mass transfer properties is examined in a subsequent chapter (see Section 5.1).

¹ This chapter is a collaboration work between the technical university Dortmund, Germany and the laboratory for catalytic processes, LGPC-CPE, Lyon, France. The L-L “slurry Taylor” flow experiments were carried out at the Laboratory for Chemical Reaction Engineering and belong to the doctoral research study of Frederik Scheiff. Contact: Prof. David W. Agar ✉ david.agar@bci.tu-dortmund.de

4.1	Introduction	71
4.2	Experimental	73
4.2.1	Principle	73
4.2.2	Set-up	75
4.2.3	Chemicals	76
4.2.4	Intrusive and non-intrusive electrical impedance based measurement devices	77
4.2.5	Mass transfer measurements in "slurry Taylor" flow	79
4.3	Results and discussion	80
4.3.1	Gas-liquid "slurry Taylor" flow	80
4.3.2	Liquid-liquid "slurry Taylor" flow	81
4.3.3	Comparison between G-L and L-L "slurry Taylor" flow	84
4.3.4	Conclusion and perspectives	85
4.4	Symbols	86

4.1 INTRODUCTION

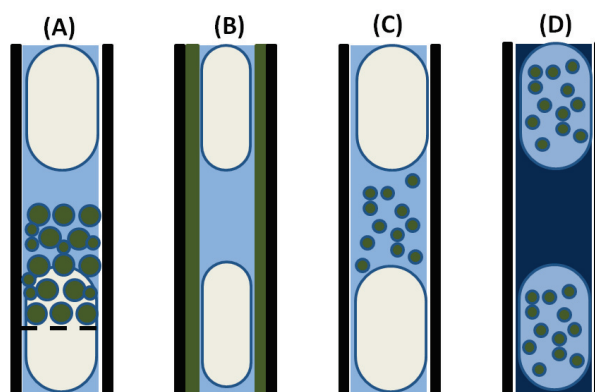


Figure 4.1: Examples for solid handling in micro or milli metric structures. (A) Micro fixed bed, (B) catalyst impregnation, "slurry Taylor" with particles transported in the continuous phase (C) and (D) discontinuous phase of Taylor flow.

The transportation and usage of micrometric particles is a subject which has been addressed in multi-phase micro reaction technology only recently [130]. Gas-liquid or liquid-liquid slug flows were studied quite extensively [10, 42, 55, 62, 72] and are accepted more and more as useful tools in continuous chemistry [43, 67]. Due to the fear of clogging or bridging of freely flowing particles [49, 50] the placement of the catalytic solid phase is, when necessary, usually resolved by immobilization either in form of a wall coating film or as a micro packed bed (see Figure 4.1 (A) and (B)). Coating the catalyst on the reactor wall asks for special procedures, unique for each catalyst type, and renders the reactor system less flexible as the removal due to deactivation or change in active phase is nearly impossible without damaging the reactor wall. Milli or micro fixed beds represent an alternative and hold interesting performances in mass transfer [59, 82, 84] but concerns might be the high linear pressure drop and complex hydrodynamics encountered (wall channelling, local dewetting, wettability problems, etc.) [84].

The approach to immobilize the solid phase is limited to catalytic systems and is not applicable when the product or the reactant itself is a solid. On the other hand the occurrence of solid particles other than catalysts should not be neglected [49]. A study by Roberge et al.[106] identified that out of 86 reactions carried out at Lonza, 31% could benefit from micro reaction technology but involve a solid phase (catalyst, reactant or product) and are thus considered to be difficult to perform in a micro reactor. Nanoparticles [67, 101, 104, 113, 117, 132] are handled quite frequently in micro reaction technology but the application of freely flowing solid particles from 10 up to 200 μm has so far only been studied rudimentarily as concerns regarding clogging due to bridging and/ or deposition [49, 50] prevailed. Taylor flow or segmented flow is a typical flow pattern often encountered in micro reaction technology due to its interesting properties [62, 72] namely:

- high surface to volume ratio
- nearly ideal plug flow conditions (Peclet numbers up to 1000 [125])
- circulation pattern in the liquid slug, intensive convective mixing

Joining beneficial properties of slug flow conditions and slurry reactors can be an interesting approach to transport the solid phase. The internal circulations occurring in the liquid slugs of G/L segmented flow [63, 72] or in the continuous and discontinuous phases of L/L

segmented flow [36, 57, 65] can be used to keep catalyst particles in motion and transport them in a stable three-phase flow. In this contact mode, catalysts can be easily removed from the reactor, simple and available commercial catalysts can be employed and good transfer performances can be expected due to the large interfacial areas available for both heat and mass transfer.

Segmented flow with slurry contact mode has been first mentioned in the literature in 2005 [33–35] and first studies were oriented mainly to the demonstration of this new contactor's applicability and interesting performance [13, 35, 80, 128]. Few investigations were addressed to hydrodynamic studies and gave first qualitative results on the placement of solid particles under varying operating conditions [73, 95]. Numerical studies on liquid-liquid and gas-liquid "slurry Taylor" flow [17, 29, 58] are also prove for the interest in this new contactor type. So far more studies focus on the transport of a liquid-solid suspension in an inert liquid continuous phase. The main argument for the preference to place the solid particles in the dispersed phase is the hindered danger of clogging as the particles are not in direct contact with the reactor wall [50, 95, 101, 109] due to the discontinuous phase. Nevertheless, for gas-liquid-solid applications the liquid phase is necessarily the continuous one.

So far the performance of this new contactor type was basically evaluated by comparing the conversion of a fast G-L-S or L-L-S reaction obtained in "slurry Taylor" flow with the conversion obtained in a classic stirred tank reactor. Nevertheless it is crucial to investigate mass transfer properties. Cai et al. [16] investigated the influence of solid charge and nature of solid phase on G-L mass transfer for G-L-S "slurry Taylor" flow. Very fine particles were chosen for this study ($d_p = 2 \mu\text{m}$ to $12 \mu\text{m}$) and the mass transfer of CO_2 into pure water was investigated. They observed that the G-L mass transfer was enhanced especially for hydrophobic activated carbon particles which would stick to the G-L interface and contribute to mass transfer due to the shuttle mechanism. We concentrate on liquid-solid mass transfer in gas-liquid and liquid-liquid slurry-Taylor flow and propose to confront the mass transfer properties of solid particles circulating either in the dispersed phase in liquid-liquid or in the continuous phase of gas-liquid Taylor flow (see Figure 4.1 (C) and (D)). Hence, either the continuous liquid or the gas phase is treated as chemically inert and only applied for inducing recirculation vortices in the suspension to mimic the real 3-phase reactive flow.

Common methods to characterize liquid-solid mass transfer of mobile particles are

- the dissolution of calibrated solid particles of β -naphthol or benzoic acid [60]
- acidic ion exchange particles and neutralisation reaction of caustic sodium hydroxide solutions [48, 98]
- fast, mass transfer limited three-phase reactions (hydrogenation of α -methyl styrene [88], oxidation of glucose [127]), knowing the transfer coefficient for the G-L or L-L transfer and the intrinsic kinetics

The production of calibrated particles between $60 \mu\text{m}$ to $200 \mu\text{m}$ and their detection and size analysis seems not suitable and sufficiently precise. We chose to work with ion exchange particles as this method is quite simple to implement and allows for a direct determination of the external L-S mass transfer coefficient. Ion exchange particles were recently used to investigate L-S mass transfer in L-L "slurry Taylor" flow by Scheiff et al. [110].

In G-L and L-L Taylor-flow the principle is the same: two non miscible phases (two liquids or a gas and a liquid) encounter each other and form a segmented flow pattern where the

disperse phase (gas bubble or liquid droplet) occupies with its height nearly the whole tubing diameter. Only a thin liquid film connects the two liquid slugs in front and behind the disperse phase. Depending on tubing and liquid properties regarding hydrophobicity and interfacial tension in L-L Taylor flow an aqueous phase can be either continuous or discontinuous. In G-L Taylor flow, the gas phase is the discontinuous phase and the liquid forms the continuous phase. In some conditions (water-air Taylor flow in Teflon tubing for example) the liquid film dries out so that both, gas and liquid form a dispersed phase [20, 75, 76, 112].

The objectives of this article are to present liquid-solid mass transfer coefficients and Sherwood numbers in gas-liquid and liquid-liquid "slurry Taylor" flow and to confront mass transfer properties for solid particles transported in either the disperse or the continuous phase. Dealing with particles in the continuous phase of G-L and the discontinuous phase of L-L Taylor-flow two phenomena have to be accounted for :

- G-L Taylor flow can be operated at higher two phase velocities than L-L Taylor flow
- the flow pattern in the continuous phase and the discontinuous phase are not necessarily comparable.

The recirculation patterns encountered in both, G-L and L-L Taylor flow are depicted in Figure 4.2. Due to the thin liquid film, the gas bubble moves with a velocity higher than the mean liquid flow. The maximum velocity of the liquid phase though is higher than the bubble velocity. As the liquid is confined between two bubbles, two counter rotating vortexes are formed [122, 124]. The vortexes fill the entire space between two subsequent bubbles and with increasing Capillary number the film thickness increases and the center of the rotation is moved towards the centreline of the tubing until at $Ca > 0.47$ the vortex vanishes [125]. In the droplets in L-L Taylor flow, the recirculation pattern depends strongly on the liquid properties (viscosity, superficial tension): two counter rotating vortexes were observed but also subvortexes in the rear end and close to the nose of the droplet [28, 31, 36, 39, 65]. In the continuous phase of either L-L or G-L flow only one vortex is present.

In literature flow regime transitions for G-L or L-L flow in micro or milli metric tubes are often given in form of Weber numbers. The dimensionless Weber number is defined as $\frac{\rho u^2 d_T}{\sigma}$. G-L and L-L Taylor flow are both located at similar Weber numbers for gas and liquid phases (around 1) [2, 21, 134]. While the surface tension is in the same order of magnitude, due to the high density difference of the gas and liquid phase this leads to operating velocities far lower for L-L flow than G-L Taylor flow where higher gas flow rates can be employed.

4.2 EXPERIMENTAL

4.2.1 Principle

To determine the liquid-solid mass transfer coefficient we work with the hydrogen form of a strong cationic ion resin and a simple neutralisation reaction (the overbar denotes the ion present in the solid ion exchange particle):



The reaction has been widely used to determine L-S mass transfer coefficients for mobilized particles [7, 48, 98, 108, 110] and the ion exchange process is well known [52].

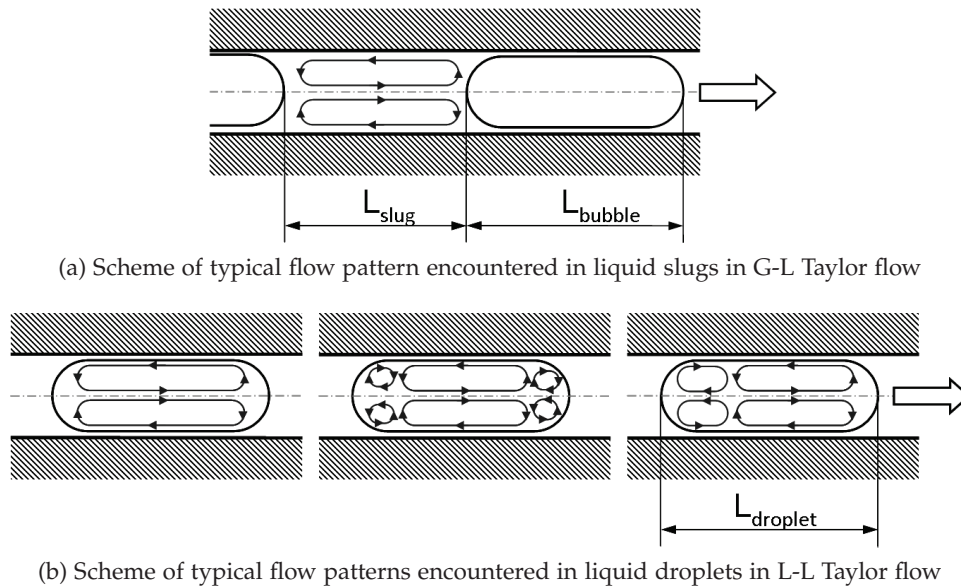


Figure 4.2: Typical flow patterns encountered in liquid slugs in G-L Taylor-flow and in liquid droplets in L-L Taylor-flow

Four processes control the ion exchange:

1. the mixture of the suspension phase with the sodium hydroxide solution
2. external diffusion through the liquid film around the ion exchange particle
3. internal diffusion in the ion exchange particle
4. the "reaction" or the exchange of both ions in the ion exchange particle.

The suspension phase and the sodium hydroxide solution are brought in contact the same time the Taylor flow is formed, therefore the mixing of both phases has to be fast enough compared to the external L-S mass transfer and the overall residence time. In G-L Taylor flow the optimum operating parameters (inlet flow rates for suspension and sodium hydroxide solution) were verified by visual experiments with a pH-colour indicator. The mixing in L-L Taylor flow was verified experimentally and numerically [110]). Both were found to be fast enough.

For ion exchange processes, the exchange of the two ions itself has been proven to be quasi instantaneous [46, 52]. In dilute sodium hydroxide conditions and at low conversion of the ion exchanger the Na^+ concentration at the L-S interface is negligible compared to the bulk concentration [52]. In this conditions migration of Na^+ ions and internal transfer limitations can be neglected. The process can be considered to be controlled mainly by the diffusion across the external film. A simple, one dimensional model for stationary conditions was established (Figure 4.3).

For a differential volume element of the aqueous liquid slug/ droplet the material balance for the Na^+ ion is given by:

$$F_{Na^+,z} = N_{Na^+} \cdot S_{LS} + F_{Na^+,z+\Delta Z} \quad (4.3)$$

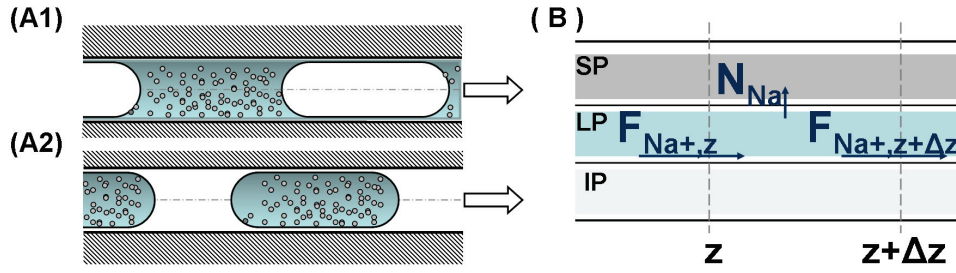


Figure 4.3: Illustration of the model used to estimate the external L-S mass transfer coefficient in G-L and L-L "slurry Taylor" flow (A). A volume element (B) is used to establish the material balance for the Na^+ ion between z and $z + \Delta z$. (LP: liquid phase, SP: solid phase, IP: inert phase)

The normalised molar flux N_A is transferred via the L-S exchange interface S_{LS} which can be defined by the solid hold-up ε_S , the specific surface area a_s and the liquid control volume ΔV_R .

$$S_{LS} = a_s \cdot \varepsilon_S \cdot \Delta V_R \quad (4.4)$$

$$N_{\text{Na}^+} = k_s \cdot (C_{A,ex} - C_{A,su}) \quad (4.5)$$

The molar flow can be defined as $F_{\text{Na}^+} = Q_L \cdot C_{\text{Na}^+}$, as the flow rates are assumed constant. The surface concentration of the sodium hydroxide ion is negligible compared to the bulk concentration and the material balance results in:

$$Q_L \frac{dC_{\text{Na}}}{dz} = -k_s \cdot C_{\text{Na},ex} \cdot a_s \cdot \varepsilon_S \cdot S_T \quad (4.6)$$

The length is linked to the residence time by the fluid velocity: $z = u_{TP} \cdot \tau$ so that the conversion profile as a function of time can be given as:

$$X_{\text{NaOH}}(\tau) = 1 - \exp\left(-\frac{3\varepsilon_S}{1 - \varepsilon_S} k_s \cdot \tau\right) \quad (4.7)$$

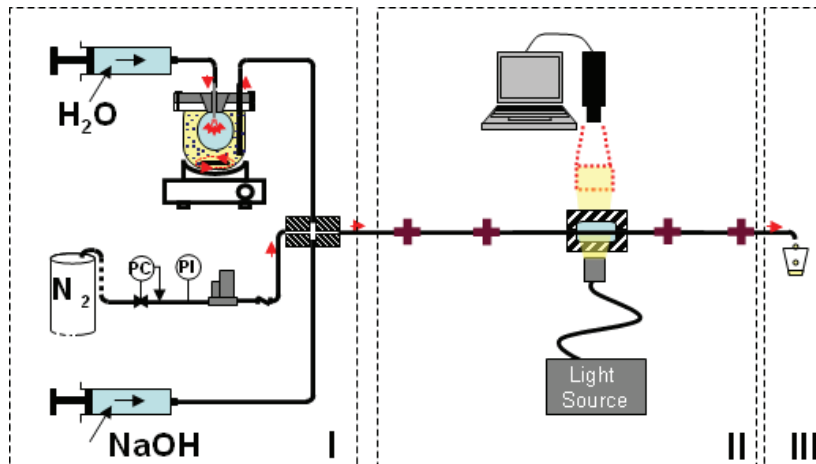
4.2.2 Set-up

Figure 4.4 gives a global view of the experimental set-up used for L-S mass transfer measurements and can roughly be divided in three main parts: A fluid and suspension supply system (I), the reactional section for L-S mass transfer measurements and a section (III) for sampling and waste collection. The fluid and suspension supply section is similar to the ones described in earlier works [80, 109, 110]. In-house built 4-port connectors (Figure 4.5) are used to mix the aqueous suspension of ion exchange particles with the sodium hydroxide solution and to generate the slug flow. The ratio $\frac{Q_{\text{NaOH}}}{Q_{\text{H}_2\text{O}} + Q_{\text{NaOH}}}$ was kept constant for all mass-transfer experiences (0.5 for L-L and 0.4 for G-L flow). The reactor used in this study consists in a simple horizontal PFA (G-L) or FEP (L-L) capillary tubing with an internal diameter of 1.65 mm for G-L and 1.6 mm for L-L flow. For G-L flow, 4 conductivity cells (in-house built, see Figure 4.6a) were installed in series over a total length of 1.5 m (15, 50, 100 and 150 cm downstream from the injector). For L-L flow, one sensor (C4D-sensor, Figure 4.6b [110]) was used and to obtain a concentration-time profile the capillary length was adjusted between 0.05 m to 0.5 m.

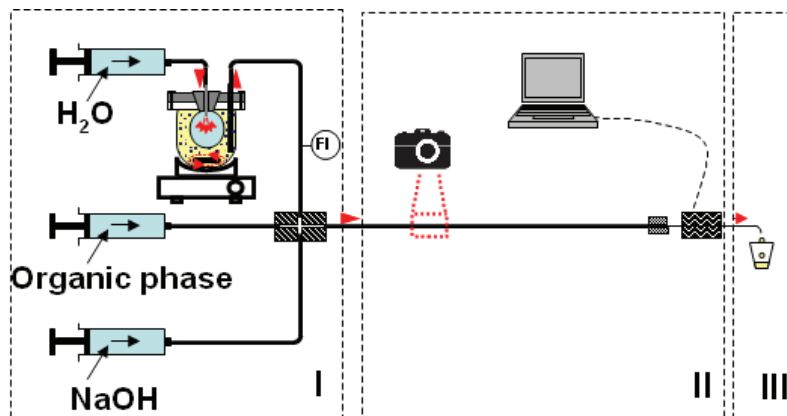
In G-L flow a visualization cell, filled with distilled water, is used to adapt the refractive index of the PFA tube in order to obtain high quality movies and pictures with a high speed camera (Optronis CR600x2, Solini 7:1 modular zoom, 0.9x-6.34x). In L-L flow snapshots of disperse

slugs and particle placement were taken with a CCD camera (Canon PowerShot A640, Canon GmbH) approximately 20 cm downstream from the point of slug generation. Stationary particle placement was attained instantaneously at the applied operating conditions.

The liquids were supplied with syringe pumps (Harvard apparatus PHD 4400 for G-L and LDP-5, BD Labortron and NE1010, New Era Pump Systems Inc. for L-L flow) and the gas phase was fed by mass flow controllers (Brooks instruments 58505 for flow rates higher 10 mL min^{-1} and Bronkhorst "el flow" for flow rates lower 12 mL min^{-1} for nitrogen). The operating conditions can be found in Table 4.1.



(a) Experimental set-up used for G-L "slurry Taylor" flow experiments



(b) Experimental set-up used for L-L "slurry Taylor" flow experiments

Figure 4.4: Experimental set-up used for G-L and L-L "slurry Taylor" flow experiments: (I) injection zone for gas/liquid and liquid-solid suspension; (II) reaction and visualization zone; (III) sample collection zone.

4.2.3 Chemicals

Cation exchange beads (Dowex 50Wx8, Sigma-Aldrich, 200-400 Mesh and 100-200 Mesh) were used in their original particle size as well as sieved to size fractions. The ion exchange particles were thoroughly pretreated by repetitive washings with 1N solution of NaOH and HCl as well as EtOH [53]. The particles were then stored in their H^+ form either in deionized water (G-L) or dried for 12 h at 70°C and stored dry (L-L). The ion exchange particles were regarded as spheres.

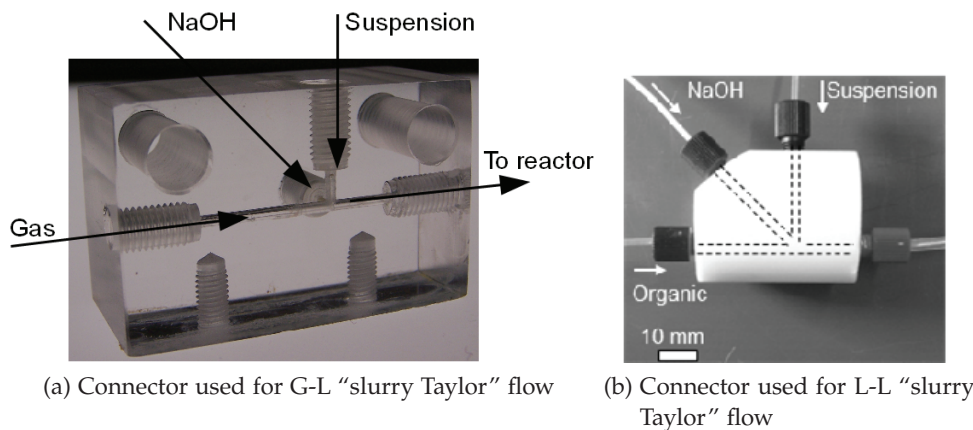


Figure 4.5: In-house fabricated 4-port connectors for suspension mixing and slug flow generation, fluids were injected as indicated on the picture, a) T-junction used in G-L flow, PMMA, internal diameter 1.6 mm, b) Y-junction used for L-L flow, Teflon, internal diameter 1.6 mm.

For G-L flow the inert medium was nitrogen and for L-L flow two different organic solvents were used to obtain different recirculation patterns: toluene (VWR International) and n-hexanol (Merck KGaA) were used as received. For the suspension phase, sodium hydroxide solutions (G-L: 0.01N standard solution, Alfa Aesar, L-L: 1N, Merck KGaA) and deionised water were used (L-L) as well as a mixture of deionised water and absolute ethanol (G-L, VWR chemicals). For G-L flow, due to the hydrophobic nature of the Teflon tubing, unsteady flow occurs when pure water is used. The liquid phase forms rather plugs than slugs [20, 75, 76, 112] and the liquid film dries out for high gas flow rates or after a certain time on stream (here after approximately 20 min). This translates in an oscillating flow (possibly linked to the alternating harsh pressure oscillations between liquid and gas phase) which is not suitable for estimating mass transfer coefficients. To improve the wettability of the liquid phase in G-L flow 0.255 wt% of liquid leak detector (Snoop, Swagelook, < 5% surfactant, nature not detailed by the supplier) was added to the ethanol/water mixture as adding a small quantity of ethanol alone did not suffice. Due to the small amount of surfactant, density and viscosity was considered to be unchanged and equal to the water/ ethanol mixture.

The liquid properties are listed in table 4.2.

4.2.4 Intrusive and non-intrusive electrical impedance based measurement devices

4.2.4.1 Intrusive measurement for G-L "slurry Taylor" flow

In gas-liquid flow the concentration of the sodium ions was measured using an in-house fabricated conductivity cell roughly based on the description in the literature [14, 37, 99]. A PEEK cross (Upchurch 0.5 mm inner diameter) was used to connect the electrodes with the reaction tube. Therefore one axis was drilled to 1.6 mm to match the inner diameter of the tube (Figure 4.6). Two platinum wires (technical wire, 0.5 mm diameter, Acros Organics) served as electrodes and were flush-mounted and connected to the cross with Upchurch fittings and a PFE tubing sleeve. The wires were connected to a function generator (TTi TG330) and over a 1 k Ω resistance to a data acquisition system (Graphtec midiLogger GL900). To avoid undesirable electrochemical processes like total polarization inducing measurement perturbation, an alternating current with a frequency of 1.36 kHz and a voltage of 20 V was applied. The voltage measured across the resistance as well as the exciting signal is recorded with a data logger which allowed for each measurement a total of 10⁶ data points and a sampling every 10 μ s. As a consequence, around 100 slugs could be covered by one measurement. Four con-

Table 4.1: Operating conditions applied in G-L and L-L “slurry Taylor” flow experiments for L-S mass transfer measurements.

	G-L flow	L-L flow
Inert phase	N ₂	toluene, n-hexanol
Q_{inert} [mL min ⁻¹]	1 - 12	0.5-3.25
Suspension phase	20 wt% EtOH in H ₂ O	H ₂ O
Q_{susp} [mL min ⁻¹]	1.5 - 7	1-2.6
Q_{NaOH}/Q_{susp} [-]	0.4	0.5
Q_{susp}/Q_{inert} [-]	0.35 - 1.67	1
$C_{NaOH,0}$ [mol L ⁻¹]	0.004	0.005
Solid phase	Dowex50Wx8	Dowex50Wx8
$d_{P,swollen}$ [μm]	40-200, 90-125	63-80, 80-90, 90-125, 125-160
w_{cat} [g L ⁻¹]	6-9	5
$n_{IE,0}/n_{NaOH,0}$ [-]	5.5 - 10	2.5-3.8
X_{IE} [%]	10	27-40
Tubing	PFA	FEP
d_T [mm]	1.65	1.6
Pressure	ambient	ambient
Temperature	ambient	ambient

Table 4.2: Properties of the liquids and mixtures used for L-S mass transfer measurements in G-L and L-L “slurry Taylor” flow.

	H ₂ O	EtOH/H ₂ O
x_{H_2O} [-]	1	0.911
$w_{surfactant}$ [-]	-	0.00013
ρ_L [g cm ⁻³]	0.9971	0.9659 [64]
μ [Pa s]	0.00089	0.0018 [64]
Sc	698	2298
D_{Na+} [m ² s ⁻¹]	$1.28 \cdot 10^{-9}$ [83]	$0.803 \cdot 10^{-9}$ [83]

ductivity cells were placed in series to obtain a concentration-time profile with a single run. The signals were then treated numerically to detect the mean voltage for each slug.

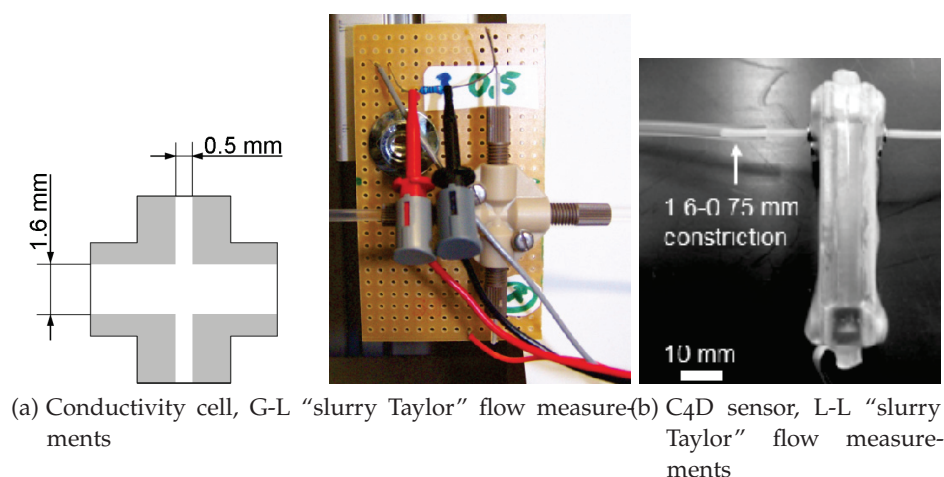


Figure 4.6: Devices for conductimetric measurements applied in L-S mass transfer experiments, a) in-house fabricated conductivity cell used in G-L “slurry Taylor” flow, b) C4D sensor (eDAQ Pty. Ltd.) and flow constriction used in L-L flow

4.2.4.2 Non intrusive measurement for L-L “slurry-Taylor” flow

In liquid-liquid flow, the neutralization of sodium hydroxide is monitored by C4D-based (Figure 4.6b, contactless, capacitively coupled) concentration measurements. A noninvasive, commercial C4D-sensor (excitation with 2 MHz, 5V and sampling frequencies of 3 kHz) in 1/16 OD plastic capillaries has been utilized, together with a data recorder and Chart™ software package (ET125 general purpose headstage, e-corder®ER125 C4D detector, eDAQ Pty. Ltd.). The sensor principle is reviewed in [22]. The sensor is only applicable to 1/16 OD capillaries. Hence, the reactional capillary (1/8 OD) was attached to the sensor tube and the sensor was placed 2 cm downstream from the reduction (1.65 to 0.75 mm ID). The distance between the restriction and the sensor is very short and the sensor is placed at the exit of the reactor. Therefore the effects due to the restriction on the L-S mass transfer can be neglected.

4.2.5 Mass transfer measurements in “slurry Taylor” flow

In G-L flow, before each run the ion exchange particles were placed in a filter funnel and converted to the H⁺-form (batch equilibria with 3x50ml 1N HCl) and subsequently washed with deionized water until the effluent solution had reached a neutral pH. The remaining water was removed as complete as possible by filtration under vacuum. In G-L flow experiments the ion exchange particles were used in their humid state whereas in L-L flow dry particles were employed. The desired solid weight was placed together with the solvent in the suspension feeding system which was then sealed and connected to the reactor.

Before each experimental run a calibration of the conductivity cells/ sensor with particle free alkaline solutions was carried out. A stabilisation time of 10 minutes was allowed before the syringe pump connected to the suspension feeding system was launched at the desired flow-rate. The inert fluid rates (gas or organic phase) were set first, then the sodium hydroxide flow was started and a time corresponding to approximately 5 residence times was considered as sufficient to reach a steady state. The conductivity measurements were launched, a video/ picture of the Taylor flow was captured and a sample collected at the reactor exit for further analysis. The operating conditions tested are listed in Table 4.1. The collected samples

were used to determine the actual solid charge within the slugs either by drying (G-L) or by reverse titration with a 0.01 N NaOH solution knowing the total exchange capacity (L-L). For both configurations uncertainties for the estimation of the L-S mass transfer coefficient have two sources: firstly fluctuating solid charge during the experimental run and its correct determination. For G-L flow experiments, this uncertainty was estimated to effect the mass transfer coefficient by 5%. Also the determination of the sodium hydroxide concentration has to be accounted for. For G-L flow for example the measured voltage deviates slightly from slug to slug. The impact on the L-S mass transfer coefficient due to this deviation is around 5%. The standard deviation for the mass transfer coefficient for G-L flow is thus 10% and for L-L flow the standard deviation was estimated to be around 38% for water-toluene and around 52% for water- n-hexanol flow.

4.3 RESULTS AND DISCUSSION

4.3.1 Gas-liquid "slurry Taylor" flow

4.3.1.1 Effect of two phase velocity

Figure 4.7 illustrates the influence of two phase velocity u_{TP} on the mass transfer coefficient. Pictures are added to give an example for the dispersion of solid particles in the liquid slug.

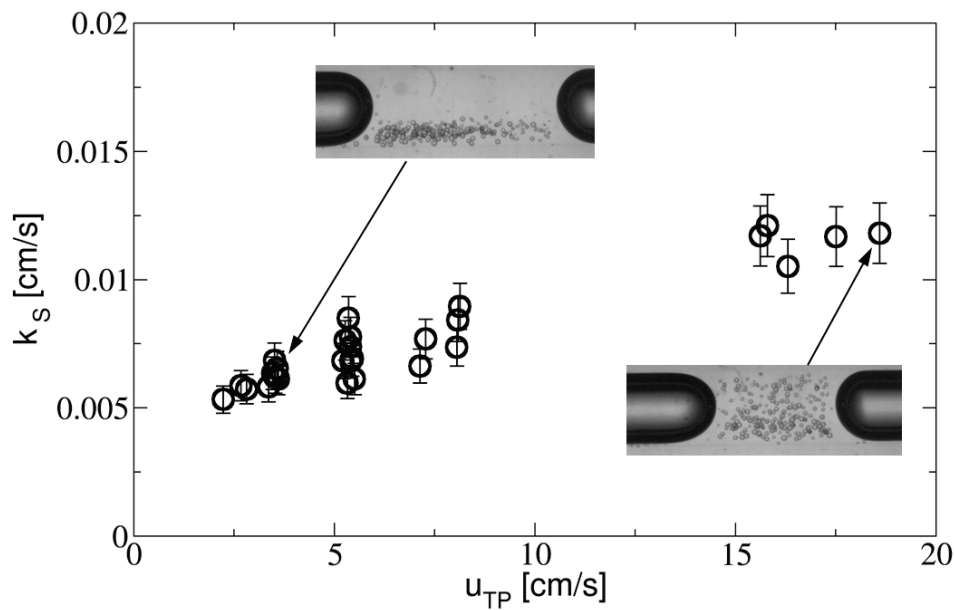


Figure 4.7: External L-S mass transfer coefficients estimated for gas-liquid "slurry Taylor" flow, pictures illustrate particle behaviour for two velocities, the two phase velocity was defined as $u_{TP} = u_{slug} + u_B$.

For the lowest two phase velocities (2.2 cm s^{-1} to 3.6 cm s^{-1}) used in this study, the resin particles are only placed in the lower part of the liquid slug and a slight accumulation in the rear part can be detected. An increase of velocity leads first to a better distribution of the particles in the lower part of the slug and successively to the appearance of particles in the upper part of the liquid slug. The increase of two phase velocity from 2.2 cm s^{-1} to 8.2 cm s^{-1} does not only affect the distribution of particles in the liquid slug but leads also to a steady increase of the mass transfer coefficient (from 0.0053 cm s^{-1} to 0.0089 cm s^{-1}). At two phase velocities higher than 15 cm s^{-1} homogeneously distributed particles over the entire

slug height could be observed. However the mass transfer coefficient for these high velocities (15 cm s^{-1} to 19 cm s^{-1}) appears to stay constant at 0.0118 cm s^{-1} ($\pm 1.6\%$). It seems as if once sufficient energy input for homogeneous distribution is reached, an increase of the fluids flow rate beyond this limit, does not lead to further increase the mass transfer coefficient.

4.3.1.2 Effect of slug length

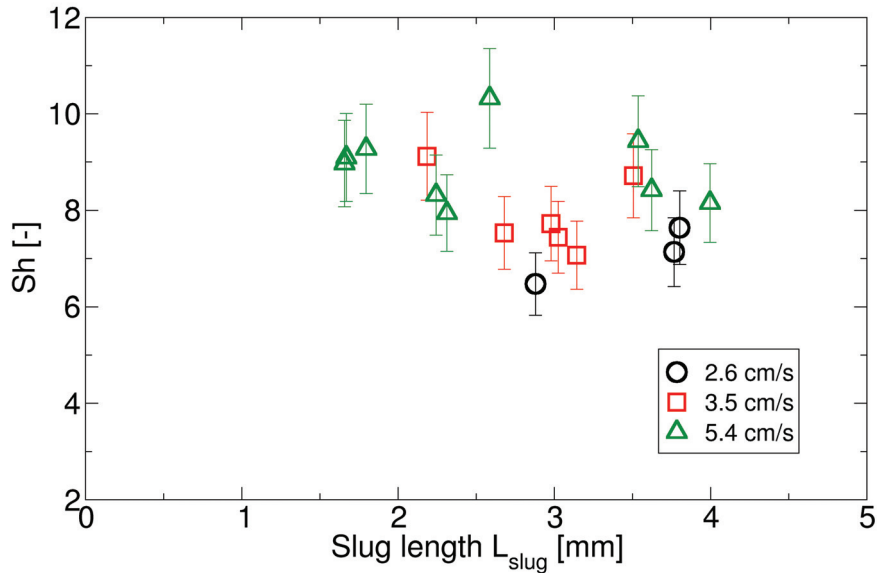


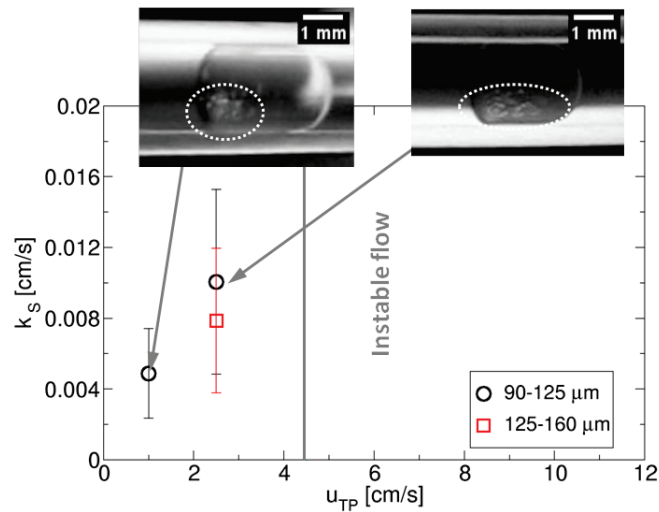
Figure 4.8: Influence of slug length on the Sherwood number for different two phase velocities in G-L “slurry Taylor” flow

For certain velocities the ratio of gas and liquid flow rate was varied to produce different slug length with the same cross mixer in order to investigate the influence of slug length on L-S mass transfer. By varying the ratio of gas and liquid flow rate the length of the liquid slug but also of the gas bubble is affected. However, the bubble length does not influence the ion exchange nor the placement of solid particles. Therefore this is an adequate method to investigate the influence of slug length on the external L-S mass transfer. For three bubble velocities (2.6 cm s^{-1} to 5.4 cm s^{-1}) different slug length between 1.7 mm to 4 mm were obtained. In Figure 4.8 the influence of slug length on the Sherwood number is illustrated. Within the accuracy of our measurements no influence on the Sherwood number could be detected. Also no real difference in hydrodynamics between small and longer slugs at these operating conditions was observed.

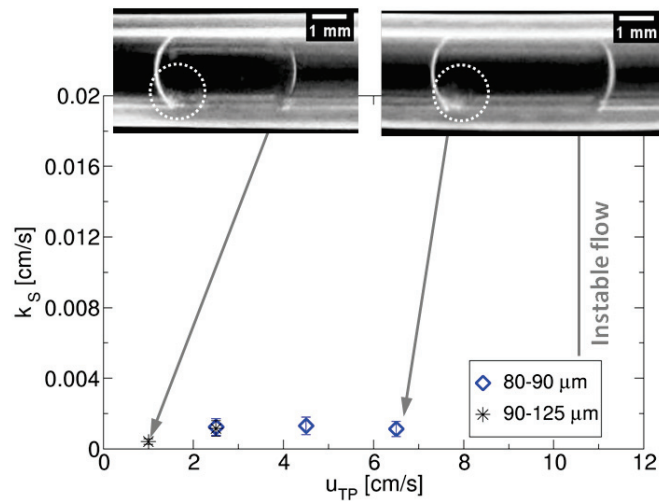
4.3.2 Liquid-liquid “slurry Taylor” flow

4.3.2.1 Effect of two phase velocity

The influence of two phase velocity on the mass transfer coefficient is illustrated for n-hexanol-aqueous flow in Figure 4.9 a). Representative snapshots of the flow conditions are added to illustrate typical particle behaviour. In n-hexanol-aqueous L-L “slurry Taylor” flow, the resin particles are circulating in the lower part of the liquid droplet for the velocity range (1 cm s^{-1} to 2.5 cm s^{-1}) studied and it could be observed that particles accumulate slightly in the rear end of the droplet. Increasing the velocity from 1 cm s^{-1} to 2.5 cm s^{-1} leads to an increase of the mass transfer coefficient from 0.005 cm s^{-1} to 0.01 cm s^{-1} . For n-hexanol water the upper limit for stable slug flow conditions is situated quite low at 4.5 cm s^{-1} . Therefore it was not



(a) aqueous- n-hexanol flow



(b) aqueous - toluene flow

Figure 4.9: Effect of two phase velocity on external L-S mass transfer coefficient in L-L “slurry Taylor” flow, pictures indicate localisation of particles, a) aqueous- n-hexanol flow, b) aqueous - toluene flow.

possible to work with more homogeneously suspended solid particles and to investigate, if by further increasing the two phase velocity the L-S mass transfer coefficient increases. Irregular slug lengths impede mass transfer measurements beyond that threshold.

4.3.2.2 Effect of particle size

In the literature the L-S mass transfer coefficient was reported to be independent from particle diameter for large particles in two phase and three phase fluidized beds [8], liquid-solid horizontal pipe flow [48] and stirred tank reactors (for $d_p > 200 \mu\text{m}$) [47, 98]. For bubble columns a negative impact of particle size ($200 \leq d_p \leq 900 \mu\text{m}$) was found [108]. In stirred tank reactors a negative influence for fine particles ($< 100 \mu\text{m}$) was likewise detected. It was shown that very fine particles approach the theoretical limit of $Sh = 2$ [7, 9, 47]. The different behaviour for small and larger particles is explained by a change of governing mechanism. Asai et al. [9] showed that for particles $\gg 200 \mu\text{m}$ the mass transfer coefficient is proportional to $D_m^{2/3}$ ($k_s \propto D_m^{2/3}$) indicating boundary layer theory and for particles $< 27 \mu\text{m}$ the Sherwood

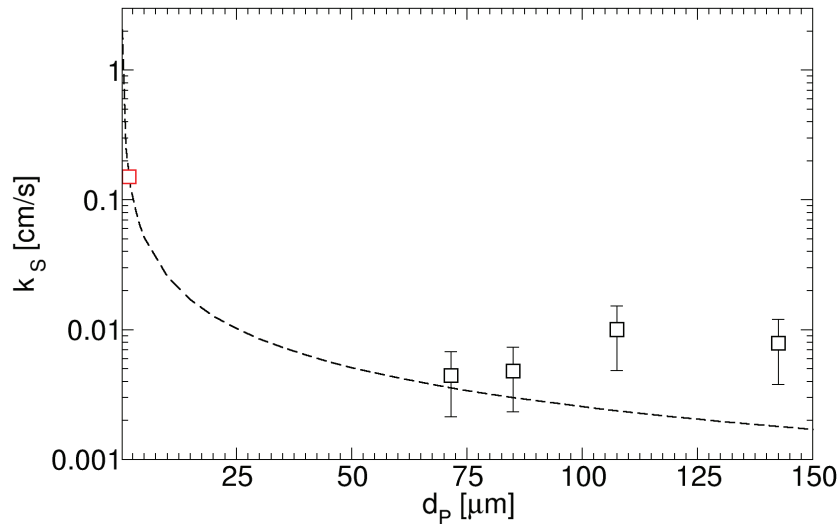


Figure 4.10: Influence of particle size on L-S mass transfer coefficient, black, square symbols represent results for aqueous - n-hexanol flow: the two phase velocity was kept constant at $u_{TP} = 2.5\text{cm/s}$, red circle symbol correspond to experiments with zeolith particles, experimental conditions are detailed in [110], $u_{TP} = 6.5\text{cm/s}$. The dashed line indicates the theoretical limit $\text{Sh} = \frac{k_s \cdot d_p}{D} = 2$.

number approaches its limiting theoretical value $\text{Sh} = 2$ which indicates that mass transfer occurs due to molecular diffusion and not turbulent diffusion.

The influence of particle size on the L-S mass transfer coefficient in “slurry Taylor” flow conditions was investigated for water - n-hexanol flow. The two phase velocity was kept constant and resin particles sieved into different size fractions (wet sieving) from $63\ \mu\text{m}$ to $160\ \mu\text{m}$ were used. The results are illustrated in Figure 4.10. Given the high errorbars, the obtained results have to be handled with care but it appears that our results reflect the tendency described in the literature: judging from the overall trend it appears that an increase of particle size leads to slightly increased Sherwood numbers. A possible explanation for this behaviour might be that smaller particles are more easily entrained by flow lines which leads to a reduction of relative velocity between particle and surrounding liquid. Similar to Asai et al. [9] we find that for small particles ($d_p < 70\ \text{m}$) the Sherwood number approaches 2.

4.3.2.3 Effect of inert fluid

Figure 4.9 b) displays the mass transfer coefficient k_s estimated for aqueous-toluene slug flow and gives pictures for typical particle behaviour. Contrary to aqueous-hexanol flow the transition of regular to irregular slug flow is at higher velocities ($u_{TP} = 10.5\ \text{cm s}^{-1}$). At small velocities of $1\ \text{cm s}^{-1}$, particles are entirely segregated in the lower rear cap. The resulting mass transfer is very low ($0.0013\ \text{cm s}^{-1}$). Not only film transfer, but also convective transport of sodium hydroxide by slow internal circulation within the slug can be attributed to this finding [110]. However, k_s inclines significantly at $2.5\ \text{cm s}^{-1}$. Still, particles segregate in the rear cap, but are mobile in the co-rotating subvortex. It is also observed that k_s remains constant for transport velocities higher than $2.5\ \text{cm s}^{-1}$. The snapshots indicate that the internal circulation is not accelerated sufficiently to provide any substantial change in particle behaviour.

The Sherwood number was calculated and found to be below 2 for water-toluene “slurry Taylor” flow ($\text{Sh} = 0.3\text{to}1$). These unsatisfying low results can possibly be attributed to the agglomeration of particles: the intense agglomeration hinders the diffusion of Na^+ ions to reach particles in the inner heart of the agglomerates [110]. To correctly determine the mass

transfer coefficient, the particle diameter of the non-agglomerated particles might be not sufficient and could be the cause for the very low mass transfer coefficients detected. Instead, a representative diameter for the agglomerates appears more appropriate, which is however unknown.

Comparison between water-toluene and water n-hexanol slug flow demonstrates that intensive circulation and high particle mobility promotes liquid-solid mass transfer. Changing the inert phase from toluene to n-hexanol increases the mass transfer coefficient by a factor of 10.

4.3.3 Comparison between G-L and L-L “slurry Taylor” flow

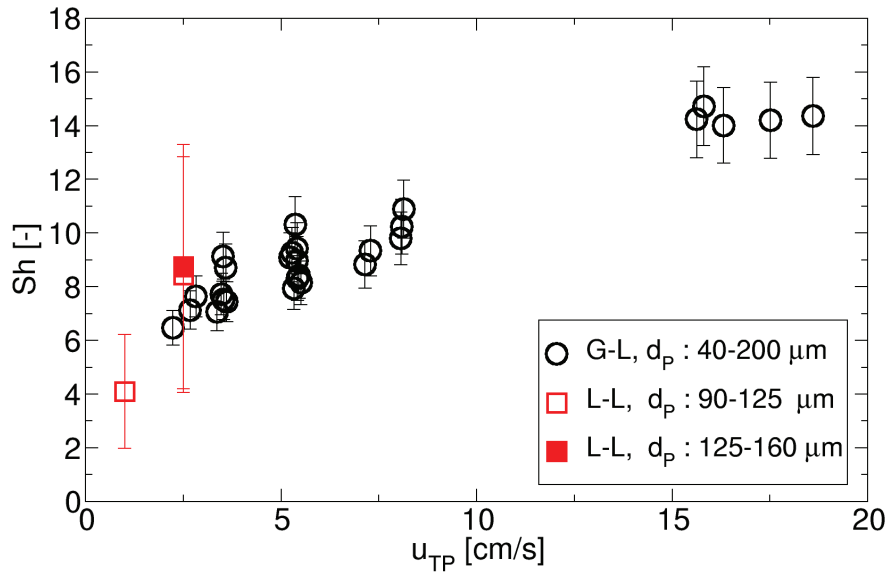


Figure 4.11: Comparison of Sherwood numbers obtained for G-L and L-L “slurry Taylor” flow, results obtained for aqueous - n-hexanol (L-L) and water/ ethanol-nitrogen flow (G-L), particle diameters as indicated in the graph.

The Sherwood numbers obtained in G-L and L-L “slurry Taylor” flow are depicted in Figure 4.11. To compare the L-S mass transfer properties of G-L and L-L “slurry Taylor” flow we concentrate first on the results obtained for aqueous - n-hexanol flow for L-L “slurry Taylor” flow. The main difference between G-L and L-L “slurry Taylor” flow is the higher operating range and thus the higher possible velocities which lead to better distribution and more effective recirculation of particles. Generally a more homogeneous particle recirculation pattern could be observed in G-L Taylor flow. Nevertheless, Sherwood numbers estimated for G-L and L-L “slurry Taylor” flow are in the same range for low velocities. This might indicate that once particles do not agglomerate but circulate freely in the liquid phase, it is not important if particles are distributed homogeneously in the entire slug/ droplet or if there is an accumulation in the lower part. Whereas for L-L flow the velocity can hardly be further increased (limit $u_{TP} = 6.5 \text{ cm s}^{-1}$) this velocity limit is only in the lower range for G-L flow. Here the total velocity could be increased from 2.8 cm s^{-1} to 19 cm s^{-1} and the Sherwood number doubled. Additionally the maximal velocity applied in these experiences does not correspond to the limit for Taylor flow conditions and it is possible to further increase the velocity. In both L-L and G-L flow an increase of velocity did not necessarily led to an increase of the L-S mass transfer coefficient. In G-L flow the Sherwood number appears to be constant ($Sh = 14.4 \pm 1.6\%$) for two phase velocities higher than 15 cm s^{-1} . Also for velocities higher than 15 cm s^{-1} particles are distributed homogeneously over the entire slug height. A

similar behaviour can be found for conventional reactors with mobilized particles: in stirred tanks k_s increases first rapidly for increasing velocities but beyond just suspended conditions augmenting the stirrer speed still increases k_s but its influence is reduced [98]. Ohashi et al [94] investigated the mass transfer for transported particles in horizontal L-S pipeflow and found that for low flow rates particles were mainly situated in the lower part of the tube and an increase of velocity did not lead to increase k_s . Only once a certain velocity was reached, k_s started to increase. Sanger and Deckwer [108] investigated the mass transfer in bubble columns and found that beyond a certain value of gas flow rate the mass transfer coefficient could not be further increased, this values roughly coincided with a change in flow pattern from homogeneous to heterogeneous churn-turbulent flow.

In G-L “slurry Taylor” flow the first increase of velocity leads to more and more homogeneously distributed particles but once the particles are well distributed over the entire slug height further increase of velocity does not influence the mass transfer coefficient any longer. A possible explanation is that the particles follow the liquid streamlines and even if the velocity is increased this does not influence the relative velocity between surrounding liquid and particle flow.

4.3.4 Conclusion and perspectives

The L-S external mass transfer was investigated for particles transported in the continuous phase of G-L and the discontinuous phase of L-L “slurry Taylor” flow. Mass transfer coefficients and Sherwood numbers were estimated using the transfer of sodium ion from aqueous solution to ion exchange particles. Overall, the Sherwood numbers obtained for “slurry Taylor” flow are comparable to those obtained in more conventional reactors with slurry catalyst. In bubble columns for example, for the same fluid and particle properties, Sherwood number from 14 to 20 can be calculated [108]). It was found that for aqueous-toluene L-L flow, particle agglomeration in the rear end of the liquid droplet leads to very low mass transfer coefficients ($k_s = 0.0012 \text{ cm s}^{-1}$). An increase of two phase velocity did not enhance particle circulation or de-agglomeration and had thus no influence on mass transfer coefficients. Once particles do not agglomerate but circulate freely in the aqueous phase, the Sherwood number increases with increasing two phase velocity. For aqueous - n-hexanol flow, the Sherwood numbers estimated for particles transported in the disperse phase are in the same range ($Sh = 4$ to 8.4 , $u_{TP} = 1 \text{ cm s}^{-1}$ to 2.5 cm s^{-1}) as for particles suspended in the continuous phase of g-l “slurry Taylor” flow ($Sh = 6$ to 9 , $u_{TP} = 2.2 \text{ cm s}^{-1}$ to 3.6 cm s^{-1}). Stable flow conditions for L-L “slurry Taylor” flow could be only achieved for velocities up to $u_{TP} = 4.5 \text{ cm s}^{-1}$. Increasing the two phase velocity in G-L “slurry Taylor” flow led to more and more suspended particles in the liquid slug and to an increase of the Sherwood number. However, once the particles are homogeneously suspended over the entire slug height ($u_{TP} > 8 \text{ cm s}^{-1}$) an increase of two phase velocity has no impact on the Sherwood number ($Sh = 14.4$). In conclusion, it seems that for freely circulating particles and no agglomeration phenomena, the recirculation efficiency and the occupied space of circulating particles has no effect on the L-S external mass transfer. At the low Reynolds numbers in Taylor flow, laminar conditions predominate and one could assume that therefore the primary source of slip velocity (between particle and surrounding liquid), and thus driving force for external L-S mass transfer, is the settling velocity of the solid particle.

To clarify these assumptions it is necessary to further investigate the l-s mass transfer coefficient in G-L and L-L “slurry Taylor” flow and the effect of recirculation pattern and efficiency. Employing other aqueous-organic phase couples might help to enlarge the operating range for L-L Taylor flow and to allow operating at conditions were the particles are homogeneously

suspended in the entire droplet. Also it might be interesting to study the influence of particle density to gain further insight on the influence of settling velocity on the L-S mass transfer coefficient.

4.4 SYMBOLS

Roman Symbols

a_s	m^{-1}	specific surface area
Ca	-	capillary number $Ca = \mu u_B / \sigma$
C_{Na}	mol L^{-1}	sodium hydroxide concentration
$C_{Na,ex}$	mol L^{-1}	sodium hydroxide concentration at the L-S interface
C_{Na}^*	mol L^{-1}	equilibrium sodium hydroxide concentration
$C_{NaOH,0}$	mol L^{-1}	initial sodium hydroxide concentration at the reactor entrance
d_p	m	particle diameter
d_T	m	internal tubing diameter
D_{Na+}	$\text{m}^2 \text{s}^{-1}$	diffusion coefficient of sodium hydroxide ions
F_{Na}	mol s^{-1}	molar flux of Na^+ -ions
k_S	m s^{-1}	L-S external mass transfer coefficient
$n_{IE,0}$	mol	initial molar amount of ion exchange site
$n_{NaOH,0}$	mol	initial molar amount of sodium hydroxide ions
N_{Na}	$\text{mol s}^{-1} \text{m}^{-2}$	normalised molar flux of Na^+ -ions
Q_{aqu}	mL min^{-1}	aqueous flow rate at the exit of the suspension supply unit before formation of Taylor flow
Q_{inert}	mL min^{-1}	flow rate of inert phase
Q_{NaOH}	mL min^{-1}	flow rate of sodium hydroxide solution at entrance of 4-port junction
Q_L	mL min^{-1}	flow rate of active liquid phase
Q_{susp}	mL min^{-1}	suspension flow rate $Q_{susp} = Q_{NaOH} + Q_{susp}$
S_{LS}	m^2	liquid-solid interface
S_T	m^2	channel cross section
Sc	-	Schmidt number $Sc = \mu / (\rho D)$
Sh	-	Sherwood number $Sh = k_s d_p / D$
u_B	m s^{-1}	bubble or droplet velocity
u_{TP}	m s^{-1}	two phase velocity (sum of discontinuous and continuous superficial velocity)
V_R	m^3	reactor volume
w_{cat}	g L^{-1}	catalyst loading
$w_{surfactant}$	-	mass fraction of surfactant
x_{H_2O}	-	molar fraction of water
X_{NaOH}	-	sodium hydroxide conversion

$z =$	m	length
<hr/>		
Greek symbols		
ε_S	-	solid volume per liquid slug (G-L) or liquid droplet (L-L)
μ	Pa s	dynamic viscosity
ρ_L	kg m ⁻³	liquid phase density
τ	s	residence time in reactor
<hr/>		
Abbreviations		
B		bubble
G		gas phase
L		liquid phase
P		particle
R		reactor
suso		suspension
S		solid phase
TP		two phase
<hr/>		

LIQUID-SOLID MASS TRANSFER IN HORIZONTAL AND VERTICAL THREE PHASE “SLURRY TAYLOR” FLOW

This chapter has been submitted for publication as A.-K. Liedtke, F. Bornette, R. Philippe, C. de Bellefon, Correlation for liquid-solid mass transfer in gas-liquid-solid three phase “slurry Taylor” flow. submitted to Industrial & Engineering Chemistry Research.

In Chapter 3 the influence of flow direction and thus gravity on particle placement was investigated and a fundamental difference between horizontal and vertical downwards flow was found: whereas for horizontal flow a minimum two phase velocity is necessary to ensure homogeneously distributed particles over the entire slug volume, for vertical flow even for very low velocities ($u_{TP} = 2 \text{ cm s}^{-1}$) particle distribution is homogeneous. For high velocities an interesting phenomena could be observed for vertical flow: solid particles follow mainly the outer streamlines where the velocity is the highest. A centrifugal force appears to be predominant and particles seem to be pushed towards the outer recirculation loop. To continue the investigation of external L-S mass transfer in “slurry Taylor” flow, the study is now expanded towards G-L vertical flow. This chapter is therefore dedicated to study the influence of flow direction, two phase velocity, solid loading and nature of the liquid phase for particles transported in the discontinuous phase of horizontal and vertical G-L “slurry Taylor” flow. The obtained results serve to propose a first correlation for the Sherwood number in “slurry Taylor” flow.

5.1	Introduction	90
5.2	Experimental	91
5.2.1	Principle	91
5.2.2	Set-up	91
5.2.3	Chemicals	92
5.2.4	Mass transfer measurements in “slurry Taylor” flow	92
5.3	Results and discussion	94
5.3.1	Influence of two phase velocity and flow direction on the liquid-solid mass transfer	94
5.3.2	Influence of solid loading and particle diameter	95
5.3.3	Correlation for L-S mass transfer coefficients in horizontal and vertical “slurry Taylor” flow	97
5.3.4	Conclusion and perspectives	98
5.4	Symbols	99

5.1 INTRODUCTION

Three phase gas-liquid-solid (G-L-S) reactions [24, 111, 126] play an important role in the chemical industry. For several reasons the use of suspension catalysts is often the best option for the handling of the solid phase. Suspension catalysts ensure efficient heat removal and prevent the build-up of hot-spots, fine powders provide good external surface area and enhanced internal mass transfer. By enabling to introduce fresh catalysts in a continuous way, they ensure an easy and on-line replacement or regeneration of fast deactivating catalysts. Three phase G-L-S contactors with suspension catalysts often employed in chemical industry are in general bubble columns, stirred tank reactors and fluidized or ebullated beds [24, 103, 111, 126]. Suspension reactors are generally characterized by good mass and heat transfer capacities, low power requirements due to overall low pressure drops and their high flexibility. However they also promote a high degree of back-mixing for the liquid and solid phases and gas phase for stirred tanks which can be a drawback for reactions with selectivity issues and/ or when very high conversions are required. For applications which require the use of suspension catalysts (e. g. deactivation, need for high internal mass transfer) and where the reaction kinetics demand plug flow behaviour, up to now no industrial technology is able to answer both demands simultaneously.

A typical flow pattern often encountered in micro reaction technology due to its interesting properties [62, 72] is the so-called Taylor flow or segmented flow. Taylor flow is characterized by a high surface to volume ratio, nearly ideal plug flow conditions (Peclet numbers up to 1000 [125]) and a circulation pattern in the liquid slug ensuring intensive convective mixing.

One possible solution to provide a G-L-S reactor system which combines suspension catalysts, plug flow behaviour and excellent heat and mass transfer capacities is the "slurry Taylor" flow where solid particles are transported in form of a suspension in the liquid slugs of G-L Taylor flow. The internal circulations present in the liquid slugs [63, 72] can be used to keep catalyst particles in motion and transport them in a stable three-phase flow. The concept of freely circulating micro-metric particles in milli-metric tubes is still quite recent as concerns regarding clogging due to bridging and/ or deposition [49, 50] generally prevail. Often studies centred on the demonstration of the interesting performances of this contact mode [13, 33–35, 80, 128] or focused on hydrodynamic investigations [73, 95]. So far only very few studies addressed mass transfer properties. Cai et al [16] investigated the influence of very fine particles ($d_p = 2\ \mu\text{m}$ to $12\ \mu\text{m}$) on the G-L mass transfer. First results for the L-S mass transfer in "slurry Taylor" flow appeared just recently for horizontal flow [79, 110].

Previous hydrodynamic studies of particle dynamics in G-L "slurry Taylor" flow in horizontal and vertical oriented capillaries showed a fundamental difference regarding particle behaviour: for a given solid in horizontal flow a minimal fluid velocity is necessary to homogeneously suspend the solid in the liquid phase whereas in vertical flow, particles are equally distributed in the slug even for low velocities. The objective of this article is therefore to investigate if this difference in hydrodynamics translates to the L-S mass transfer properties. The external L-S mass transfer coefficient is thus investigated for horizontal and vertical flow. Furthermore, the influence of fluid velocity, solid charge, fluid media and particle diameter is investigated and a first correlation is proposed.

5.2 EXPERIMENTAL

5.2.1 Principle

The experimental method to determine the L-S mass transfer has been described in Section 4.2.1. The hydrogen form of a strong cationic ion resin and a simple neutralisation reaction with sodium hydroxide aqueous solution (the overbar denotes the ion present in the solid ion exchange particle) are used:

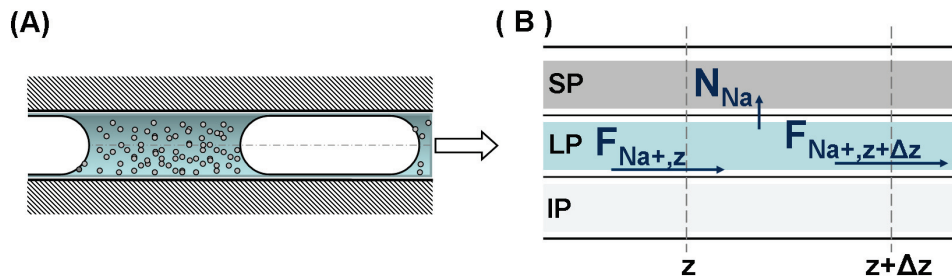


Figure 5.1: Illustration of the model used to estimate the external L-S mass transfer coefficient in G-L “slurry Taylor” flow (A). A volume element (B) is used to establish the material balance for the Na^+ ion between z and $z + \Delta z$. (LP: liquid phase, SP: solid phase, IP: inert phase)

Ion exchange and the neutralisation reaction of dilute caustic sodium hydroxide solutions have been widely used to determine L-S mass transfer coefficients for mobilized particles [7, 48, 98, 108, 110] and the ion exchange process is well known [52]. The exchange of the two ions is considered to be quasi instantaneous [46, 52] and the Na^+ concentration at the L-S interface is negligible low compared to the bulk concentration [52] for dilute sodium hydroxide conditions and at low conversion of the ion exchanger. It is therefore possible to neglect the migration of Na^+ ions and internal transfer limitations and consider the process to be mainly controlled by the diffusion across the external film. The one dimensional model for stationary conditions has been derived in Section 4.2.1 and is illustrated in Figure 5.1. The conversion profile allows to calculate the L-S mass transfer coefficient according to Equation 5.3.

$$X_{NaOH}(\tau) = 1 - \exp\left(-\frac{3\varepsilon_S}{1 - \varepsilon_S} k_s \cdot \tau\right) \quad (5.3)$$

5.2.2 Set-up

The experimental set-up is illustrated in Figure 5.2 and has been described in Section 4.2.2. The aqueous suspension of ion exchange particles is mixed with the sodium hydroxide solution in an in-house built 4-port connector which generates the slug flow. The reactor consists in a simple PFA capillary tubing with an internal diameter of 1.65 mm. Four (horizontal) respectively five (vertical) conductivity cells (in-house built, Section 4.2.4.1) were installed in series over a total length of 1.5 m to 1.8 m. The tubing was straightened and placed with the help of a water-level as horizontal/ vertical as possible. In order to obtain high quality films and pictures a visualization cell, filled with distilled water is used to adapt the refractive index of the PFA tube. The liquids were supplied with syringe pumps (Harvard apparatus

PHD 4400) and the gas phase was fed by mass flow controllers (Brooks instruments 58505 for flow rates higher 10 N mL min^{-1} and Bronkhorst "el flow" for flow rates lower 12 N mL min^{-1} for nitrogen). The operating conditions can be found in Table 5.1.

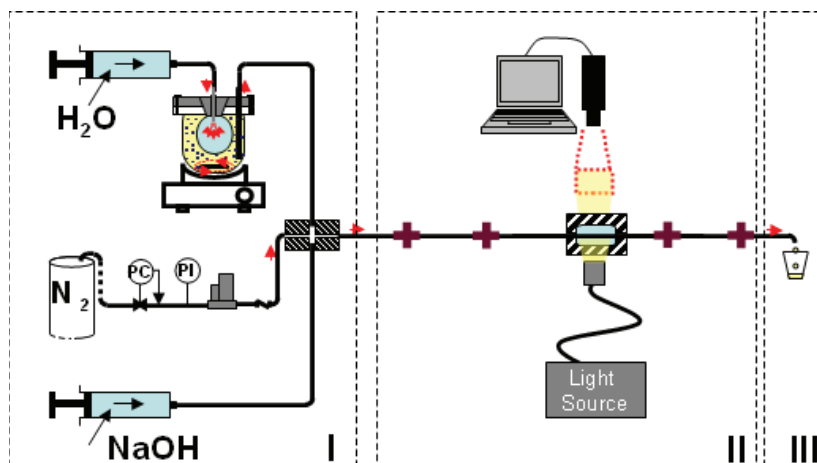


Figure 5.2: Experimental set-up used to determine L-S mass transfer coefficients of "slurry Taylor" flow: (I) fluid supply, 4-port junction for generation of segmented flow; (II) reaction and visualization zone; (III) sample collection zone.

5.2.3 Chemicals

Cation exchange beads (Dowex 50Wx8, Sigma-Aldrich, 200-400Mesh, 100-200 Mesh) were used in their original particle size as well as sieved to size fractions. The ion exchange particles were thoroughly pretreated by repetitive washings with 1N solution of NaOH and HCl as well as EtOH [53]. The particles were then stored in their H^+ form in deionized water. The inert medium was nitrogen. For the suspension phase, sodium hydroxide solutions (0.01N standard solution, Alfa Aesar) and mixtures of deionised water and absolute ethanol (VWR chemicals) or acetonitrile (Sigma Aldrich) were used. In order to ensure steady and invariable flow conditions 0.255 wt% of liquid leak detector (Snoop, Swagelook, < 5% surfactant, nature not detailed by the supplier) was added to the ethanol/water mixture. Due to the small amount of surfactant, density and viscosity was considered to be unchanged and equal to the water/ ethanol mixture. The liquid properties are listed in Table 5.2. The diffusion in the acetonitrile/ water mixture was estimated to be close to the diffusivity in pure water as the viscosity is approximately the same.

5.2.4 Mass transfer measurements in "slurry Taylor" flow

The employed protocol for the mass transfer measurements is similar to the one described in Section 4.2.5. The desired solid weight of the pretreated ion exchange particles (washed, converted to the H^+ -form, filtrated under vacuum) was placed together with the solvent in the suspension feeding system. A calibration of the conductivity cells with particle free alkaline solutions was carried out before each experimental run. The gas and liquid flow rates were set and a time corresponding to approximately 5 residence times was considered sufficient to reach steady state. The conductivity measurements were launched and for each run a video of the Taylor flow was captured and one to three samples were collected at the reactor exit for further analysis. The operating conditions tested are listed in Table 5.1. The standard deviation for the mass transfer coefficient was considered to be around 10% accounting for the difficult

Table 5.1: Operating conditions applied in G-L “slurry Taylor” flow experiments for L-S mass transfer measurements. Experiments were conducted in two different fluid media: an aqueous-ethanol (EtOH/H₂O) and an aqueous-acetonitrile (ACN/H₂O) mixture.

	EtOH/H ₂ O	ACN/H ₂ O
Inert phase	N ₂	N ₂
Q_{inert} [mL min ⁻¹]	1-8	2-12
Suspension phase	20 wt% EtOH in H ₂ O	15.5wt % ACN in H ₂ O
$Q_{susp} = Q_{NaOH} + Q_{aqu}$ [mL min ⁻¹]	2	4-7
Q_{NaOH}/Q_{susp} [-]	0.4	0.4
Q_{susp}/Q_{inert} [-]	0.25-2	0.5-2
$C_{NaOH,0}$ [mol l ⁻¹]	0.004	0.004
Solid phase	Dowex50Wx8	Dowex50Wx8
$d_{p,swollen}$ [μm]	100	100, 160
w_{cat} [g L ⁻¹]	6-20	6
Tubing	PFA	PFA
d_T [mm]	1.65	1.65
Pressure	ambient	ambient
Temperature	ambient	ambient

Table 5.2: Properties of the liquids used for L-S mass transfer measurements in G-L “slurry Taylor” flow. The properties are given for ethanol/ water (EtOH/H₂O), acetonitrile/ water (ACN/H₂O) mixtures and for the sake of comparison also for pure water.

	H ₂ O	EtOH/H ₂ O	ACN/H ₂ O
x_{H_2O} [-]	1	0.911	0.926
$w_{surfactant}$ [-]	-	0.00013	-
ρ_L [g cm ⁻³]	0.9971	0.9659 [64]	0.9705
μ [Pa s]	0.000891	0.001781 [64]	0.00098 [129]
Sc	698	2298	789
D_{Na^+} [m ² /s]	$1.28 \cdot 10^{-9}$ [83]	$0.803 \cdot 10^{-9}$ [83]	$1.28 \cdot 10^{-9}$

measurement of the correct solid charge as well as the determination of the sodium hydroxide concentration as the measured voltage deviates slightly from slug to slug.

5.3 RESULTS AND DISCUSSION

5.3.1 Influence of two phase velocity and flow direction on the liquid-solid mass transfer

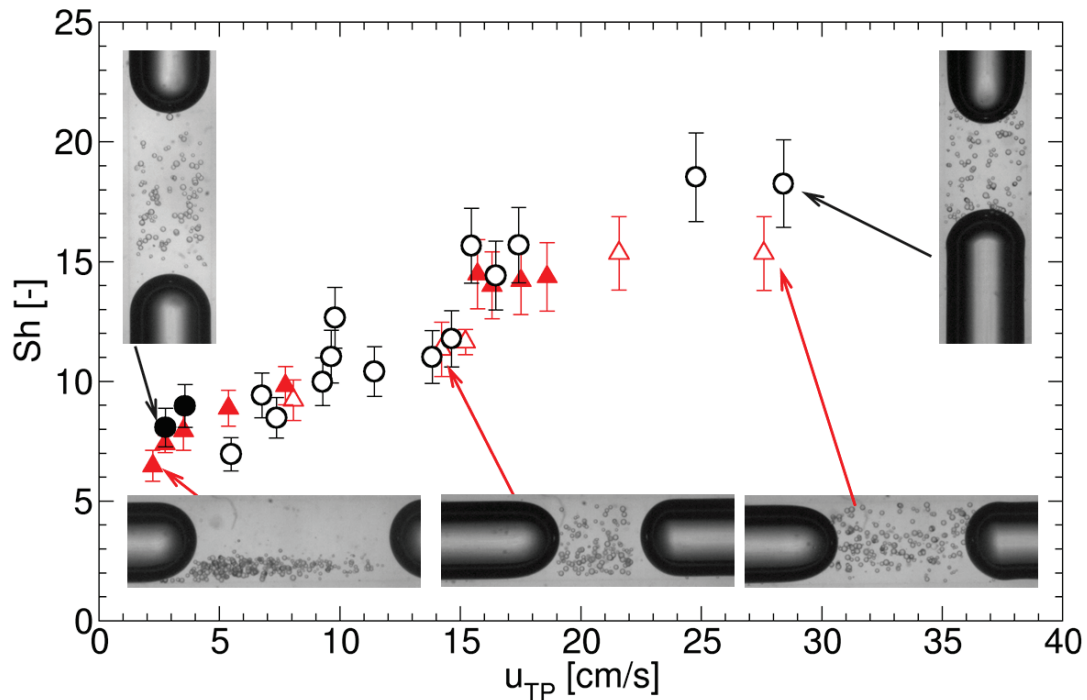


Figure 5.3: Influence of two phase velocity on Sherwood numbers for horizontal (Δ , \blacktriangle) and vertical (\circ , \bullet) "slurry Taylor" flow, filled symbols represent experiments conducted with ethanol/water and empty symbols with acetonitrile/water mixtures. The pictures illustrate typical flow patterns for the indicated operating conditions.

In Figure 5.3 the resulting Sherwood numbers for horizontal and vertical flow are illustrated for increasing two phase velocity. Whereas the flow pattern differs for horizontal and vertical flow, no influence of flow direction on the L-S mass transfer coefficient could be observed. For vertical flow, over the whole operating range particles were always observed as uniformly distributed of the entire slug. In horizontal flow, however, for low velocities, the particles were placed preferentially in the lower part of the liquid slug and a certain minimal velocity was needed to homogeneously suspend the solid particles over the entire tubing section.

For horizontal and vertical flow, the Sherwood number increases with increasing two phase velocity ($Sh = 6.5$ to 15.3 for $u_{TP} = 2.2 \text{ cm s}^{-1}$ to 16 cm s^{-1}). In horizontal as well as vertical flow, once a certain velocity is reached ($u_{TP} = 16 \text{ cm s}^{-1}$), a further increase seems to not or only slightly influence the Sherwood number and a plateau like behaviour is observed. This velocity appears to coincide with the minimal velocity necessary for homogeneous distribution in horizontal flow.

Ohashi et al. studied L-S mass transfer in horizontal [94] and vertical [93] small tubes ($d_T = 2 \text{ cm}$ to 5.5 cm) for two phase liquid-solid flow. In spite of the differences ($d_T = 2 \text{ cm}$ to 5.5 cm vs 1.65 mm , liquid-solid flow vs. "slurry Taylor" flow, $u_{TP} > 50 \text{ cm s}^{-1}$ vs. $u_{TP} < 30 \text{ cm s}^{-1}$)

their results report on solid particles circulating in cylindrical tubes and therefore a comparable physical systems.

Ohashi et al. could apply the same mass transfer correlation for horizontal as well as vertical flow, even though the flow profiles in both configurations differ: particles were uniformly distributed in vertical flow and largely located close to the bottom for horizontal flow respectively. The particle distribution does not seem to affect the L-S mass transfer and cannot explain the decreasing influence of two phase velocity on the mass transfer coefficient for higher two phase velocities ($u_{TP} > 16 \text{ cm s}^{-1}$) in “slurry Taylor” flow. More detailed studies such as μ -PIV appear necessary to further investigate this finding.

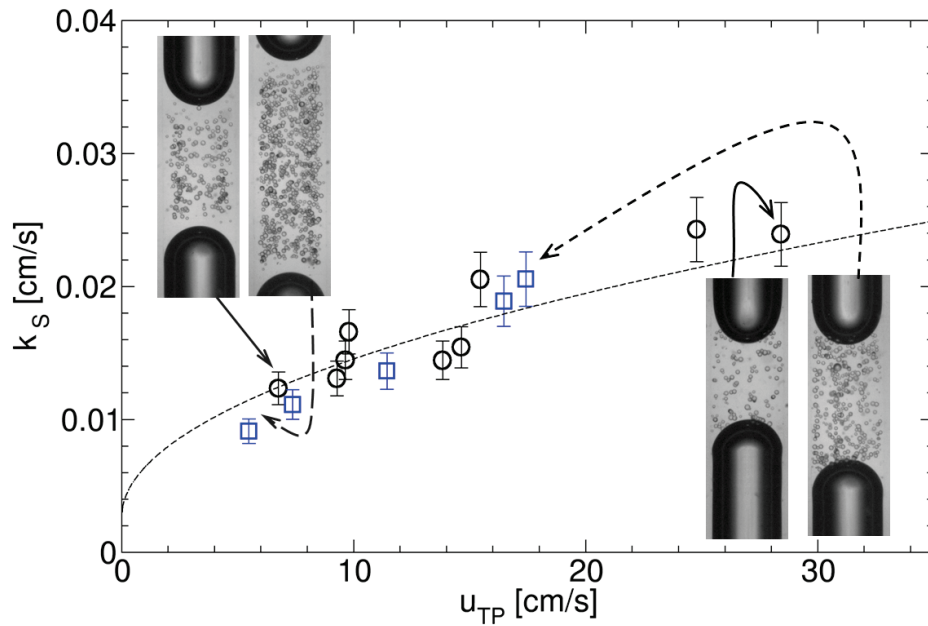
5.3.2 Influence of solid loading and particle diameter

In Figure 5.4a the profile of the L-S mass transfer coefficient for increasing two phase velocity is depicted for two different solid loadings. Pictures demonstrate the placement of solid particles for the corresponding operating conditions. The increase of solid charge from 5.4 g L^{-1} to 17.5 g L^{-1} does not seem to affect the L-S mass transfer. For both solid loadings the particles circulate undisturbed in the liquid slugs. The settling velocity in higher concentrated suspensions is hindered [105, 120] which could possibly change the relative velocity between solid particles and surrounding fluids for different suspension concentrations. However, for the solid loading used in this study, the settling velocity is only reduced by 15%. This appears to be not enough to observe any influence on the L-S mass transfer.

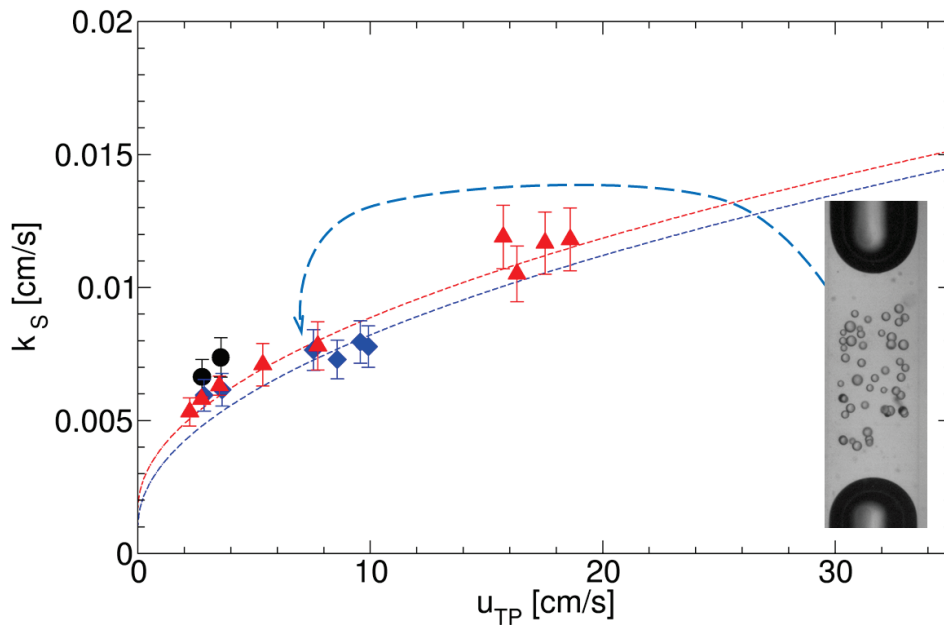
To investigate the influence of particle diameter on L-S mass transfer properties we used two different particle classes ($d_{p,s} = 100$ and $160 \mu\text{m}$). This increase of particle diameter translates in an increase of settling velocity from 0.7 to 1.9 mm s^{-1} . At the low Reynolds numbers present in Taylor flow, and the low particle densities, it is adequate to assume that the particles follow closely the liquid streamlines and the only source of slip velocity comes from the gravity influence. As we did not detect an impact of flow direction we confront the experiments for both particle diameters in vertical flow with the results obtained in horizontal flow. Figure 5.4b illustrates that a similar behaviour could be observed for both particle classes studied.

In conventional contactors which also apply freely circulating solid particles, the impact of particle diameter has been the subject of several studies. In stirred tanks it was found that the L-S mass transfer coefficient is almost independent from particle diameter for particles larger than $200 \mu\text{m}$, for fine particles ($d_p < 100 \mu\text{m}$) a steep increase of mass transfer with decreasing particle size approaching the theoretical limit of $Sh = 2$ could be observed [7, 9, 98]. In bubble columns a negative impact of particle diameter ($200 \leq d_p \leq 900 \mu\text{m}$) on the L-S mass transfer was observed [108].

In contrast to the studies in conventional reactors, the average velocities in “slurry Taylor” flow are rather low and laminar flow is characteristic. Therefore a more pronounced impact of settling velocity (and thus particle diameter and density difference) appears possible for very low two phase velocities. In this study the fluid velocity was always high compared to the settling velocity and sedimentation of particles was not visually detected, which is one reason, why no impact of particle diameter on L-S mass transfer was detected. To better understand a possible influence of particle diameter, solid charge and particle density, experiments with two phase velocities close to the limit of particle settling velocity could be interesting, and might reveal an effect of gravity and therefore flow direction.



(a) Influence of solid charge, experiments were conducted with $\text{H}_2\text{O}/\text{ACN}$ mixtures in vertical flow, $w_s = 5.4 \text{ g l}^{-1}$ (\circ) and 17.5 g l^{-1} (\square).



(b) Influence of particle diameter, experiments were conducted with $\text{H}_2\text{O}/\text{EtOH}$ mixtures, in vertical flow ($d_p = 100 \mu\text{m}$, \bullet and $d_p = 160 \mu\text{m}$, \blacklozenge) and horizontal flow ($d_p = 100 \mu\text{m}$, \blacktriangle).

Figure 5.4: Effect of solid charge and particle diameter on L-S mass transfer in "slurry Taylor" flow. The dashed lines indicate the theoretical results calculated with the proposed correlation in Equation 5.8.

5.3.3 Correlation for L-S mass transfer coefficients in horizontal and vertical “slurry Taylor” flow

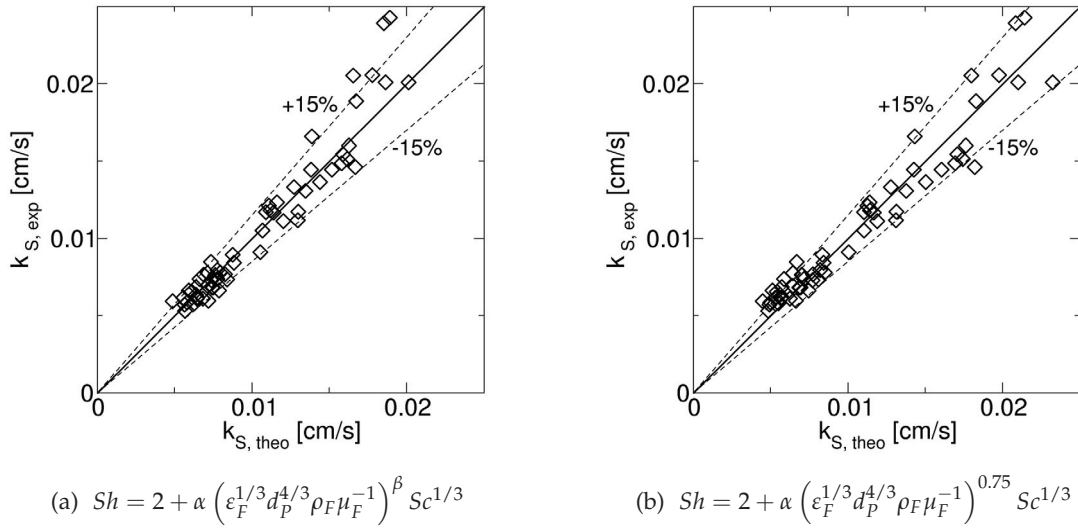


Figure 5.5: Parity diagram illustrating experimental and theoretical L-S mass transfer coefficients calculated with two correlations for the Sherwood number: $Sh = 2 + \alpha (Re_\varepsilon)^\beta Sc^{1/3}$. The dotted lines indicate an uncertainty of 15%. The mean standard deviation is with 8.2% and 9.7% equally good. Fixing β at 0.75, illustrated in (b) to account for the negligible influence of particle diameter on the mass transfer coefficient k_S appears to allow a better fitting for the high range of two phase velocities.

L-S mass transfer experiments were performed for two different fluid media over the same two phase velocity range allowing to establish a first correlation for the Sherwood number. Typically Sherwood number correlations are expressed in function of Reynolds and Schmidt number as $Sh = 2 + \alpha Re^\beta Sc^\gamma$. For stirred tanks and bubble columns the Reynolds number is often based on the energy dissipation rate Equation 5.4 either taking into account the stirring speed or the energy introduced by the gas phase. Ohashi et al. [94] proposed a new approach for particles transported in tubular two phase L-S flow. They introduced the energy dissipation rate for particles circulating in conducts as the sum two effects (i) ε_F accounts for pressure drop due to friction and wall shear rate (Equation 5.5) and (ii) ε_P describes the impact of relative velocity and thus gravity (Equation 5.6).

$$\varepsilon = \varepsilon_F + \varepsilon_P \quad (5.4)$$

$$\varepsilon_F = 2 \cdot f \cdot u_{TP}^3 / d_T \quad (5.5)$$

$$\varepsilon_P = 0.5 \cdot C_D \cdot u_T^3 / d_p \quad (5.6)$$

Even though the flow pattern differs in L-S flow, solid particles are exposed to the same effects in “slurry Taylor” flow. Assuming that the presence of solid particles does not alter the pressure drop; the correlation for the friction factor f for G-L Taylor flow by Kreutzer et al. [71] (Equation 5.7) was used to calculate ε_F .

$$f = \frac{16}{Re} \left[1 + 0.17 \frac{d_T}{L_{slug}} \left(\frac{Re}{Ca} \right)^{0.33} \right] \quad (5.7)$$

The impact of ε_p and thus settling velocity on the overall energy dissipation rate ε is negligible (<5%) for the operating range studied here. However, it dominates the energy dissipation rate for denser ($\Delta\rho > 800 \text{ kg m}^{-3}$, for $d_p = 100 \mu\text{m}$) and/ or bigger particles ($d_p > 200 \mu\text{m}$, for $\Delta\rho = 600 \text{ kg m}^{-3}$) at slow two phase velocities ($u_{TP} < 10 \text{ cm s}^{-1}$). For the correlation proposed here, only ε_F was taken into account and further studies are necessary to investigate and confirm the effect of settling velocity on the L-S mass transfer. The exponent of the Schmidt number was fixed as $\gamma = 1/3$. In agreement with correlations for stirred tank reactors and bubble columns, where the mass transfer coefficient does not directly depend on the particle diameter the exponent of the Reynolds number can be set at $3/4$. Figure 5.5 illustrates the agreement of theoretical and experimental L-S mass transfer coefficients. An other approach would be to fit the data for both parameters (αRe^β). The standard mean deviation is similar for both approaches (9.7% vs. 8.2%) but fixing $\beta = 3/4$ appears to be a better fit for mass transfer coefficients at higher two phase velocities. The dashed lines in Figure 5.4a and 5.4b were obtained using Equation 5.8 and also confirm the good agreement of the proposed correlation with our data.

$$Sh = 2 + 0.34Re^{3/4}Sc^{1/3} \quad (5.8)$$

$$Re = \varepsilon_F^{1/3} d_p^{4/3} \rho_F \mu_F^{-1} \quad (5.9)$$

As discussed above, this correlation is valid for operating conditions where the settling velocity and thus gravity influence can be safely ignored ($\varepsilon_p/\varepsilon < 0.1$). The influence of fluid properties was only investigated for two different fluids, having rather similar properties and the impact of tubing diameter and particle density on the L-S mass transfer coefficient was not addressed in this study. Therefore the proposed correlation (Equation 5.8) represents only a first indication and further studies are necessary to confirm our findings.

5.3.4 Conclusion and perspectives

The L-S mass transfer coefficient was investigated for solid particles transported in horizontal and vertical "slurry Taylor" flow using strong cationic ion exchange beads and the neutralisation of a diluted sodium hydroxide solution. It was found that solid charge (5 g L^{-1} to 18 g L^{-1}) and flow direction do not affect the mass transfer coefficient. For increasing two phase velocity ($u_{TP} = 2.2 \text{ cm s}^{-1}$ to 17.4 cm s^{-1}) the mass transfer coefficient increases ($Sh = 6.5$ to 16). Over the whole velocity range the solid particles were always in motion, in vertical flow they always covered the whole slug, in horizontal flow for low velocities the particles were mainly situated in the lower part and started to populate the upper part of the liquid slug for higher velocities. However, as long as the particles are in motion, their placement does not seem to affect the L-S mass transfer coefficient as the results for both flow orientations are comparable. For horizontal and vertical flow, once a certain two phase velocity ($u_{TP} > 16 \text{ cm s}^{-1}$) was reached, the mass transfer coefficient appears to stay constant. The reason behind this behaviour still needs to be investigated and $\mu - PIV$ seems to be a good method to better evaluate the slip velocity between solid particles and surrounding liquid phase. Particle diameter and density have both an impact on settling velocity and affect therefore the slip velocity. The impact of bigger and denser particles as well as smaller and less dense particles seems interesting to investigate. Due to the external constraints (clogging and settling should be avoided) the settling velocity cannot be increased by all means especially at low fluid velocities. In particular for scale-up the influence of tubing size can be an issue and therefore any influence of tubing diameter and thus flow profile is worth investigating.

These future experiments should also aim to verify and confirm the first correlation that was proposed for the L-S mass transfer in G-L-S “slurry Taylor” flow.

5.4 SYMBOLS

Roman Symbols

a_s	m^{-1}	specific surface area
Ca	-	capillary number $Ca = \mu u_B / \sigma$
C_{Na}	mol L^{-1}	sodium hydroxide concentration
$C_{Na,ex}$	mol L^{-1}	sodium hydroxide concentration at the L-S interface
C_{Na}^*	mol L^{-1}	equilibrium sodium hydroxide concentration
$C_{NaOH,0}$	mol L^{-1}	initial sodium hydroxide concentration at the reactor entrance
C_D	-	drag coefficient for a single particle at u_T
d_p	m	particle diameter
$d_{p,S}$	m	Sauter particle mean diameter
d_T	m	internal tubing diameter
D_{Na+}	$\text{m}^2 \text{s}^{-1}$	diffusion coefficient of sodium hydroxide ions
f	-	friction factor
F_{Na}	mol s^{-1}	molar flux of Na^+ -ions
g	m s^{-3}	gravitational acceleration
k_S	m s^{-1}	L-S external mass transfer coefficient
$n_{IE,0}$	mol	initial molar amount of ion exchange site
$n_{NaOH,0}$	mol	initial molar amount of sodium hydroxide ions
N_{Na}	$\text{mol s}^{-1} \text{m}^{-2}$	normalised molar flux of Na^+ -ions
Q_{aqu}	mL min^{-1}	aqueous flow rate at the exit of the suspension supply unit before formation of Taylor flow
Q_{inert}	mL min^{-1}	flow rate of inert phase
Q_{NaOH}	mL min^{-1}	flow rate of sodium hydroxide solution at entrance of 4-port junction
Q_L	mL min^{-1}	flow rate of active liquid phase
Q_{susp}	mL min^{-1}	suspension flow rate $Q_{susp} = Q_{NaOH} + Q_{susp}$
Sc	-	Schmidt number $Sc = \mu / (\rho D)$
Sh	-	Sherwood number $Sh = k_s d_p / D$
u_B	m s^{-1}	bubble or droplet velocity
u_T	m s^{-1}	terminal settling velocity for a single particle in a still liquid
u_{TP}	m s^{-1}	two phase velocity (sum of discontinuous and continuous superficial velocity)
w_S	g L^{-1}	solid loading
$w_{surfactant}$	-	mass fraction of surfactant

x_{H_2O}	-	molar fraction of water
X_{NaOH}	-	sodium hydroxide conversion
z	m	length
<hr/>		
Greek symbols		
ε	$m^3 s^{-3}$	energy dissipation rate per unit mass of liquid
ε_F	$m^3 s^{-3}$	energy dissipation rate per unit mass of liquid representing the influence of the liquid velocity
ε_S	-	solid volume per liquid slug (G-L)
ε_P	$m^3 s^{-3}$	energy dissipation rate per unit mass of liquid representing the gravity influence
μ	Pa s	dynamic viscosity
ρ_L	$kg m^{-3}$	liquid phase density
τ	s	residence time in reactor
<hr/>		
Abbreviations		
B		bubble
exp		experimental
G		gas phase
L		liquid phase
susp		suspension
S		solid phase
theo		theoretical
TP		two phase
<hr/>		

Part V

CONCLUSION AND PERSPECTIVES

CONCLUSION AND PERSPECTIVES

6.0.1 Conclusion

The G-L-S “slurry Taylor” contact mode was investigated in a single capillary reactor in horizontal and vertical flow configuration. A L-S suspension supplier has been designed and was successfully validated with non-reactive and reactive experiments with silica and alumina based catalysts and ion exchange beads in water, ethanol and ethanol/ glycerine. Mean diameters up to 200 μm and solid loadings up to 50 g L^{-1} have been used successfully. A stable G-L-S “slurry Taylor” flow was generated with a homogeneous and targeted content of particles fluidized in the vortex existing in the liquid slugs.

This contacting mode was used under a pressurized flow of H_2 for the catalytic hydrogenation reaction of 3-methyl-1-pentyn-3-ol. Results were in agreement with those obtained in a conventional batch reactor confirming the good mass transfer performances attainable with this contact mode. Conversion levels for all experiments did not vary over several hours on stream indicating the efficiency and the regularity of the flow and particularly the stability of the L-S suspension feed throughout time. A method of monitoring reaction progress via bubble shrinkage was also exemplified and validated for the first time in a G-L-S media.

The hydrodynamics of G-L-S “slurry Taylor” flow were investigated for two distinct fluid couples: ethanol-nitrogen- SiO_2 and ethanol/glycerol-nitrogen- SiO_2 flow and the influence of flow direction, solid charge and two phase velocity on solid particle placement was investigated. For solid loadings up to 50 g L^{-1} a stable and repeatable solid supply is possible, which encourages the utilisation of even higher loadings. For the operating conditions examined in this study no clogging of the contactor nor the tubing fittings was observed.

For horizontal flow five different flow patterns were observed: at low fluid velocities particles circulate in the lower part of the liquid slug and some amount of the solid is settled on the channel bottom as a stationary bed. By increasing the velocity, particles start to populate also the upper part of the liquid slug. Thus, less particles are settled on the bottom and particle dispersion becomes more homogeneous. In vertical flow, particles were observed to be homogeneously distributed over the entire slug volume even for very low velocities ($u_{TP} > 2 \text{ cm s}^{-1}$). For the operating conditions studied, no accumulation on the rear end of the gas bubble, nor sticking to subsequent bubble nose was observed at any point, even for high solid loadings. Increasing the fluid velocity pushes the particles in the outer recirculation loop depopulating the inner center of the vortex. For horizontal as well as vertical flow, at high velocities ($u_{TP} > 15 \text{ cm s}^{-1}$) the amount of particles trapped in the stationary liquid film at the channel wall increases again. This indicates that there exists an upper limit concerning two phase velocity for good operating conditions. A simplified analysis of the relevant mechanisms affecting the solid dynamics showed that for the operating conditions studied here, the injection of suspension phase as well as entrainment of settled particles is mostly influential. Sedimentation appears to be only secondary.

The mapping of the flow was achieved by using a coefficient of Shields parameter and boundary Reynolds number ΘRe^* for horizontal flow. For vertical flow, as gravity and flow direction are aligned, the two phase velocity seems to impact mostly the placement of particles.

The L-S external mass transfer was investigated for particles transported in the continuous phase of G-L and the discontinuous phase of L-L “slurry Taylor” flow. Mass transfer

coefficients were estimated using the transfer of sodium ion from aqueous solutions to ion exchange particles.

For aqueous-toluene L-L flow it was found that particle agglomeration in the rear end of the liquid droplet leads to very low mass transfer coefficients ($k_s = 0.0012 \text{ cm s}^{-1}$). An increase of two phase velocity did not enhance particle circulation or de-agglomeration and had thus no influence on mass transfer coefficients.

Once particles do not agglomerate but circulate freely in the aqueous phase, the Sherwood number increases with increasing two phase velocity. For aqueous - n-hexanol flow, the Sherwood numbers estimated for particles transported in the disperse phase are in the same range ($Sh = 4$ to 8.4 , $u_{TP} = 1 \text{ cm s}^{-1}$ to 2.5 cm s^{-1}) as for particles suspended in the continuous phase of G-L "slurry Taylor" flow ($Sh = 6$ to 9 , $u_{TP} = 2.2 \text{ cm s}^{-1}$ to 3.6 cm s^{-1}). However, stable flow conditions for L-L "slurry Taylor" flow could be only achieved for velocities up to $u_{TP} = 4.5 \text{ cm s}^{-1}$.

In G-L "slurry Taylor" flow, increasing the two phase velocity led to more and more homogeneously suspended particles in the liquid slug and to an increase of the Sherwood number. However, once the particles are equally distributed over the entire slug height ($u_{TP} > 8 \text{ cm s}^{-1}$) an increase of two phase velocity has no impact on the Sherwood number ($Sh = 14.4$).

The L-S mass transfer coefficient in horizontal and vertical G-L-S "slurry Taylor" flow was also compared. In spite of a quite different hydrodynamic behaviour, it was found that the flow direction does not effect the mass transfer coefficient.

In conclusion, it seems that for freely circulating particles and no agglomeration phenomena, the recirculation efficiency and the occupied space of circulating particles has no effect on the L-S external mass transfer. At the low Reynolds numbers in Taylor flow, laminar conditions are dominating therefore the primary source of slip velocity (between particle and surrounding liquid) is the settling velocity of the solid particles.

A first correlation for the L-S mass transfer in G-L-S "slurry Taylor" flow was established and the mean relative deviation was found to be around 9.7%.

6.0.2 Perspectives

This work pictured the interesting performances of G-L-S "slurry Taylor" flow and gave a first inside into hydrodynamics and external liquid-solid mass transfer properties. This new contact mode is very promising and appears to be a good alternative to conventional G-L-S slurry reactors. So far the understanding of this contactor is still in the beginning and further studies are needed. Future challenges for further research can be grouped into two aspects:

- Broadening the operating parameters:
 - Tubing diameter: it was shown that lift force plays an essential role for particle entrainment. Also the L-S mass transfer experiments indicate a possible influence of shear rate and tubing diameter on the mass transfer coefficient. Therefore it is interesting to investigate this parameter and evaluate its relevance. The tubing diameter is additionally a crucial parameter for scale-up. For horizontal flow bigger channel diameters might require higher two phase velocities for homogeneous particle distribution. Smaller tubing diameters might lead to increased mass transfer coefficients but also a higher risk of clogging.
 - It was found that the initial formation of Taylor flow plays an important role on the particle behaviour and the flow pattern. To better understand this impact and to predict the affect of the injector, it seems interesting to study the initial formation more in detail and to experiment with different injector types.

- Material properties: Studying the influence of material properties on the placement of particles and the required conditions to achieve homogeneous suspension is necessary to predict if a certain reaction can be carried out in this new contact mode. Particles having a higher or lower density as the fluid media, hydrophilic particles in hydrophobic fluid media and the influence of gas phase (CO_2 vs. N_2) are parameters worth investigating.
- Using more sophisticated experimental methods to better understand the physics of this new contact mode and to better describe its properties:
 - One characteristic property of Taylor flow are the nearly ideal plug flow conditions. In horizontal “slurry Taylor” flow, particles settled on the tubing bottom possibly enlarge the liquid film leading to a modified residence time distribution compared to simple G-L Taylor flow. Therefore it is necessary to investigate in how far the particles present in the film alter the plug flow behaviour.
 - The residence time distribution of the solid particle has to be further investigated. Solid particles present in the film have not the same residence time in the reactor as the ones circulating in the liquid slug. Further analysis could show, if the amount of particles trapped in the film is negligible or not and how these particles affect future applications as catalytic reactions or synthesis of nanoparticles for example. In this particular contact mode, investigating the residence time of the micrometric particles is challenging due to the small and rather light particles employed and the susceptible operation of “slurry Taylor” flow. One method could be the use of caged fluorescent particles which are activated by laser impulse.
 - To better understand the different flow patterns detected as well as the results for the L-S mass transfer with its stagnant behaviour for high two phase velocities, τ -PIV appears to be a good method to evaluate the slip velocity between the solid particles and the surrounding fluid.

BIBLIOGRAPHY

- [1] R. Abdallah, V. Meille, J. Shaw, D. Wenn, and C. de Bellefon. Gas-liquid and gas-liquid-solid catalysis in a mesh microreactor. *Chemical Communications*, (4):372–373, February 2004.
- [2] M. K. Akbar, D. A. Plummer, and S. M. Ghiaasiaan. On gas-liquid two-phase flow regimes in microchannels. *International Journal of Multiphase Flow*, 29(5):855–865, May 2003.
- [3] Katherine Albion, Lauren Briens, Cedric Briens, and Franco Berruti. Flow regime determination in horizontal hydrotransport using non-intrusive acoustic probes. *Canadian Journal of Chemical Engineering*, 86(6):989–1000, December 2008.
- [4] R. Aleixo and R. Maia. The beginning of sediment transport - a different approach. In R. M. L. Ferreira, C. T. L. Alves, G. a. B. Leal, and A. H. Cardoso, editors, *Proceedings and Monographs in Engineering, Water and Earth Sciences*, volume Vols 1 and 2 of *Conference: International Conference on Fluvial Hydraulics Location: Lisbon, PORTUGAL Date: SEP 06-08, 2006*, pages 919–926. 2006.
- [5] Abdullah S. Alkindi, Yahya M. Al-Wahaibi, and Ann H. Muggeridge. Physical properties (density, excess molar volume, viscosity, surface tension, and refractive index) of ethanol + glycerol. *Journal of Chemical & Engineering Data*, 53(12):2793–2796, December 2008.
- [6] Hamed Amini, Elodie Sollier, Westbrook M. Weaver, and Dino Di Carlo. Intrinsic particle-induced lateral transport in microchannels. *Proceedings of the National Academy of Sciences of the United States of America*, 109(29):11593–11598, July 2012.
- [7] Piero M. Armenante and Donald J. Kirwan. Mass-transfer to microparticles in agitated systems. *Chemical Engineering Science*, 44(12):2781–2796, 1989.
- [8] David C. Arters and Liang-Shih Fan. Solid liquid mass-transfer in a gas-liquid solid fluidized-bed. *Chemical Engineering Science*, 41(1):107–115, 1986.
- [9] S. Asai, Y. Konishi, and Y. Sasaki. Mass-transfer between fine particles and liquids in agitated vessels. *Journal of Chemical Engineering of Japan*, 21(2):107–112, April 1988.
- [10] Joelle Aubin, Montse Ferrando, and Vladimir Jiricny. Current methods for characterising mixing and flow in microchannels. *Chemical Engineering Science*, 65(6):2065–2093, March 2010.
- [11] P. Aussillous and D. Quere. Quick deposition of a fluid on the wall of a tube. *Physics of Fluids*, 12(10):2367–2371, October 2000.
- [12] H. Brenner. The slow motion of a sphere through a viscous fluid towards a plane surface. *Chemical Engineering Science*, 16(3-4):242–251, 1961.
- [13] B. Buisson, S. Donegan, D. Wray, A. Parracho, J. Gamble, P. Caze, J. Jorda, and C. Guermur. Slurry hydrogenation in a continuous flow reactor for pharmaceutical application. *Chem. Today*, 27(6):12–16, December 2009.

- [14] K. Burlage, C. Gerhardy, H. Praefke, M. A. Liauw, and W. K. Schomburg. Slug length monitoring in liquid-liquid taylor-flow integrated in a novel PVDF micro-channel. *Chemical Engineering Journal*, 227:111–115, July 2013.
- [15] Francisco J. Cabrejos and George E. Klinzing. Incipient motion of solid particles in horizontal pneumatic conveying. *Powder Technology*, 72(1):51–61, October 1992.
- [16] Wangfeng CAI, Jiao ZHANG, Xubin ZHANG, Yan WANG, and Xiangjuan QI. Enhancement of CO₂ absorption under taylor flow in the presence of fine particles. *Chinese Journal of Chemical Engineering*, 21(2):135–143, February 2013.
- [17] Tang Can, Liu Mingyan, and Xu Yonggui. 3-d numerical simulations on flow and mixing behaviors in gas-liquid-solid microchannels. *AIChE Journal*, 59(6):1934–1951, June 2013.
- [18] Dino Di Carlo. Inertial microfluidics. *Lab on a Chip*, 9(21):3038–3046, November 2009.
- [19] Dino Di Carlo, Daniel Irimia, Ronald G. Tompkins, and Mehmet Toner. Continuous inertial focusing, ordering, and separation of particles in microchannels. *Proceedings of the National Academy of Sciences*, 104(48):18892–18897, November 2007.
- [20] Zhizhao Che, Teck Neng Wong, and Nam-Trung Nguyen. An analytical model for plug flow in microcapillaries with circular cross section. *International Journal of Heat and Fluid Flow*, 32(5):1005–1013, October 2011.
- [21] Siva Kumar Reddy Cherlo, Sreenath Kariveti, and S. Pushpavanam. Experimental and numerical investigations of two-phase (liquid-liquid) flow behavior in rectangular microchannels. *Industrial & Engineering Chemistry Research*, 49(2):893–899, January 2010.
- [22] Wendell Karlos Tomazelli Coltro, Renato Sousa Lima, Thiago Pinotti Segato, Emanuel Carrilho, Dosil Pereira de Jesus, Claudimir Lucio do Lago, and José Alberto Fracassi da Silva. Capacitively coupled contactless conductivity detection on microfluidic systems?ten years of development. *Analytical Methods*, 4(1):25–33, January 2012.
- [23] Raymond G. Cox and Howard Brenner. The slow motion of a sphere through a viscous fluid towards a plane surface - ii small gap widths, including inertial effects. *Chemical Engineering Science*, 22(12):1753–1777, December 1967.
- [24] Leonid B. Datsevich. Technological reasons for the selection of fixed-bed reactors. In *Conventional Three-Phase Fixed-Bed Technologies*, number 7 in SpringerBriefs in Applied Sciences and Technology, pages 7–9. Springer New York, January 2012.
- [25] C. de Bellefon, T. Lamouille, N. Pestre, F. Bornette, H. Pennemann, F. Neumann, and V. Hessel. Asymmetric catalytic hydrogenations at micro-litre scale in a helicoidal single channel falling film micro-reactor. *Catalysis Today*, 110(1-2):179–187, December 2005.
- [26] Subhasish Dey. Sediment threshold. *Applied Mathematical Modelling*, 23(5):399–417, May 1999.
- [27] Subhasish Dey. Entrainment threshold of loose boundary streams. In P. Rowinski, editor, *Experimental Methods in Hydraulic Research*, pages 29–48. Springer verlag edition, 2011.
- [28] N. Di Miceli Raimondi, L. Prat, C. Gourdon, and J. Tasselli. Experiments of mass transfer with liquid-liquid slug flow in square microchannels. *Chemical Engineering Science*, 105:169–178, February 2014.

- [29] Ina Dittmar and Peter Ehrhard. Numerical study of a liquid-liquid slug flow in a capillary microreactor. *Chemie Ingenieur Technik*, 85(10):1612–1618, October 2013.
- [30] GN Doku, W Verboom, DN Reinhoudt, and A van den Berg. On-microchip multiphase chemistry - a review of microreactor design principles and reagent contacting modes. *Tetrahedron*, 61(11):2733–2742, March 2005.
- [31] Valentina Dore, Dimitrios Tsaoulidis, and Panagiota Angeli. Mixing patterns in water plugs during water/ionic liquid segmented flow in microchannels. *Chemical Engineering Science*, 80:334–341, October 2012.
- [32] P. Doron and D. Barnea. Flow pattern maps for solid-liquid flow in pipes. *International Journal of Multiphase Flow*, 22(2):273–283, April 1996.
- [33] D. I. Enache, G. J. Hutchings, S. H. Taylor, R. Natividad, S. Raymahasay, J. M. Winterbottom, and E. H. Stitt. Experimental evaluation of a three-phase downflow capillary reactor. *Industrial & Engineering Chemistry Research*, 44(16):6295–6303, August 2005.
- [34] D. I. Enache, G. J. Hutchings, S. H. Taylor, and E. H. Stitt. The hydrogenation of isophorone to trimethyl cyclohexanone using the downflow single capillary reactor. *Catalysis Today*, 105(3-4):569–573, August 2005.
- [35] D. I. Enache, G. J. Hutchings, S. H. Taylor, S. Raymahasay, J. M. Winterbottom, M. D. Mantle, A. J. Sederman, L. F. Gladden, C. Chatwin, K. T. Symonds, and E. H. Stitt. Multiphase hydrogenation of resorcinol in structured and heat exchange reactor systems influence of the catalyst and the reactor configuration. *Catalysis Today*, 128(1-2):26–35, October 2007.
- [36] Wei-Feng Fang, Shang-Chieh Ting, Ching-Wen Hsu, Yu-Tzu Chen, and Jing-Tang Yang. Locally enhanced concentration and detection of oligonucleotides in a plug-based microfluidic device. *Lab on a Chip*, 12(5):923–931, 2012.
- [37] M. Fossa. Design and performance of a conductance probe for measuring the liquid fraction in two-phase gas-liquid flows. *Flow Measurement and Instrumentation*, 9(2):103–109, June 1998.
- [38] Hitoshi Fujimoto, Masahiro Kubo, Takayuki Hama, and Hirohiko Takuda. Transport phenomena of solid particles in pulsatile pipe flow. *Advances in Mechanical Engineering*, 2010.
- [39] Aras Ghaini, Axel Mescher, and David W. Agar. Hydrodynamic studies of liquid-liquid slug flows in circular microchannels. *Chemical Engineering Science*, 66(6):1168–1178, March 2011.
- [40] A. J. Goldman, R. G. Cox, and H. Brenner. Slow viscous motion of a sphere parallel to a plane wall .2. couette flow. *Chemical Engineering Science*, 22(4):653–660, 1967.
- [41] B. González, Calvar N., and Domínguez A. Gómez, E. Density, dynamic viscosity, and derived properties of binary mixtures of methanol or ethanol with water, ethyl acetate, and methyl acetate at $t = (293.15, 298.15, \text{ and } 303.15) \text{ k}$. *The Journal of Chemical Thermodynamics*, 39(12):1578–1588, December 2007.
- [42] A. Gunther, S. A. Khan, M. Thalmann, F. Trachsel, and K. F. Jensen. Transport and reaction in microscale segmented gas-liquid flow. *Lab on a Chip*, 4(4):278–286, 2004.

- [43] Axel Gunther and Klavs F. Jensen. Multiphase microfluidics: from flow characteristics to chemical and materials synthesis RID b-9013-2008. *Lab on a Chip*, 6(12):1487–1503, December 2006.
- [44] S. Haase and T. Bauer. New method for simultaneous measurement of hydrodynamics and reaction rates in a mini-channel with Taylor flow. *Chemical Engineering Journal*, 176-77:65–74, December 2011.
- [45] Youngbae Han and Naoki Shikazono. Measurement of the liquid film thickness in micro tube slug flow. *International Journal of Heat and Fluid Flow*, 30(5):842–853, October 2009.
- [46] C. E. Harland. The kinetics and mechanism of ion exchange. In *Ion Exchange*, pages 134–165. Royal Society of Chemistry, Cambridge, 2 edition, 1994.
- [47] P. Harriott. Mass transfer to particles .2. suspended in a pipeline. *Aiche Journal*, 8(1): 101–102, 1962.
- [48] P. Harriott. Mass transfer to particles .1. suspended in agitated tanks. *Aiche Journal*, 8 (1):93–101, 1962.
- [49] Ryan L. Hartman. Managing solids in microreactors for the upstream continuous processing of fine chemicals. *Organic Process Research & Development*, 16(5):870–887, May 2012.
- [50] Ryan L. Hartman, John R. Naber, Nikolay Zaborenko, Stephen L. Buchwald, and Klavs F. Jensen. Overcoming the challenges of solid bridging and constriction during Pd-catalyzed C-N bond formation in microreactors. *Organic Process Research & Development*, 14(6):1347–1357, November 2010.
- [51] K. S. Hayden, K. Park, and J. S. Curtis. Effect of particle characteristics on particle pickup velocity. *Powder Technology*, 131(1):7–14, March 2003.
- [52] F. Helfferich. Ion-exchange kinetics .v. ion exchange accompanied by reactions. *Journal of Physical Chemistry*, 69(4):1178–1187, 1965.
- [53] Friedrich G. Helfferich. *Ion Exchange*. Courier Dover Publications, 1962. ISBN 9780486687841.
- [54] E. J. Helley. Field measurement of initiation of large bed particle motion in blue creek California. *Transactions-American Geophysical Union*, 50(2):57–&, 1969.
- [55] V. Hessel, P. Angeli, A. Gavriilidis, and H. Lowe. Gas-liquid and gas-liquid-solid microstructured reactors: Contacting principles and applications RID g-7353-2011. *Industrial & Engineering Chemistry Research*, 44(25):9750–9769, December 2005.
- [56] Edward J. Hickin. Sediment transport. In *River Geomorphology*. John Wiley & Sons Ltd, Chichester ; New York, July 1995.
- [57] S. R. Hodges, O. E. Jensen, and J. M. Rallison. The motion of a viscous drop through a cylindrical tube. *Journal of Fluid Mechanics*, 501:279–301, February 2004.
- [58] I. Iliuta and F. Larachi. New scrubber concept for catalytic CO₂ hydration by immobilized carbonic anhydrase II and in-situ inhibitor removal in three-phase monolith slurry reactor. *Separation and Purification Technology*, 86(0):199–214, February 2012.

- [59] T. Inoue, M. A. Schmidt, and K. F. Jensen. Microfabricated multiphase reactors for the direct synthesis of hydrogen peroxide from hydrogen and oxygen. *Industrial & Engineering Chemistry Research*, 46(4):1153–1160, February 2007.
- [60] Said Irandoust and Bengt Andersson. Concentration-dependent diffusivity of benzoic acid in water and its influence on the liquid-solid mass transfer. *The Canadian Journal of Chemical Engineering*, 64(6):954–959, December 1986.
- [61] Josef Janca, Vera Halabalova, Vladimir Polasek, Martin Vasina, and Anastasia Yu Men-shikova. Relaxation of microparticles exposed to hydrodynamic forces in microfluidic conduits. *Analytical and Bioanalytical Chemistry*, 399(4):1481–1491, February 2011.
- [62] Madhvanand N. Kashid and Liubov Kiwi-Minsker. Microstructured reactors for mul-tiphase reactions: State of the art. *Industrial & Engineering Chemistry Research*, 48(14): 6465–6485, July 2009.
- [63] Semih Kececi, Martin Woerner, Alexandru Onea, and Hakan Serhad Soyhan. Recircu-lation time and liquid slug mass transfer in co-current upward and downward taylor flow. *Catalysis Today*, 147:S125–S131, September 2009.
- [64] Ibrahim Sadek Khattab, Farzana Bandarkar, Mohammad Amin Abolghassemi Fakhree, and Abolghasem Jouyban. Density, viscosity, and surface tension of water+ethanol mixtures from 293 to 323K. *Korean Journal of Chemical Engineering*, 29(6):812–817, June 2012.
- [65] Haruyuki Kinoshita, Shohei Kaneda, Teruo Fujii, and Marie Oshima. Three-dimensional measurement and visualization of internal flow of a moving droplet using confocal micro-PIV. *Lab Chip*, 7(3):338–346, March 2007.
- [66] L Kiwi-Minsker and A Renken. Microstructured reactors for catalytic reactions. *Cataly-sis Today*, 110(1-2):2–14, December 2005.
- [67] Andrea Knauer and J. Michael Köhler. Micro continuous-flow synthesis of metal nanoparticles using micro fluid segment technology. In J. Michael Köhler and Brian P. Cahill, editors, *Micro-Segmented Flow*, Biological and Medical Physics, Biomedical Engi-neering, pages 149–200. Springer Berlin Heidelberg, January 2014.
- [68] Michael R. Krecic and Daniel M. Hanes. An analysis of particle saltation dynamics. *Coastal Engineering Proceedings*, 1(25), January 2001.
- [69] M. T. Kreutzer, F. Kapteijn, and J. A. Moulijn. Monoliths as biocatalytic reactors: Smart gas-liquid contacting for process intensification. *Industrial & Engineering Chemistry Re-search*, 44(25):9646–9652, December 2005.
- [70] M. T. Kreutzer, F Kapteijn, J. A. Moulijn, B. Andersson, and Cybulski. Two-phase seg-mented flow in capillaries and monolith reactors. In J. G. and Speight, editor, *Structured Catalysts and Reactors*, Chemical Industries, pages 393–434. CRC Press, November 2005.
- [71] M. T. Kreutzer, F. Kapteijn, J. A. Moulijn, C. R. Kleijn, and J. J. Heiszwolf. Inertial and interfacial effects on pressure drop of taylor flow in capillaries. *Aiche Journal*, 51(9):2428–2440, September 2005. ISSN 0001-1541. doi: 10.1002/aic.10495. WOS:000231237200010.
- [72] M. T. Kreutzer, F. Kapteijn, J.A. Moulijn, and J.J. Heiszwolf. Multiphase monolith re-actors: Chemical reaction engineering of segmented flow in microchannels. *Chemical Engineering Science*, 60(22):5895–5916, November 2005.

- [73] G. K. Kurup and Amar S. Basu. Field-free particle focusing in microfluidic plugs. *Biomicrofluidics*, 6(2):022008–1–022008–10, June 2012.
- [74] A. Leclerc, M. Alamé, D. Schweich, P. Pouteau, C. Delattre, and C. de Bellefon. Gas-liquid selective oxidations with oxygen under explosive conditions in a microstructured reactor. *Lab Chip*, 8(5):814–817, April 2008.
- [75] Chi Young Lee and Sang Yong Lee. Pressure drop of two-phase plug flow in round mini-channels: Influence of surface wettability. *Experimental Thermal and Fluid Science*, 32(8):1716–1722, September 2008.
- [76] Chi Young Lee and Sang Yong Lee. Influence of surface wettability on transition of two-phase flow pattern in round mini-channels. *International Journal of Multiphase Flow*, 34(7):706–711, July 2008.
- [77] David Leighton and Andreas Acrivos. The lift on a small sphere touching a plane in the presence of a simple shear flow. *Zeitschrift für angewandte Mathematik und Physik ZAMP*, 36(1):174–178, January 1985.
- [78] Sharon S.Y. Leung, Raghvendra Gupta, David F. Fletcher, and Brian S. Haynes. Gravitational effect on taylor flow in horizontal microchannels. *Chemical Engineering Science*, 69(1):553–564, February 2012.
- [79] A.-K. Liedtke, F. Scheiff, F. Bornette, R. Philippe, D. Agar, and C. de Bellefon. Liquid-solid mass transfer for microchannel suspension catalysis in gas-liquid and liquid-liquid segmented flow. submitted to *Ind. Eng. Chem. Res.*
- [80] Anne-Kathrin Liedtke, Frederic Bornette, Regis Philippe, and Claude de Bellefon. Gas-liquid-solid "slurry taylor" flow: Experimental evaluation through the catalytic hydrogenation of 3-methyl-1-pentyn-3-ol. *Chemical Engineering Journal*, 227:174–181, July 2013.
- [81] Alexander E. Lobkovsky, Ashish V. Orpe, Ryan Molloy, Arshad Kudrolli, and Daniel H. Rothman. Erosion of a granular bed driven by laminar fluid flow. *Journal of Fluid Mechanics*, 605:47–58, June 2008.
- [82] M. W. Losey, M. A. Schmidt, and K. F. Jensen. Microfabricated multiphase packed-bed reactors: Characterization of mass transfer and reactions. *Industrial & Engineering Chemistry Research*, 40(12):2555–2562, June 2001.
- [83] Arthur A. Marcinkowsky, Harold O. Phillips, and Kurt A. Kraus. Properties of organic-water mixtures .v. self-diffusion coefficients of na+ in alcohol-water mixtures at 25 degrees. *Journal of Physical Chemistry*, 69(11):3968–3972, 1965.
- [84] N. Marquez, P. Castano, J. A. Moulijn, M. Makkee, and M. T. Kreutzer. Transient behavior and stability in miniaturized multiphase packed bed reactors. *Industrial & Engineering Chemistry Research*, 49(3):1033–1040, February 2010.
- [85] J. P. Matas, J. F. Morris, and E. Guazzelli. Lateral forces on a sphere. *Oil & Gas Science and Technology-Revue D Ifp Energies Nouvelles*, 59(1):59–70, February 2004.
- [86] I. McEwan and J. Heald. Discrete particle modeling of entrainment from flat uniformly sized sediment beds. *Journal of Hydraulic Engineering-Asce*, 127(7):588–597, July 2001.
- [87] V. Meille. Review on methods to deposit catalysts on structured surfaces. *Applied Catalysis a-General*, 315:1–17, November 2006.

- [88] V. Meille, N. Pestre, P. Fongarland, and C. de Bellefon. Gas/liquid mass transfer in small laboratory batch reactors: Comparison of methods. *Industrial & Engineering Chemistry Research*, 43(4):924–927, February 2004.
- [89] Othmane Merkak, Laurent Jossic, and Albert Magnin. Dynamics of particles suspended in a yield stress fluid flowing in a pipe. *Aiche Journal*, 54(5):1129–1138, May 2008.
- [90] G.V. Middleton and J. B. Southard. *Mechanics of Sediment Movement*. Society of Economic Paleontologists and Mineralogists. Eastern Section, Tulsa, Ok, 1984.
- [91] P. L. Mills and R. V. Chaudhari. Multiphase catalytic reactor engineering and design for pharmaceuticals and fine chemicals. *Catalysis Today*, 37(4):367–404, September 1997.
- [92] T.A. Nijhuis, G van Koten, F Kapteijn, and J. A. Moulijn. Separation of kinetics and mass-transport effects for a fast reaction: the selective hydrogenation of functionalized alkynes. *Catalysis Today*, 79(1-4):315–321, April 2003.
- [93] H. Ohashi, T. Sugawara, K. Kikuchi, and T. Henmi. Mass-transfer between particles and liquid in solid-liquid 2-phase upflow in vertical tubes. *Journal of Chemical Engineering of Japan*, 12(3):190–195, 1979. doi: 10.1252/jcej.12.190. WOS:A1979GY92800004.
- [94] H. Ohashi, T. Sugawara, K. Kikuchi, and M. Takeda. Mass-transfer between particles and liquid in solid-liquid 2-phase flow through horizontal tubes. *Journal of Chemical Engineering of Japan*, 15(4):311–313, 1982.
- [95] K. Olivon and F. Sarrazin. Heterogeneous reaction with solid catalyst in droplet-flow millifluidic device. *Chemical Engineering Journal*, 227:97–102, July 2013.
- [96] Aluf Orell. The effect of gas injection on the hydraulic transport of slurries in horizontal pipes. *Chemical Engineering Science*, 62(23):6659–6676, December 2007.
- [97] Nicole Pamme. Continuous flow separations in microfluidic devices. *Lab on a Chip*, 7(12):1644–1659, 2007.
- [98] V. G. Pangarkar, A. A. Yawalkar, M. M. Sharma, and Aacm Beenackers. Particle-liquid mass transfer coefficient in two-/three-phase stirred tank reactors. *Industrial & Engineering Chemistry Research*, 41(17):4141–4167, August 2002.
- [99] Sidharth Paranjape, Susan N. Ritchey, and Suresh V. Garimella. Electrical impedance-based void fraction measurement and flow regime identification in microchannel flows under adiabatic conditions. *International Journal of Multiphase Flow*, 42:175–183, June 2012.
- [100] N. A. Patankar, T. Ko, H. G. Choi, and D. D. Joseph. A correlation for the lift-off of many particles in plane poiseuille flows of newtonian fluids. *Journal of Fluid Mechanics*, 445:55–76, October 2001.
- [101] Sarah L. Poe, Meredith A. Cummings, Michael P. Haaf, and D. Tyler McQuade. Solving the clogging problem: Precipitate-forming reactions in flow. *Angewandte Chemie International Edition*, 45(10):1544–1548, 2006.
- [102] Evgeny Rabinovich and Haim Kalman. Flow regime diagram for vertical pneumatic conveying and fluidized bed systems. *Powder Technology*, 207(1-3):119–133, February 2011.

- [103] P. A. Ramachandran and R. V. Chaudhari. *Three-phase catalytic reactors*. Gordon and Breach Science Publishers, 1983.
- [104] D. V. Ravi Kumar, B. L. V. Prasad, and A. A. Kulkarni. Segmented flow synthesis of ag nanoparticles in spiral microreactor: Role of continuous and dispersed phase. *Chemical Engineering Journal*, 192:357–368, June 2012.
- [105] J. F. Richardson and W. N. Zaki. Sedimentation and fluidisation: Part i. *Trans. Instn Chem. Engrs*, 32:S82–S99, 1954.
- [106] D. M. Roberge, L. Ducry, N. Bieler, P. Cretton, and B. Zimmermann. Microreactor technology: A revolution for the fine chemical and pharmaceutical industries? *Chemical Engineering & Technology*, 28(3):318–323, 2005.
- [107] P. G. Saffman. The lift on a small sphere in a slow shear flow. *Journal of Fluid Mechanics*, 22(02):385–400, 1965.
- [108] P. Sanger and Wd Deckwer. Liquid-solid mass-transfer in aerated suspensions. *Chemical Engineering Journal and the Biochemical Engineering Journal*, 22(3):179–186, 1981.
- [109] Frederik Scheiff and David William Agar. Solid particle handling in microreaction technology: Practical challenges and application of microfluid segments for particle-based processes. In J. Michael Köhler and Brian P. Cahill, editors, *Micro-Segmented Flow, Biological and Medical Physics, Biomedical Engineering*, pages 103–148. Springer Berlin Heidelberg, January 2014.
- [110] Frederik Scheiff, Frank Neemann, Sylwia J. Tomasiak, and David W. Agar. Suspension-skatalyse im pfpfenströmungs-Mikroreaktor - experimentelle und numerische stofftransportbewertung. *Chemie Ingenieur Technik*, 86(4):504–518, April 2014.
- [111] Daniel Schweich. *Génie de la réaction chimique*. Paris, TEC & DOC edition, 2001.
- [112] A. Serizawa, Z. P. Feng, and Z. Kawara. Two-phase flow in microchannels. *Experimental Thermal and Fluid Science*, 26(6-7):703–714, August 2002.
- [113] Ilya Shestopalov, Joshua D. Tice, and Rustem F. Ismagilov. Multi-step synthesis of nanoparticles performed on millisecond time scale in a microfluidic droplet-based system. *Lab on a Chip*, 4(4):316–321, July 2004.
- [114] Jelle R. A. Sietsma, Johannes D. Meeldijk, Marjan Versluijs-Helder, Alfred Broersma, A. Jos van Dillen, Petra E. de Jongh, and Krijn P. de Jong. Ordered mesoporous silica to study the preparation of Ni/SiO₂ ex nitrate catalysts: Impregnation, drying, and thermal treatments. *Chemistry of Materials*, 20(9):2921–2931, May 2008.
- [115] Frits Byron Soepyan, Selen Cremaschi, Cem Sarica, Hariprasad J. Subramani, and Gene E. Kouba. Solids transport models comparison and fine-tuning for horizontal, low concentration flow in single-phase carrier fluid. *AIChE Journal*, 60(1):76–122, January 2014.
- [116] Martin Sommerfeld, Karl-Ernst Wirth, and Ulrich Muschelknautz. L₃ two-phase gas-solid flow. In *VDI Heat Atlas, VDI-Buch*, pages 1181–1238. Springer Berlin Heidelberg, January 2010.
- [117] Helen Song, Delai L. Chen, and Rustem F. Ismagilov. Reactions in droplets in microfluidic channels. *Angewandte Chemie-International Edition*, 45(44):7336–7356, 2006.

- [118] P Stevenson, R. B Thorpe, J. E Kennedy, and C McDermott. The transport of particles at low loading in near-horizontal pipes by intermittent flow. *Chemical Engineering Science*, 56(6):2149–2159, March 2001.
- [119] P Stevenson, R. B Thorpe, and J. F Davidson. Incipient motion of a small particle in the viscous boundary layer at a pipe wall. *Chemical Engineering Science*, 57(21):4505–4520, November 2002.
- [120] Professor Dr-Ing Matthias Stieß. Fluidmechanische Grundlagen. In *Mechanische Verfahrenstechnik - Partikeltechnologie 1*, Springer-Lehrbuch, pages 105–160. Springer Berlin Heidelberg, January 2009.
- [121] R. Sun and T. Cubaud. Dissolution of carbon dioxide bubbles and microfluidic multi-phase flows. *Lab on a Chip*, 11(17):2924–2928, 2011.
- [122] G. I. Taylor. Deposition of a viscous fluid on the wall of a tube. *Journal of Fluid Mechanics*, 10(2):161–165, 1961.
- [123] Rex B. Thorpe and Paul Stevenson. Suspension of particles from the bottom of pipes and stirred tanks by gassed and ungassed flows. *The Canadian Journal of Chemical Engineering*, 81(3-4):351–359, June 2003.
- [124] T. C. Thulasidas, M. A. Abraham, and R. L. Cerro. Flow patterns in liquid slugs during bubble-train flow inside capillaries. *Chemical Engineering Science*, 52(17):2947–2962, September 1997.
- [125] T. C. Thulasidas, M. A. Abraham, and R. L. Cerro. Dispersion during bubble-train flow in capillaries. *Chemical Engineering Science*, 54(1):61–76, January 1999.
- [126] Pierre Trambouze and Jean-Paul Euzen. *Chemical Reactors*. Technip, Paris, edition technip edition, 2002.
- [127] Roman Tschentscher, Tjeerd Alexander Nijhuis, John van der Schaaf, and Jaap C Schouten. Glucose oxidation in slurry reactors and rotating foam reactors. *Industrial & Engineering Chemistry Research*, 51(4):1620–1634, February 2012.
- [128] A. Ufer, D. Sudhoff, A. Mescher, and D.W. Agar. Suspension catalysis in a liquid-liquid capillary microreactor. *Chemical Engineering Journal*, 167(2-3):468–474, March 2011.
- [129] Ch Wohlfarth. Viscosity of the mixture (1) water; (2) acetonitrile. In M. D. Lechner, editor, *Supplement to IV/18*, number 25 in Landolt-Börnstein - Group IV Physical Chemistry, pages 716–718. Springer Berlin Heidelberg, January 2009.
- [130] K. Wu and S. Kuhn. Strategies for solids handling in microreactors. *chimica oggi*, 32(3):62–67, 2014.
- [131] Xiangchun Xuan, Junjie Zhu, and Christopher Church. Particle focusing in microfluidic devices. *Microfluidics and Nanofluidics*, 9(1):1–16, July 2010.
- [132] Liang Yu, Yichang Pan, Chongqing Wang, and Lixiong Zhang. A two-phase segmented microfluidic technique for one-step continuous versatile preparation of zeolites. *Chemical Engineering Journal*, 219:78–85, March 2013.
- [133] Lanying Zeng, Fady Najjar, S. Balachandar, and Paul Fischer. Forces on a finite-sized particle located close to a wall in a linear shear flow. *Physics of Fluids (1994-present)*, 21(3):033302–1–033302–18, March 2009.

- [134] Yuchao Zhao, Guangwen Chen, and Quan Yuan. Liquid-liquid two-phase flow patterns in a rectangular microchannel. *Aiche Journal*, 52(12):4052–4060, December 2006.
- [135] Jian Zhou and Ian Papautsky. Fundamentals of inertial focusing in microchannels. *Lab on a chip*, 13(6):1121–32, February 2013.